CHAPTER 8

# X-Ray Spectroscopy*

**Contributing authors: Alexander Seyfarth† and Eileen Skelly Frame**

## 8.1 ORIGIN OF X-RAY SPECTRA

X-rays were discovered in 1895 by Wilhelm Conrad Röntgen who received the first Nobel Prize in Physics, awarded in 1901, for his discovery. X-ray absorption, emission, and fluorescence spectra are used in the qualitative and quantitative determination of elements in solid and liquid samples. XRA is used in the nondestructive evaluation of flaws in objects, including voids or internal cracks in metals, cavities in teeth, and broken bones in humans, a technique called radiography or X-ray fluoroscopy. This same technique is used to perform security screening of baggage at airports. A computerized version of radiography, computed tomography (CT) scanning or computed axial tomography (CAT), provides a powerful, high-resolution medical diagnostic tool by giving a 3D cross-sectional image of body tissues. Diffraction of X-rays by crystalline materials, a technique called X-ray crystallography, provides crystal structure identification, orientation of atomic planes in materials, and other physical information about samples. X-ray astronomy uses cosmic X-rays to study the universe, and X-ray spectrometers have been sent to the moon and Mars to study the surface rocks *in situ*. This chapter will focus primarily on X-ray fluorescence (XRF) spectrometry and X-ray diffractometry (XRD), the techniques of most use to analytical chemists.

X-rays consist of electromagnetic radiation with a wavelength range from 0.005 to 10 nm (0.05–100 Å). X-rays have shorter wavelengths and higher energy than ultraviolet (UV) radiation. X-rays are generated in several ways, by deceleration of electrons in matter or by electronic transitions of inner core electrons.

### 8.1.1 Energy Levels in Atoms

An atom is composed of a nucleus and electrons. The electrons are arranged in shells around the nucleus with the valence electrons in the outer shell. The different shells correspond to the different principal quantum numbers of the possible quantum states. The principal quantum number, $n$, can have integral values beginning with 1. The shells are named starting with the shell closest to the nucleus, which is called the K shell. The K shell is the lowest in energy and corresponds to the quantum level with $n = 1$. The shells moving out from the nucleus are named the L shell, M shell, and so on alphabetically. The letters used for the two lowest shells are historical; K is from the German word *kurz*, meaning short, and L is from the German word *lang*, meaning long. An atom is shown

* Dedicated to the memory of Dr. Ron Jenkins and Dr. Eugene Bertin, outstanding X-ray spectroscopists and excellent teachers.

† Dr. Seyfarth is Sr. Product Manager, HHXRF, Bruker Elemental, Kennewick, WA.

schematically in Figure 8.1a, with $\Phi_K$, $\Phi_L$, and $\Phi_M$ representing the energy of the K, L, and M shells, respectively. A partial list of elements and their electron configurations is given in Table 8.1. For example, a sodium atom contains filled K and L shells and one electron in the M shell.

When an X-ray photon or a fast-moving electron collides with an atom, its energy may be absorbed by the atom. If the X-ray photon or electron has sufficient energy, it knocks an electron out of one of the atom's inner shells (e.g., the K shell), and the atom becomes ionized as shown in Figure 8.1b. An electron from a higher-energy shell (e.g., the L shell) then falls into the position vacated by the dislodged inner electron, and an X-ray photon is emitted as the electron drops from one energy level to the other (Figure 8.1c). The wavelength/energy of this emitted X-ray photon is characteristic of the element being bombarded.

A fourth process can also occur, as shown in Figure 8.1d. Instead of emitting an X-ray photon, the energy released knocks an electron out of the M shell. This electron is called an Auger electron. This Auger process is the basis for a sensitive surface analysis technique. Auger electron spectroscopy (AES) and the related method of X-ray photoelectron spectroscopy, based on the measurement of the emitted electron shown in Figure 8.1b, are discussed in Chapter 14.

If we plot the energy levels of the K, L, and M shells for a given element, we get a diagram similar to Figure 8.2.

Note that the K shell has only one energy level, while the higher shells have sublevels within each shell. If an electron is dislodged from the K shell, an electron from an L or an M shell may replace it. The resulting ion emits radiation with energy $E$ equal to the energy difference between the electronic energy levels, such as

$$E_{\text{X-ray}} = \Phi_L - \Phi_K \tag{8.1}$$

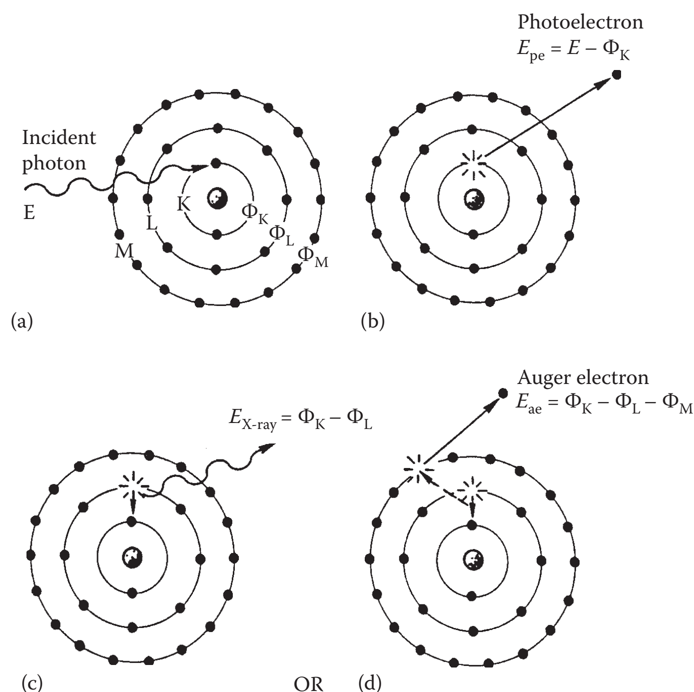


**Figure 8.1** A schematic atom showing the steps leading to the emission of an X-ray photon (c) or an Auger electron (d). (From Jenkins, R. et al., *Quantitative X-Ray Spectrometry*, Marcel Dekker, Inc., New York, 1981. With permission.)

**Table 8.1 Electron Configurations of Various Elements**

| | | K | L | | M | | | N | |
|---|---|---|---|---|---|---|---|---|---|
| **Element** | **Z** | **1s** | **2s** | **2p** | **3s** | **3p** | **3d** | **4s** | **4p** |
| H | 1 | 1 | | | | | | | |
| He | 2 | 2 | | | | | | | |
| Li | 3 | 2 | 1 | | | | | | |
| Be | 4 | 2 | 2 | | | | | | |
| B | 5 | 2 | 2 | 1 | | | | | |
| C | 6 | 2 | 2 | 2 | | | | | |
| N | 7 | 2 | 2 | 3 | | | | | |
| O | 8 | 2 | 2 | 4 | | | | | |
| F | 9 | 2 | 2 | 5 | | | | | |
| Ne | 10 | 2 | 2 | 6 | | | | | |
| Na | 11 | Neon core (10) | | | 1 | | | | |
| Mg | 12 | | | | 2 | | | | |
| Al | 13 | | | | 2 | 1 | | | |
| Si | 14 | | | | 2 | 2 | | | |
| P | 15 | | | | 2 | 3 | | | |
| S | 16 | | | | 2 | 4 | | | |
| Cl | 17 | | | | 2 | 5 | | | |
| Ar | 18 | | | | 2 | 6 | | | |
| K | 19 | | Argon core (18) | | | | | 1 | |
| Ca | 20 | | | | | | | 2 | |
| Sc | 21 | | | | | | 1 | 2 | |
| Ti | 22 | | | | | | 2 | 2 | |
| V | 23 | | | | | | 3 | 2 | |
| Cr | 24 | | | | | | 5 | 1 | |
| Mn | 25 | | | | | | 5 | 2 | |
| Fe | 26 | | | | | | 6 | 2 | |
| Co | 27 | | | | | | 7 | 2 | |
| Ni | 28 | | | | | | 8 | 2 | |
| Cu | 29 | | | | | | 10 | 1 | |
| Zn | 30 | | $Cu^+$ core (28) | | | | | 2 | |
| Ga | 31 | | | | | | | 2 | 1 |
| Ge | 32 | | | | | | | 2 | 2 |
| As | 33 | | | | | | | 2 | 3 |
| Se | 34 | | | | | | | 2 | 4 |
| Br | 35 | | | | | | | 2 | 5 |
| Kr | 36 | | | | | | | 2 | 6 |

where $\Phi_L$ is the energy of the electron in a specific electronic state within the L shell that "drops" to the K shell. Similar equations may be written for other transitions, such as between an M shell sublevel and an L shell sublevel, using the appropriate energy of the electron in the M shell sublevel that drops into the L shell and so on. As we know from Chapter 2,

$$E = h\nu = \frac{hc}{\lambda}$$

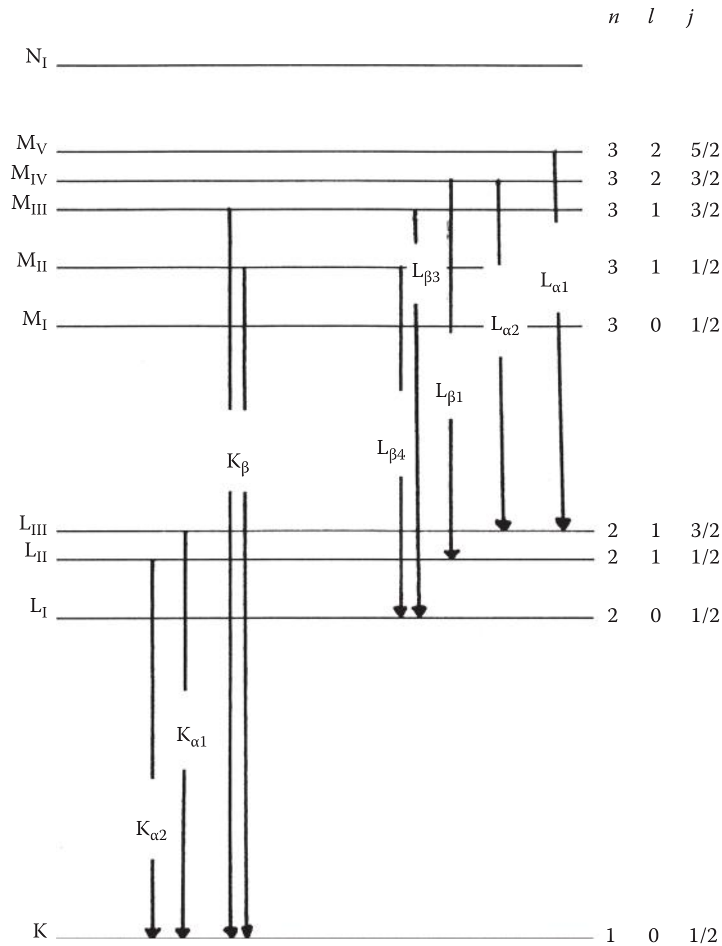


**Figure 8.2** Atomic energy levels and symbols used for some common X-ray transitions. (Modified from Parsons, M.L., X-ray methods, in Ewing, G.W. (ed.), *Analytical Instrumentation Handbook*, 2nd edn., Marcel Dekker, Inc., New York, 1997. Used with permission.)

This relationship relates the energy of the emission to the wavelength and can be used to convert wavelength and energy. Most X-ray systems express wavelength in angstroms and energy in keV. To convert between these units, Equation 8.2 gives

$$\text{Energy (keV)} = \frac{12.4}{\lambda}(\text{Å}) \tag{8.2}$$

Therefore, for the X-ray photon released when an L electron in a specific sublevel drops down to fill a vacancy in the K shell,

$$h\nu = \frac{hc}{\lambda} = \Phi_L - \Phi_K$$

Hence the frequency of the emitted X-ray is

$$\nu = \frac{\Phi_L - \Phi_K}{h} \tag{8.3}$$

The frequency or wavelength for transitions between other sublevels and shells is calculated in the same manner. Transitions are not possible between all available energy levels.

As in all forms of spectroscopy, transitions are governed by quantum mechanical *selection rules*. Some transitions are allowed by these rules while others are forbidden. For a brief discussion of the selection rules, the interested student should consult the texts by Jenkins or Bertin listed in the bibliography.

X-ray emission lines from electron transitions **terminating** in the K shell are called K lines, lines from transitions terminating in the L shell are called L lines, and so on. There are three L levels differing by a small amount of energy and five M levels. These sublevels are different quantum states, as shown in Figure 8.2; the quantum numbers and states will not be discussed here in detail. An electron that drops from an L shell sublevel to the K shell emits a photon with the energy difference between these quantum states. This transition results in a $K_\alpha$ line. There are two possible $K_\alpha$ lines for atoms with atomic number >9: $K_{\alpha_1}$ and $K_{\alpha_2}$, which originate in different sublevels of the L shell. The $K_\alpha$ lines are often not resolved, and only one peak is seen. These lines are illustrated in Figure 8.2. The use of a Greek letter and numerical subscript to identify an X-ray emission line is called the *Siegbahn* notation. For the purposes of this text, the notation is just a "name" for the peak. An electron that drops from an M shell sublevel to the K shell generates a $K_\beta$ X-ray. There is more than one $K_\beta$ line, but the energy differences are so small between $K_{\beta_1}$ and $K_{\beta_3}$ that only a single $K_\beta$ line is seen unless a high-resolution spectrometer is used. If an electron is ejected from an L shell, an electron from an M shell may fall into its place and emit an X-ray of characteristic wavelength with energy equivalent to the difference between the L and M shell sublevels. These are designated as L lines. A number of L lines are possible, as indicated by Figure 8.2. Table 8.2 indicates the actual transition that gives rise to selected X-ray emission lines. Electrons originating in an N or O shell and falling into the L shell also generate L lines. The energy levels of the K, L, M, and higher shells are characteristic of the element being examined, and the sharp emission lines resulting from electronic transitions are called *characteristic lines* or characteristic radiation. A schematic X-ray emission spectrum obtained under certain conditions by bombarding a solid metal, such as rhodium or lead or silver, with high-energy electrons is shown in Figure 8.3. The characteristic lines are shown as sharp peaks on a broad continuous background. The characteristic K X-ray emission lines from some elements are given in Table 8.3. A more comprehensive table of K and L lines for the elements is found in Appendix 8.A and in handbooks such as the *CRC Handbook of Chemistry and Physics* and the *CRC Handbook of Spectroscopy*, Vol. 1. Not all X-ray lines have a Siegbahn designation, so the International Union of Pure and Applied Chemistry (IUPAC) established

**Table 8.2 Electron Transitions for Selected X-Ray Emission Lines**

| Siegbahn Line Designation | Electron Transition | Siegbahn Line Designation | Electron Transition |
|---|---|---|---|
| $K_{\alpha_1}$ | $L_{III} \rightarrow K$ | $L_{\beta_1}$ | $M_{IV} \rightarrow L_{II}$ |
| $K_{\alpha_2}$ | $L_{II} \rightarrow K$ | $L_{\beta_3}$ | $M_{III} \rightarrow L_I$ |
| $K_{\beta_1}$ | $M_{III} \rightarrow K$ | $L_{\beta_4}$ | $M_{II} \rightarrow L_I$ |
| $K_{\beta_3}$ | $M_{II} \rightarrow K$ | $L_\eta$ | $M_I \rightarrow L_{II}$ |
| $K_{\beta_5}$ | $M_{IV,V} \rightarrow K$ | $L_{\gamma_{2,3}}$ | $N_{II,III} \rightarrow L_I$ |
| $K_{\beta_2}$ | $N_{II,III} \rightarrow K$ | $L_{\beta_6}$ | $N_I \rightarrow L_{III}$ |
| $K_{\beta_4}$ | $N_{IV,V} \rightarrow K$ | $M_{\xi_1}$ | $N_{III} \rightarrow M_V$ |
| $L_{\alpha_1}$ | $M_V \rightarrow L_{III}$ | $M_{\xi_2}$ | $N_{II} \rightarrow M_{IV}$ |
| $L_{\alpha_2}$ | $M_{IV} \rightarrow L_{III}$ | | |

*Note:* Not all lines are seen for all elements, and many of the lines are not resolved with standard X-ray spectrometers. Many M → M, N → M, O → L, and O → M transitions have no Siegbahn notation associated with them.

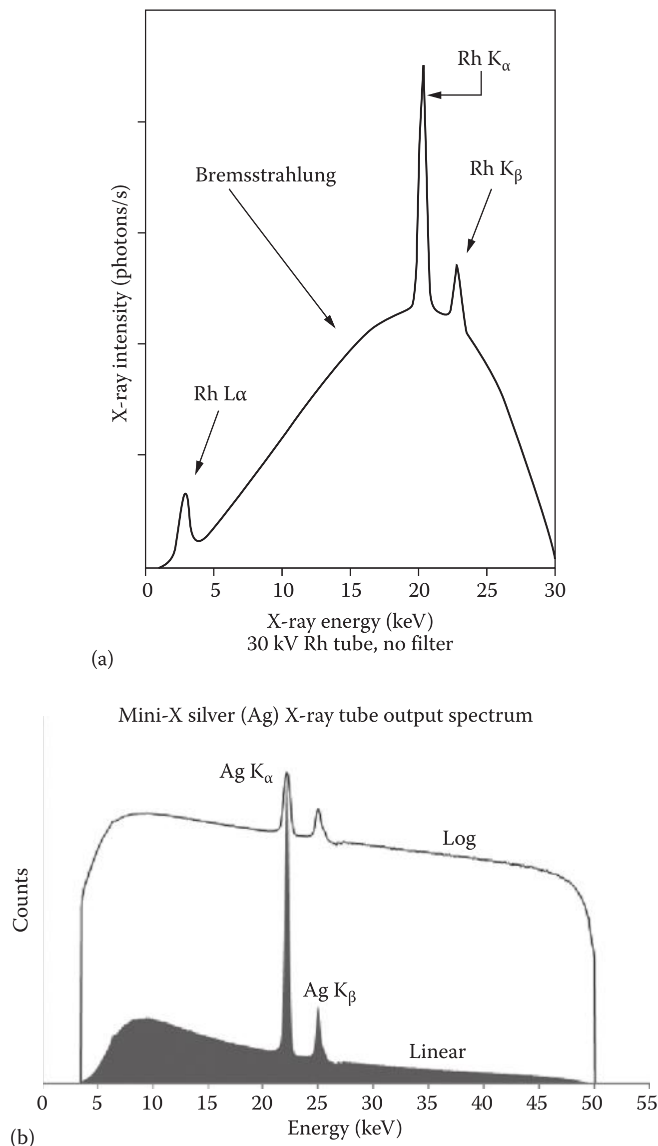


**Figure 8.3** X-ray emission spectrum obtained by bombarding (a) rhodium metal (Rh) and (b) silver metal (Ag) with electrons. Both a broad continuum (Bremsstrahlung) and sharp characteristic emission lines from the metal are seen. (a: © Thermo Fisher Scientific. www.thermofisher.com. Used with permission; b: Amptek Mini-X silver (Ag) XRF tube output spectrum; Courtesy of Amptek, Inc., Bedford, MA, www.amptek.com.)

a new identification system for X-ray lines in 1991. Appendix 8.A contains a list of the Siegbahn notation for lines and the IUPAC designation for these lines. For all new publication purposes, the IUPAC designation should be used.

The wavelengths and energies of the characteristic lines depend only on the element, because the inner electrons do not take part in bonding. Therefore, the lines are independent of oxidation state and bonding and physical state, making the use of the characteristic lines an *elemental* analysis technique. No molecular information is obtained from these lines.

**Table 8.3 Wavelengths of Absorption Edges and Characteristic Emission Lines of Various Elements**

| | | Emission (Å) | |
|---|---|---|---|
| Element | K Absorption Edge (Å) | $K_{\beta_{1,3}}$ [a] | $K_{\alpha_{1,2}}$ [b] |
| Mg | 9.512 | 9.559 | 9.890 |
| Ti | 2.497 | 2.514 | 2.748, 2.752 |
| Cr | 2.070 | 2.085 | 2.290, 2.294 |
| Mn | 1.896 | 1.910 | 2.102, 2.106 |
| Ni | 1.488 | 1.500 | 1.658, 1.662 |
| Ag | 0.4858 | 0.4971, 0.4977 | 0.5594, 0.5638 |
| Pt | 0.1582 | 0.1637, 0.1645 | 0.1855, 0.1904 |
| Hg | 0.1492 | 0.1545, 0.1553 | 0.1751, 0.1799 |

[a] When more than one number is listed, $K_{\beta_1}$ is listed first.
[b] When more than one number is listed, $K_{\alpha_1}$ is listed first.

The broad continuous "background" emission of x-radiation seen in Figure 8.3 is due to a second process that occurs when high-energy electrons strike a solid. The continuous radiation results from the collision of electrons with the atoms of the solid. At each collision, the electron loses some energy and decelerates, with the production of an X-ray photon. The energy of the photon is equal to the kinetic energy difference of the electron as a result of the collision. Each electron generally undergoes a series of collisions with each collision resulting in a photon of slightly different energy. The result of these many collisions is emission of a continuum of X-rays over a wide wavelength range. This continuous radiation is called *Bremsstrahlung* or *white radiation*.

When all the energy of the impinging electrons is turned into X-rays, as would occur if the electrons transferred all their energy in one collision, the wavelength of the emitted photons is the shortest attainable. This is termed the minimum λ or $\lambda_{min}$. The radiation with the highest energy (and therefore the shortest wavelength) is deduced as follows. When all the energy of the electrons is converted to radiant energy, then the energy of the electrons equals the energy of the radiation. The energy of the radiation is given by $E = h\nu$, whereas the energy of the electrons is given by $E = eV$. When they are equal, $h\nu = eV$, where $e$ is the charge of the electron; $V$, the applied voltage; and $\nu$, the frequency of the radiation. But

$$\nu = \frac{c}{\lambda}$$

where
$c$ is the speed of light
λ is the wavelength of radiation

Therefore,

$$h\nu = \frac{hc}{\lambda} = eV \tag{8.4}$$

Rearranging, we get

$$\lambda = \frac{hc}{eV} \tag{8.5}$$

When all the energy of the electron is converted to x-radiation, the wavelength of the radiation is a minimum, and we achieve minimum λ conditions:

$$\lambda_{min} = \frac{hc}{eV} \tag{8.6}$$

Inserting the values for $h$, $c$, and $e$, which are constants, we have the **Duane–Hunt law**,

$$\lambda_{min} = \frac{(6.626 \times 10^{-34}\ \mathrm{J\ s})(3.00 \times 10^{8}\ \mathrm{m/s})(10^{10}\ \mathrm{\AA/m})}{(1.60 \times 10^{-19}\mathrm{C}) \times V} = \frac{12{,}400}{V} \tag{8.7}$$

where

$h$ is Planck's constant
$c$ is the speed of light
$e$ is the charge of an electron
$V$ is the applied voltage (in volts)
$\lambda_{min}$ is the shortest wavelength of X-rays radiated (in angstroms)

The continuum radiation spectrum from a solid metal therefore has a well-defined short-wavelength limit. This limit is a function of the accelerating voltage, but not of the solid metal. The same $\lambda_{min}$ would be obtained by bombardment of lead or tungsten or rhodium at the same accelerating voltage.

An X-ray emission spectrum is similar for all elements, in that $K_\alpha$, $K_\beta$, and $L_\beta$ lines may be seen, if the element possesses enough electrons to populate the appropriate levels. However, the actual wavelengths of these lines vary from one element to another, depending on the *atomic number* of the particular element. A mathematical relationship was discovered between the wavelengths of the K series and the atomic number of the element, and similar relationships were found for the L lines, and others.

### 8.1.2 Moseley's Law

Henry Moseley, a young graduate student working at Cambridge, UK, in 1913, discovered the relationship between wavelength for characteristic X-ray lines and atomic number. After recording the X-ray spectra from numerous elements in the periodic table, he deduced the mathematical relationship between the atomic number of the element and the wavelength of the $K_\alpha$ line. A similar relationship was found between the atomic number and the $K_\beta$ line, the $L_\alpha$ line, and so on. The relationships were formulated in **Moseley's law**, which states that

$$\nu = \frac{c}{\lambda} = a(Z - \sigma)^2 \tag{8.8}$$

where

$c$ is the speed of light
$\lambda$ is the wavelength of the X-ray
$a$ is the constant for a particular series of lines (e.g., $K_\alpha$ or $L_\alpha$ lines)
$Z$ is the atomic number of the element
$\sigma$ is the screening constant that accounts for the repulsion of other electrons in the atom

A partial Moseley's law plot for the $K_\alpha$, $K_\beta$, $L_\alpha$, and $L_\beta$ emission lines is shown in Figure 8.4. Shortly after this monumental discovery, Moseley was killed in action in World War I. The impact of Moseley's law on chemistry was substantial, in that it provided a method of unequivocally assigning an atomic number to newly discovered elements, of which there were several at that time. In addition, it clarified disputes concerning the positions of all known elements in the periodic table, some of which were still in doubt in the early part of the twentieth century.

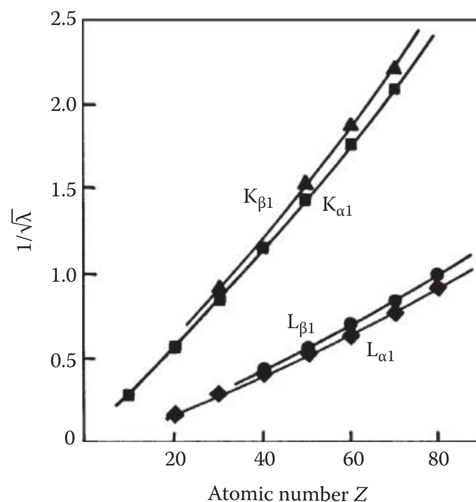


**Figure 8.4** Partial Moseley's law plots for selected K and L lines, showing the relationship between the X-ray emission wavelength and atomic number of the element. Using this relationship, it was possible to predict undiscovered elements and to correctly assign atomic numbers to known elements. (From Helsen, L.A. and Kuczumow, A., in Van Griekin, R.E.; Markowicz, A.A. (eds.), *Handbook of X-Ray Spectrometry*, 2nd edn. Marcel Dekker, Inc.: New York, 2002. Used with permission.)

### 8.1.3 X-Ray Methods

There are several distinct fields of X-ray analysis used in analytical chemistry and materials characterization, namely, XRA, XRD, XRF, and X-ray emission. The basic principles of each are described in the following. X-ray emission is generally used for microanalysis, with either an electron microprobe (Chapter 14) or a scanning electron microscope (SEM).

#### *8.1.3.1 X-Ray Absorption Process*

The absorption spectrum obtained when a beam of X-rays is passed through a thin sample of a pure metal is depicted in Figure 8.5.

As is the case with other forms of radiation, some of the intensity of the incident beam may be absorbed by the sample while the remainder is transmitted. We can write a Beer's law expression for the absorption of X-rays by a thin sample:

$$I(\lambda) = I_0(\lambda)e^{-(\mu_m)\rho x} \tag{8.9}$$

where

$I(\lambda)$ is the transmitted intensity at wavelength $\lambda$
$I_0(\lambda)$ is the incident intensity at the same wavelength
$\mu_m$ is the **mass absorption coefficient** ($cm^2/g$)
$\rho$ is the density of the sample ($g/cm^3$)
$x$ is the sample thickness (cm)

The mass absorption coefficient is a constant for a given element at a given wavelength and is independent of both the chemical and physical state of the element. An updated compilation of mass absorption coefficients can be found online at the NIST website: http://www.nist.gov/pml/data/xraycoef/index.cfm (J.H. Hubbell and S.M. Seltzer) or in the text by Bertin or handbooks listed in the bibliography or references in the literature.

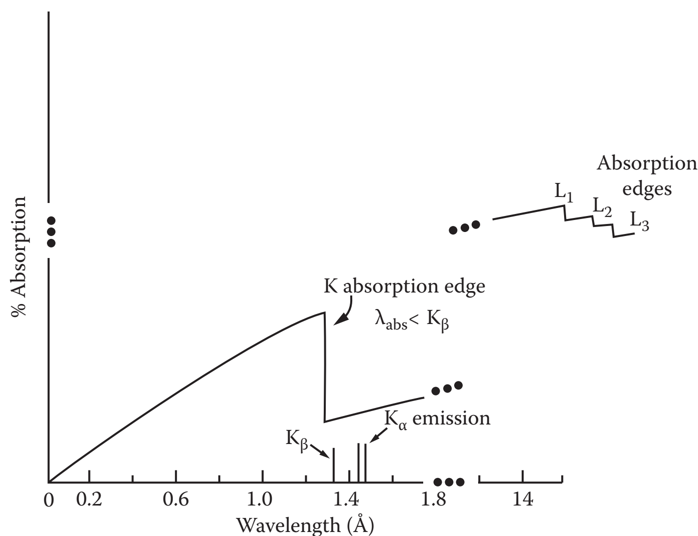


**Figure 8.5** The X-ray absorption spectrum of a pure metal. Longer wavelengths are more readily absorbed than shorter wavelengths. The absorption spectrum is characterized by absorption edges, which are abrupt increases in absorption at energies sufficient to eject an electron from one of the atomic shells. The K absorption edge occurs at an energy sufficient to eject an electron from the K shell of the given metal.

Of course, most samples do not consist of a single pure element. The total mass absorption coefficient for a sample can be calculated by adding the product of the individual mass absorption coefficients for each element times the weight fraction of the element present in the sample. That is, for a metal alloy like steel,

$$\mu_{\text{total}} = w_{\text{Fe}}\mu_{\text{Fe}} + w_{\text{Cr}}\mu_{\text{Cr}} + w_{\text{Ni}}\mu_{\text{Ni}} + \cdots \tag{8.10}$$

where

$w_{\text{Fe}}$ is the weight fraction of iron
$\mu_{\text{Fe}}$ is the mass absorption coefficient for pure iron
$w_{\text{Cr}}$ is the weight fraction of chromium, and so on for all the elements in the alloy

For accurate quantitative work, the *mass attenuation coefficient* is used in place of the mass absorption coefficient. The mass attenuation coefficient takes into account both absorption and scattering of X-rays by the sample.

The amount of light absorbed increases as the wavelength increases. This is reasonable since longer wavelengths have less energy, and a less energetic photon has less "penetrating power" and is more likely to be absorbed. Only a few absorption peaks are seen in an X-ray absorption spectrum, but there is a very distinct feature in these spectra. An abrupt change in absorptivity (or the mass absorption coefficient) occurs at the wavelength of the X-ray necessary to eject an electron from an atom. These abrupt changes in X-ray absorptivity are termed ***absorption edges***. Looking at Figure 8.5, it can be seen that radiation with a wavelength of 1.8 Å has a certain percent absorption value. As the wavelength of the X-ray *decreases*, its energy increases, its penetrating power increases, and the percent absorption decreases. This can be seen by the downward slope of the absorption trace, moving to the left along the *x*-axis from a wavelength of 1.8 Å. As the wavelength decreases further, the X-ray eventually has sufficient energy to displace electrons from the K shell. This results in an abrupt *increase* in absorption. This is manifested by the **K absorption edge**.

After the absorption edge, the penetrating power continues to increase as the wavelength decreases further until finally the degree of absorption is extremely small at very small wavelengths. At wavelengths less than 0.2 Å, penetrating power is extremely high, and we are approaching the properties of interstellar radiation such as cosmic rays, which have extremely high penetrating power. Wavelengths shorter than the K absorption edge have sufficient energy to eject K electrons; the bombarded sample will exhibit both continuum radiation and the characteristic K lines for the sample. This process is called XRF and will be discussed in detail. Wavelengths just slightly longer than the K absorption edge do not have enough energy to displace K electrons. The absorption spectrum is unique for each element; portions of the absorption spectrum showing the position of the K absorption edge for several pure elements are shown in Figure 8.6.

Another way of looking at X-ray absorption is to plot the mass absorption coefficient as a function of wavelength or energy. For a thin sample of pure metal and a constant incident intensity, Equation 8.9 indicates that if the percent absorption changes as a function of wavelength, it must be that $\mu_m$ changes. A plot of $\mu_m$ versus X-ray energy for the element lead is shown in Figure 8.7. The K, L, and M absorption edges are seen.

The wavelengths of the absorption edges and of the corresponding emission lines do not quite coincide, as seen in Figure 8.6b. This is because the energy required to dislodge an electron from an atom (the absorption edge energy) is not quite the same as the energy released when the dislodged electron is replaced by an electron from an outer shell (emitted X-ray energy). The amount of energy required to displace the electron must dislodge it from its orbital and remove it completely from the atom. This is more than the energy released by an electron in an atom falling from one energy level to another. A few absorption edge values are given in Table 8.3. Figure 8.6b shows that the energy of the K absorption edge is greater than the energy of the K emission lines. As opposed to emission spectra, only one K absorption edge is seen per element, since there is only one energy level in the K shell. Three absorption edges of different energies are observed for the L levels, five for the M levels, and so on; these can be seen in Figure 8.7. A comprehensive table of absorption edge wavelengths is located in Appendix 8.B.

#### *8.1.3.2 X-Ray Fluorescence Process*

X-rays can be emitted from a sample by bombarding it with electrons, alpha particles, or with other X-rays. When electrons or alpha particles are used as the excitation source, the process is called X-ray emission or particle-induced X-ray emission (PIXE). This is the basis of X-ray microanalysis using an electron microprobe (Chapter 14) or an SEM. An alpha particle X-ray spectrometer (APXS) is currently on the Mars Curiosity rover collecting data on Martian rock composition.

When the excitation source is a beam of X-rays, that is, photons, the process of X-ray emission is called fluorescence. This is analogous to molecular fluorescence discussed in Chapter 5 and atomic fluorescence discussed in Chapter 7, because the wavelength of excitation is shorter than the emitted wavelengths. The beam of exciting X-rays is called the *primary* beam; the X-rays emitted from the sample are called *secondary* X-rays. The use of an X-ray source to produce secondary X-rays from a sample is the basis of XRF spectroscopy. The primary X-ray beam must have a $\lambda_{min}$ that is shorter than the absorption edge of the element to be excited.

#### *8.1.3.3 X-Ray Diffraction Process*

Crystals consist of atoms, ions, or molecules arranged in a regular, repeating 3D pattern called a crystal lattice. This knowledge came from the pioneering work of German physicist Max von Laue and the British physicists W.H. Bragg and W.L. Bragg. Max von Laue demonstrated in 1912 that a crystal would diffract X-rays, just as a ruled grating will diffract light of a wavelength close to the distance between the ruled lines on the grating. The fact that diffraction occurs indicates that the

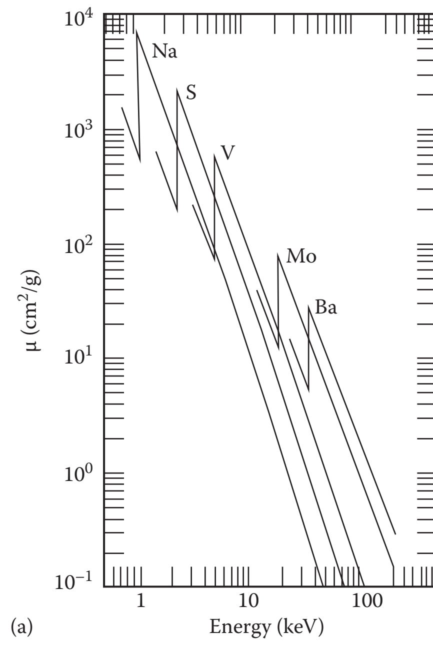


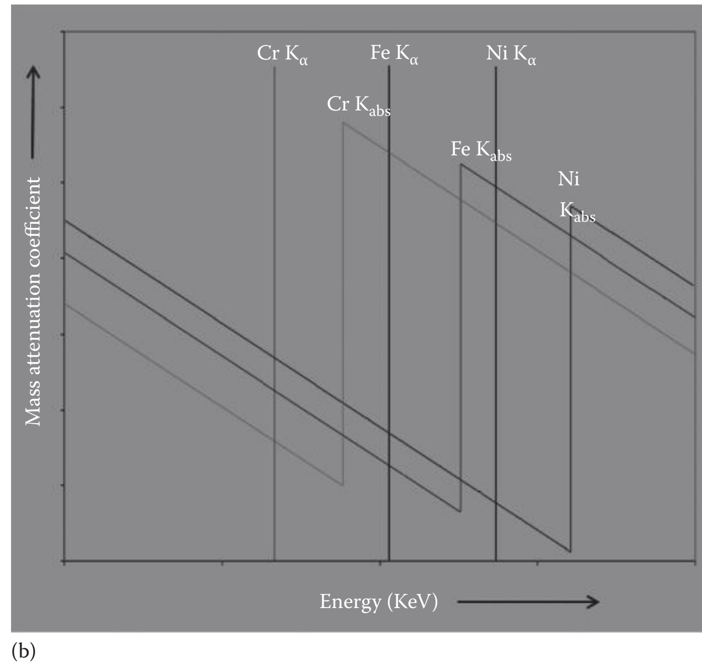


**Figure 8.6** (a) Energies of the K absorption edges for several pure elements. (Courtesy of ORTEC (Ametek). www.ortec-online.com; From Jenkins, R. et al., *Quantitative X-Ray Spectrometry*, Marcel Dekker, Inc., New York, 1981. Used with permission.) (b) Energies of the K absorption edge plotted schematically for the main elements in steel. (Courtesy of the University of Western Ontario XRF Short Course, London, Ontario, Canada.)

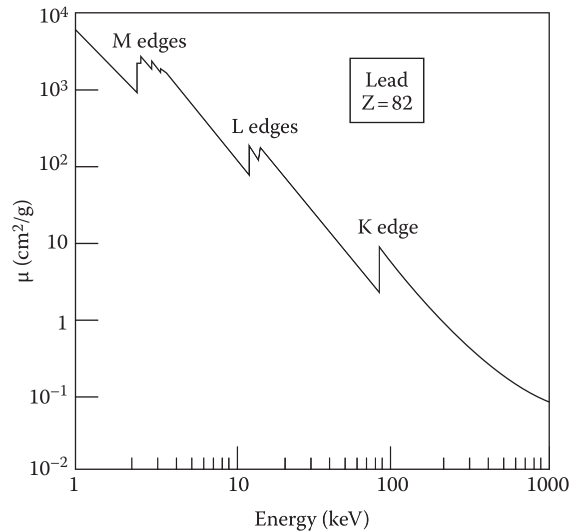


**Figure 8.7** The mass absorption coefficient for Pb as a function of energy. The K, L, and M absorption edges are seen. (Courtesy of ORTEC (Ametek). www.ortec-online.com; From Jenkins, R. et al., *Quantitative X-Ray Spectrometry*, Marcel Dekker, Inc., New York, 1981. Used with permission.)

atoms are arranged in an ordered pattern, with the spacing between the planes of atoms on the order of short-wavelength electromagnetic radiation in the X-ray region. The diffraction pattern could be used to measure the atomic spacing in crystals, allowing the determination of the exact arrangement in the crystal, the *crystal structure*. The Braggs used von Laue's discovery to determine the arrangement of atoms in several crystals and to develop a simple 2D model to explain XRD.

If the spacing between the planes of atoms is about the same as the wavelength of the radiation, an impinging beam of X-rays is reflected at each layer in the crystal, as shown in Figure 8.8. Assume that the X-rays falling on the crystal are parallel waves that strike the crystal surface at angle θ. That is, the waves O and O′ are in phase with each other and reinforce each other. In order for the waves to emerge as a reflected beam after scattering from atoms at points B and D, they must still be in phase with each other, that is, waves Y and X must still be parallel and coherent. If the waves are completely out of phase, their amplitudes cancel each other; they are said to interfere destructively and no beam emerges. In order to get reinforcement, it is necessary that the two waves stay in phase with each other after diffraction at the crystal planes.

It can be seen in Figure 8.8 that the lower wave travels an extra distance AB + BC compared with the upper wave. If AB + BC is a whole number of wavelengths, the emerging beams Y and X

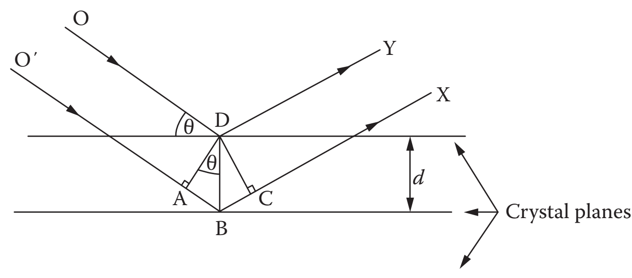


**Figure 8.8** Diffraction of X-rays by crystal planes.

will remain in phase and reinforcement will take place. From this deduction, we can calculate the relationship between the wavelengths of x-radiation, the distance $d$ between the lattice planes, and the angle at which a diffracted beam can emerge. We employ the following derivation.

X-ray waves O and O′ are parallel. The extra distance traveled by wave O′ in traveling through the crystal is AB + BC. For diffraction to occur, it is necessary that this distance be a whole number of wavelengths, $n$; that is,

$$\text{distance AB} + \text{BC} = n\lambda \tag{8.11}$$

but

$$\text{AB} + \text{BC} = 2\text{AB} \tag{8.12}$$

and

$$\text{AB} = \text{DB}\sin\theta \tag{8.13}$$

where θ is the angle of incidence of the X-ray beam with the crystal; therefore

$$\text{AB} = d\sin\theta \tag{8.14}$$

where $d$ is the distance between the crystal planes, called the interplanar distance. (Note from Figure 8.8 that $d$ = DB.)

Therefore

$$\text{AB} + \text{BC} = n\lambda = 2\text{AB} = 2d\sin\theta$$

or

$$n\lambda = 2d\sin\theta \tag{8.15}$$

The equation $n\lambda = 2d\sin\theta$ is known as the **Bragg equation**. The important result of this equation is that at any particular angle of incidence θ, only X-rays of a particular wavelength fulfill the requirement of staying in phase and being reinforced and are therefore diffracted by the crystal. Diffraction of X-rays by crystals forms the basis of XRD for crystal structure determination and is also the reason XRF spectrometry is possible, as will be seen.

## 8.2 X-RAY FLUORESCENCE

Instrumentation for X-ray spectrometry requires a source, a wavelength (or energy) selector, a detector, and beam conditioners. Component parts of the instrument are similar for XRF, XRD, and the other fields, but the optical system varies for each one. One major point to note is that some systems have the source located above the sample (the sample is faceup to the X-ray beam); other systems have the source located below the sample, with the sample facedown to the beam. There are advantages and disadvantages to both designs, as will be discussed later in this chapter.

Generally, we can distinguish between two main techniques in XRF, energy-dispersive XRF (EDXRF) and wavelength-dispersive XRF (WDXRF), as can be seen in Figure 8.9. EDXRF is based on a detector, which can discriminate the various photon energies and count them individually, whereas WDXRF is based on a set of analyzer crystals, which only diffract one energy/wavelength into a detector that counts all the photons. The subsequent instrumentation section will illustrate the components and setups used in today's commercially available instrumentation. EDXRF is sometimes called EDX or energy-dispersive spectroscopy (EDS). It must be stressed that

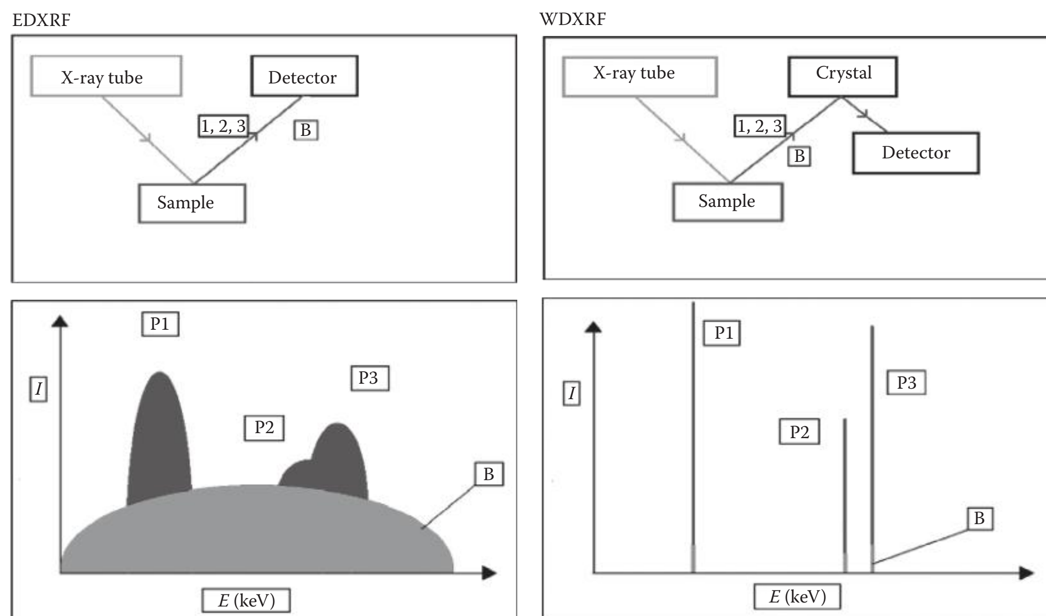


**Figure 8.9** Schematic comparison of EDXRF and WDXRF. The upper squares show the differences in instrument configuration, while the lower squares show the resulting spectra. B indicates the background radiation, while 1, 2, and 3 (P1, P2, P3) are photons of different energies.

all X-ray systems use ionizing radiation, which poses significant health hazards. X-ray systems of all types are regulated, and commercial systems have the proper shielding and safety interlocks to comply with regulatory requirements and prevent accidental exposure to radiation.

### 8.2.1 X-Ray Source

Three common methods of generating X-rays for analytical use in the laboratory or the field are

1. Use of a beam of high-energy electrons to produce a broadband *continuum* of x-radiation resulting from their deceleration upon impact with a metal target as well as element-specific X-ray *line* radiation by ejecting inner core electrons from the target metal atoms; this is the basis of the X-ray tube, the most common source used in XRD and XRF
2. Use of an X-ray beam of sufficient energy (the primary beam) to eject inner core electrons from a sample to produce a secondary X-ray beam (XRF)
3. Use of a radioactive isotope, which emits very-high-energy X-rays (also called gamma radiation) in its decay process

A fourth method of producing X-rays employs a massive, high-energy particle accelerator called a synchrotron. These are available at only a few locations around the world, such as the Brookhaven National Laboratory or the Stanford Accelerator Center in the United States, and are shared facilities servicing a large number of clients. X-rays may be generated when alpha particles or other heavy particles bombard a sample; this technique is called PIXE and requires a suitable accelerator facility. The use of an electron beam to generate X-rays from a microscopic sample as well as an image of the sample surface is the basis of X-ray microanalysis using an electron microprobe or scanning electron microscopy.

These different X-ray sources may produce either broadband (continuum) emission or narrow line emission, or both simultaneously, depending on how the source is operated. Figure 8.3

displays the simultaneous generation of both a broad continuum of X-ray energies with element-specific lines superposed upon it, obtained by bombarding rhodium metal with electrons in an **X-ray tube**.

#### *8.2.1.1 X-Ray Tube*

A schematic X-ray tube is depicted in Figure 8.10. The X-ray tube consists of an evacuated glass or ceramic envelope containing a wire filament cathode and a pure metal anode. A thin beryllium window sealed in the envelope allows X-rays to exit the tube. The envelope is encased in lead shielding and a heavy steel jacket with an opening over the window, to protect the tube. When a cathode (a negatively charged electrode) in the form of a metal wire is electrically heated by the passage of current, it gives off electrons, a process called thermionic emission. If a positively charged metallic electrode (called an anode) is placed near the cathode *in a vacuum*, the

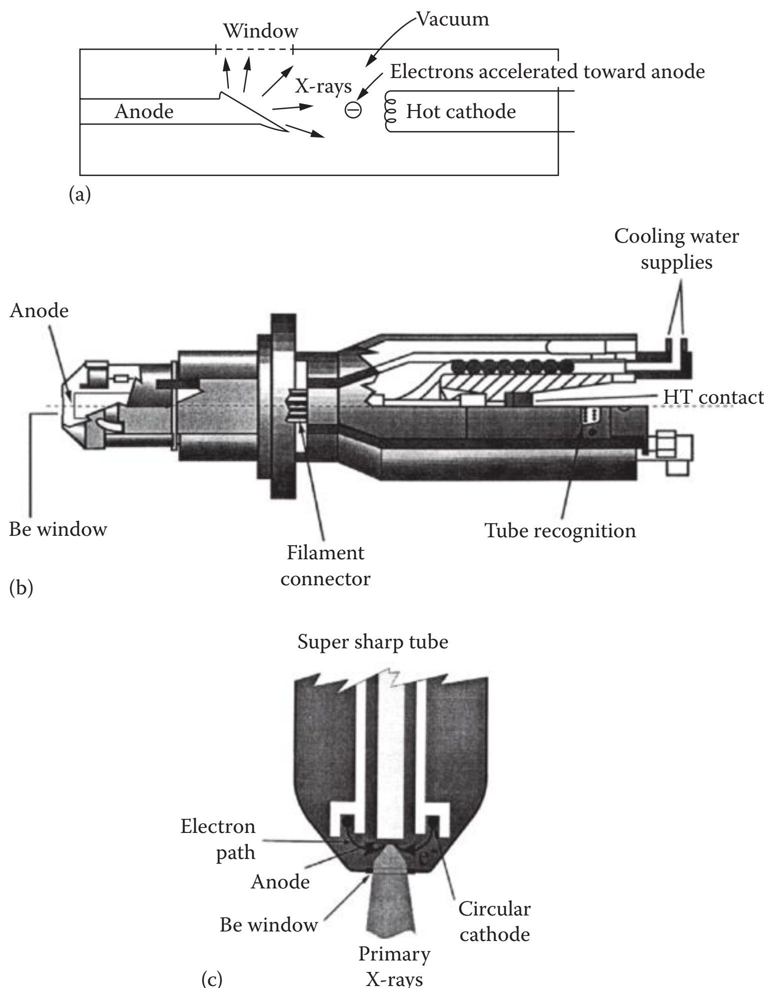


**Figure 8.10** (a) Schematic diagram of a side-window X-ray tube used for XRD. (b) Schematic of the 4.0 kW ceramic end-window X-ray tube, called the Super Sharp Tube™. (c) Close-up of the window end of the Super Sharp Tube, showing the circular cathode design of this tube. (b and c: Courtesy of PANalytical, Inc., The Netherlands, www.panalytical.com.).

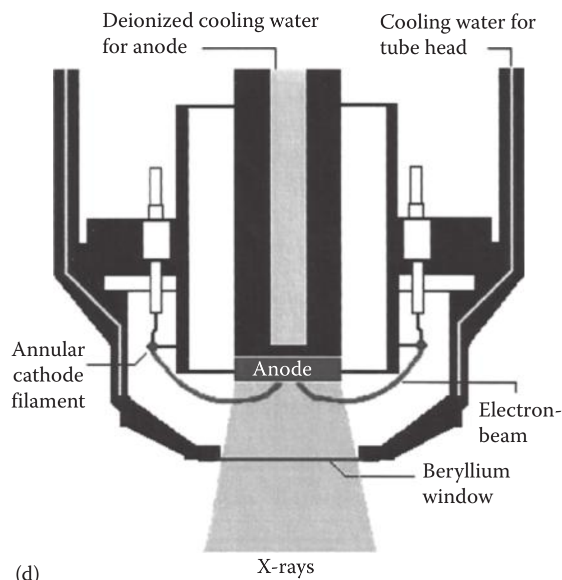


**Figure 8.10 (continued)** (d) Schematic side view of an end-window X-ray tube showing the Be window and cooling water. (© 2013 Bruker, Inc., www.bruker.com. Used with permission.)

negatively charged electrons will be accelerated toward the anode. Upon striking it, the electrons give up their energy at the metallic surface of the anode. If the electrons have been accelerated to a high enough velocity by a sufficiently high voltage between the cathode and anode, energy is released as radiation of short wavelength (0.1–100 Å), called x-radiation or X-rays. X-ray tubes are generally operated at voltage differentials of 2–100 kV between the wire filament cathode and the anode.

The cathode is normally a tungsten-based wire filament. The anode is called the target. The X-ray tube is named for the anode; a copper X-ray tube has a copper anode, a rhodium tube has a rhodium anode, a tungsten tube has a tungsten anode; all have tungsten-based wire cathodes. The target is usually not a solid metal but a copper slug coated with a layer of the desired target material. Numerous metals have been used as target materials, but common target elements are titanium, copper, chromium, molybdenum, rhodium, gold, silver, palladium, and tungsten. The target material determines the characteristic emission lines and affects the intensity of the continuum. The voltage between the anode and cathode determines how much energy the electrons in the beam acquire, and this in turn determines the overall intensity of the wide range of X-ray intensities in the continuum distribution and the maximum X-ray energy (shortest wavelength or $\lambda_{min}$, as shown by the Duane–Hunt law, Equation 8.7). Figure 8.11 shows how both the intensity of the continuum radiation and the short-wavelength/high-energy cutoff vary as the applied voltage to this silver (Ag) X-ray tube varies. This illustration also shows that the Ag L line emission varies as a function of the excitation.

In choosing the element to be used for the target, it should be remembered that it is necessary for the energy of the X-rays emitted by the source to be greater than that required to excite the element being irradiated in an XRF analysis. As a simple rule of thumb, the target element of the source should have a greater atomic number than the elements being examined in the sample. This ensures that the energy of radiation is more than sufficient to cause the sample element to fluoresce. This is not a requirement in X-ray absorption or XRD, where excitation of the analyte atoms is not necessary. In XRD, the target is chosen to avoid the excitation of characteristic X-ray (XRF)

emissions from the sample. For example, copper (Cu) target-based XRD units can excite the iron (Fe) commonly found in geological samples, and the fluorescence from the sample will increase the background of the measurement. Using a cobalt (Co) target will avoid this.

In many high-power (>200 W) X-ray tube designs, the anode, or target, gets very hot in use because it is exposed to a constant stream of high-energy electrons, with most of the energy being dissipated as heat on collision. This problem is overcome by water-cooling the anode. Modern low-power and compact X-ray tubes have been designed to operate at lower voltages and do not require any liquid-based cooling of the anode.

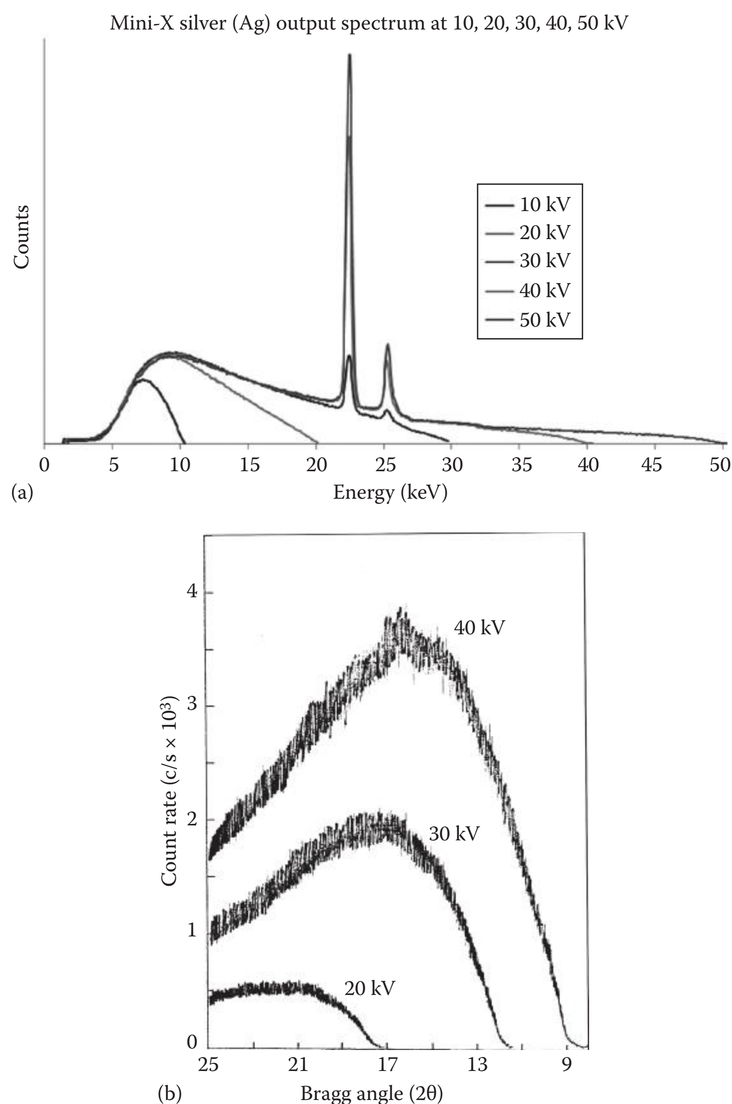


**Figure 8.11** (a) Amptek Mini-X silver output spectrum at various voltages. Ten kV starts on the left side of the diagram; the curves increase in voltage moving from left to right. Below 30 kV, only continuum radiation is seen. The high-energy cutoff increases as the voltage increases, and the Ag L line emission intensity increases with voltage. (Courtesy of Amptek, Inc., Bedford, MA, www.amptek.com.) (b) The intensity of the continuum radiation from an X-ray tube and the short-wavelength cutoff vary as the applied voltage varies. This plot is of a tungsten X-ray tube.

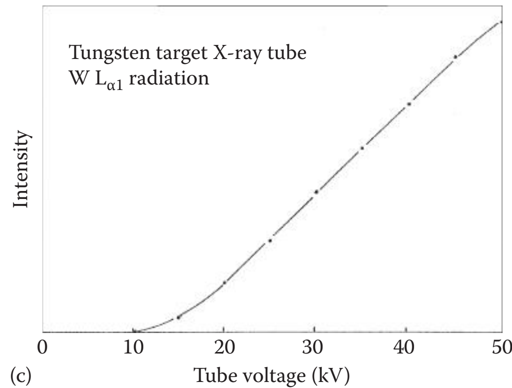


**Figure 8.11 (continued)** (c) The characteristic radiation from an X-ray tube also varies as the applied voltage varies. Below 20 kV, the intensity of the tungsten $L_{\alpha_1}$ line is very low. The intensity of this characteristic line increases as the applied voltage increases.

The exit window of the X-ray tube is usually made of beryllium, which is essentially transparent to X-rays. The Be window is thin, generally 0.3–0.5 mm thick, and is very fragile. The window may be on the side of the tube, as shown in Figure 8.10a, or in the end of the tube (Figure 8.10b through d). Side-window tubes are common, but end-window tubes permit the use of a thinner beryllium window. This makes end-window tubes good for low-energy X-ray excitation by improving the low-energy output of the tube. To minimize the tube size, a transmission target can be used. The target is a layer of the target element on the beryllium window. For example, a silver transmission target can be constructed from a 0.75 μm thick layer of Ag on a 127 μm thick Be window. Figure 8.12 shows both the schematic of a side and transmission target rhodium X-ray tube.

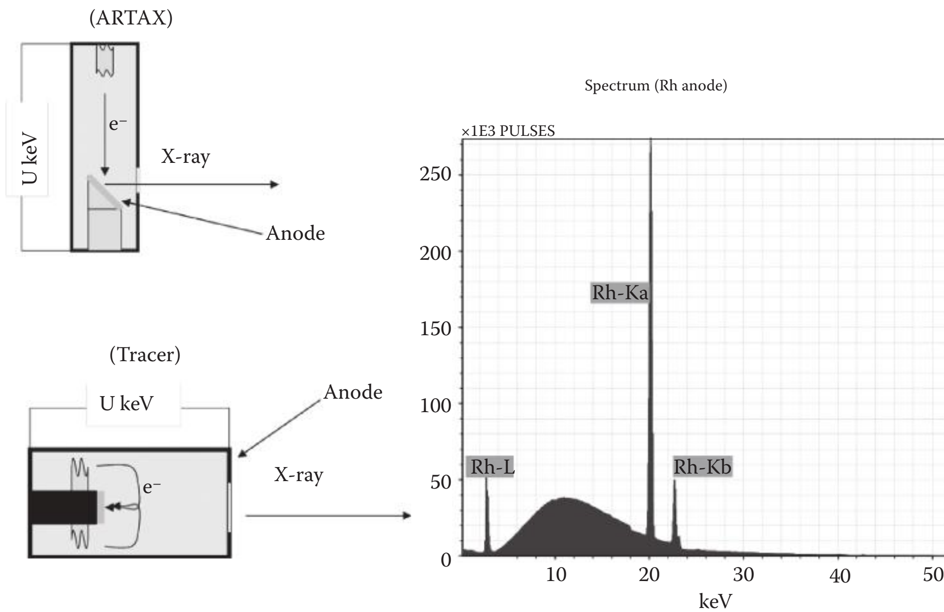


**Figure 8.12** Schematic diagrams of a Rh target side-window tube (ARTAX system) and a modern handheld transmission target design (TRACER system). (Courtesy of Roald Tagle, BRUKER NANO GmbH, Berlin, Germany. © 2013 Bruker, Inc. Used with permission.)

X-ray tubes must provide adequate intensity over a relatively wide spectral range for XRF in order to excite a reasonable number of elements. In some applications, monochromatic or nearly monochromatic X-rays are desired; that is accomplished by using filters or a monochromator as described later or by using a secondary fluorescent source, described subsequently. The tube output must be stable over short time periods for the highest precision and over long time periods for accuracy without frequent recalibration. The X-ray emission lines from the anode element must not interfere with the sample spectrum. Tube lines can be scattered into the detector and be mistaken for an element present in the sample.

#### *8.2.1.2 Secondary XRF Sources*

If it is necessary to prevent the continuum emission from an X-ray tube from scattering on a sample, a standard tube can be used to excite another pure metal target. The resulting XRF from the secondary target is used as the source of X-ray excitation for the sample. Such an example is shown in Figure 8.13. A standard tungsten X-ray tube is used to produce the emission spectrum on the left, with the tungsten characteristic lines superimposed on the continuum radiation. The radiation from this tube is used to strike a secondary pure copper target. The resulting emission from the copper is the copper XRF spectrum on the right.

This source emits very little or no continuum radiation but does emit quite strongly at the copper K and L lines. Of course, the metal used in the target of the first source must have a higher atomic number than copper to generate fluorescence. The Cu lines then can be used as an excitation source, although the intensity of the secondary source is much less than that of a Cu X-ray tube. However,

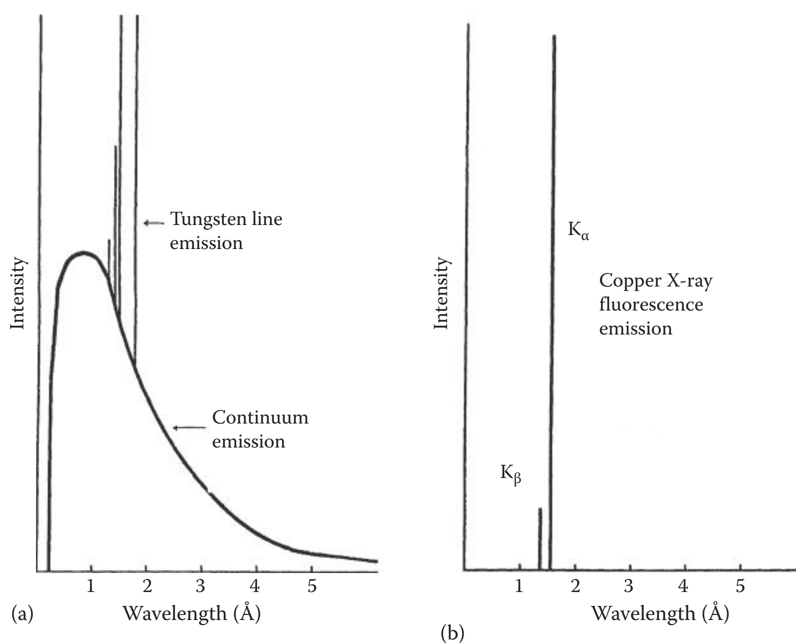


**Figure 8.13** (a) The primary X-ray emission from a tungsten target. (b) The secondary emission from a copper target. Note the removal of the continuum radiation and the nearly monochromatic output from the secondary target. (From Parsons, M.L., X-ray methods, in Ewing, G.W. (ed.), *Analytical Instrumentation Handbook*, 2nd edn., Marcel Dekker, Inc., New York, 1997. Used with permission.)

**Table 8.4 Characteristics of Radioisotope Sources for XRF Spectrometry**

| Isotope | Primary Decay Mode | Half-Life (Years) | Useful Photon Energies Emitted | % Theoretical Yield (Photons per 100 Decay Transformations) | Typical Activity (mCi) |
|---|---|---|---|---|---|
| $^{55}Fe$ | EC | 2.7 | 5.9, 6.4 keV Mn K X-rays | 28.5 | 5–100 |
| $^{109}Cd$ | EC | 1.3 | 22.2–25.5 keV Ag K X-rays | 102 | 0.5–100 |
| | | | 88.2 keV γ-ray | 4 | |
| $^{241}Am$ | Alpha | 458 | 14–21 keV Np L X-rays | 37 | 1–50 |
| | | | 59.6 keV γ-ray | 36 | |
| $^{57}Co$ | EC | 0.74 | 6.4, 7.1 keV Fe K X-rays | 51 | 1 |
| | | | 14.4 keV γ-ray | 8.2 | |
| | | | 122 keV γ-ray | 88.9 | |
| | | | 136 keV γ-ray | 8.8 | |
| $^{3}H$[a] | Beta | 12.3 | Bremsstrahlung source, endpoint at 18.6 keV | | 3000–5000 |
| $^{147}Pm$ | Beta | 2.6 | Bremsstrahlung source, endpoint at 225 keV | | 500 |

*Source:* Table from Jenkins, R. et al., *Quantitative X-Ray Spectrometry*, Marcel Dekker, Inc., New York, 1981. Used with permission.

[a] Radioactive tritium gas is adsorbed on nonradioactive metal foil, such as titanium foil.

when monochromatic or nearly monochromatic radiation is required, the loss of intensity is more than offset by the low background from the secondary source.

#### *8.2.1.3 Radioisotope Sources*

X-radiation is a product of radioactive decay of certain isotopes. The term gamma ray is often used for an X-ray resulting from such a decay process. Alpha and beta decay and electron capture (EC) processes can result in the release of gamma rays. Table 8.4 lists some common radioisotopes used as XRF sources.

The advantages of radioisotope sources are that they are small, rugged, and portable and do not require a power supply. They are ideal for obtaining XRF spectra from large samples or field measurements while not requiring any power, enabling small compact units with long operation times. Examples include the analysis of bulky objects that cannot have pieces cut from them, such as aircraft engines, ship hulls, and art objects. The disadvantage is that the intensity of these sources is weak compared with that of an X-ray tube, the source cannot be optimized by changing voltage as can be done with an X-ray tube, and the source intensity decreases with time depending on the half-life of the source. In addition, the source cannot be turned off. This requires care on the part of the analyst to avoid exposure to the ever-present ionizing radiation. Isotope sources are more regulated than tube-based sources, and although isotope sources are convenient for portable XRF systems, tube-based portable and handheld devices are more common. Isotope source uses are currently limited to K line excitation approaches as well as for economical dedicated analyzers, such as for Pb in paint.

### 8.2.2 Instrumentation for Energy Dispersive X-Ray Spectrometry

In EDXRF spectrometry, there is no physical separation of the fluorescence radiation from the sample. There is no dispersing device prior to the detector. All the photons of all energies arrive at the detector simultaneously. Any EDXRF is designed around the following components—a source of primary excitation, a sample holder, and a detector, seen in Figure 8.14.

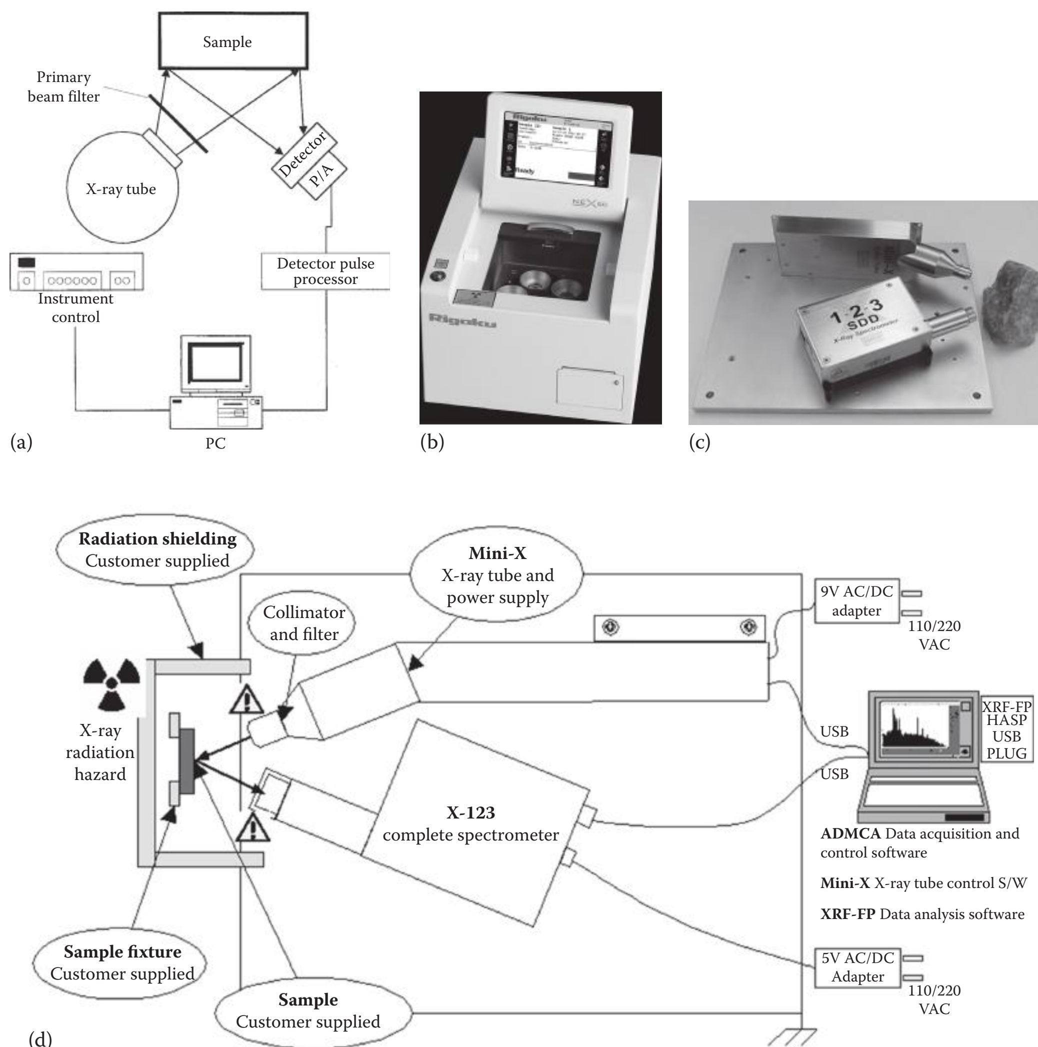


**Figure 8.14** (a) A schematic EDXRF system with an X-ray tube source. There is no dispersion device between the sample and the detector. Photons of all energies are collected simultaneously. (From Ellis, A.T., in Van Griekin, R.E.; Markowicz, A.A. (eds.), *Handbook of X-Ray Spectrometry*, 2nd edn., Marcel Dekker, Inc.: New York, 2002. Used with permission.) (b) A commercial benchtop EDXRF spectrometer, the Rigaku NEX QC, setup to measure sulfur in crude oil. (Courtesy of Applied Rigaku Technologies, Inc., Austin, TX, www.rigakuedxrf.com.) (c) Component-based compact XRF kit, showing relative positions of the X-ray tube (top), the sample (right), and the X-ray spectrometer (bottom). (d) The compact component kit as part of a complete XRF system. (c and d: Courtesy of AMPTEK, Inc. www.amptek.com.)

All EDXRF systems are able to modify the primary signal to control the excitation of the sample. This is achieved by different means, which result in three groups of systems: direct excitation, secondary or 3D excitation, and total reflectance XRF (TXRF).

In direct excitation systems, the source is directed toward the sample thus exciting the sample directly with the radiation from the target or isotope source (Figure 8.15). To modify the excitation or attenuate undesired parts of the excitation spectra, primary beam filters are used. To reduce the spot size and enable "micro" spot analysis, pinhole masks are in use as well. For micro spots below

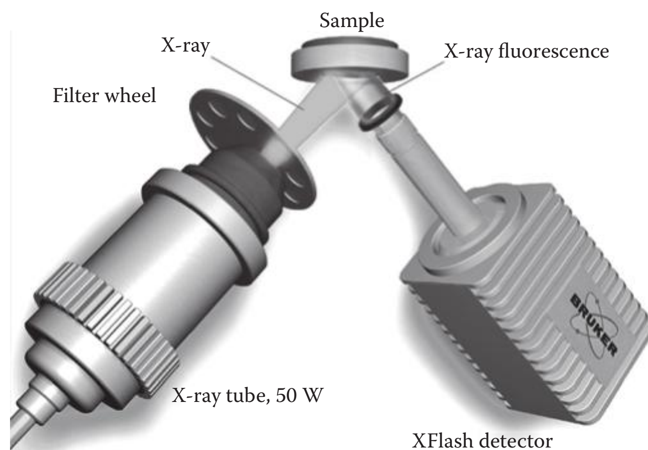


**Figure 8.15** Schematic 3D view of a direct excitation EDXRF system. (© 2013 Bruker, Inc. www.bruker.com. Used with permission.)

100 μm in certain units, capillary optics are used. Typical direct excitation units are all handheld units, isotope-based units, the majority of low-power and medium-power benchtop EDXRF systems, as well as the micro-XRF and dedicated plating thickness XRF units.

In secondary excitation units, the source is used to illuminate a selectable secondary target, which is made of specific material to either scatter the beam or to act as a new "source." The geometric arrangement is such that the signal from the secondary target illuminates the sample and also ensures that the X-ray beam is polarized (Figure 8.16).

TXRF systems use a secondary target and the principle of Bragg diffraction to create a more monochromatic beam. This beam is directed at very low incident angle to the sample to achieve "total reflectance." The signal from the sample, which has to be prepared as very thin film or

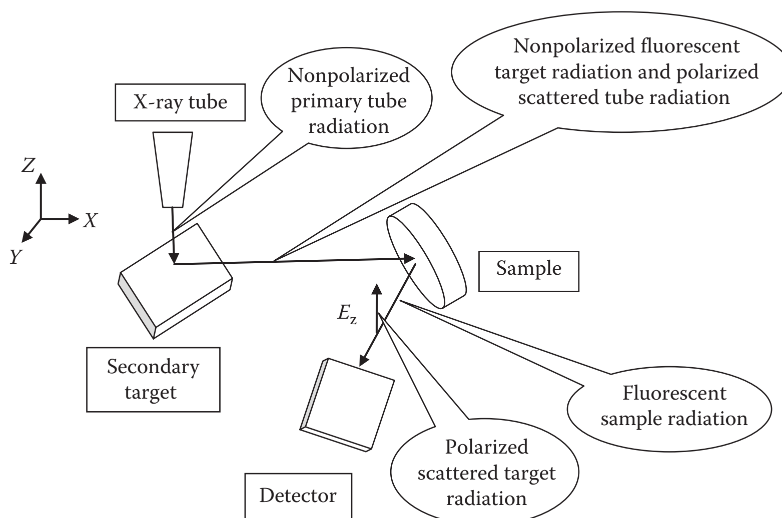


**Figure 8.16** Schematic drawing of a 3D beam of a secondary target EDXRF system. (Modified from a diagram provided by Bruno Vrebos, 2009, PANaltyical Inc., The Netherlands. www.panalytical.com.)

(a)

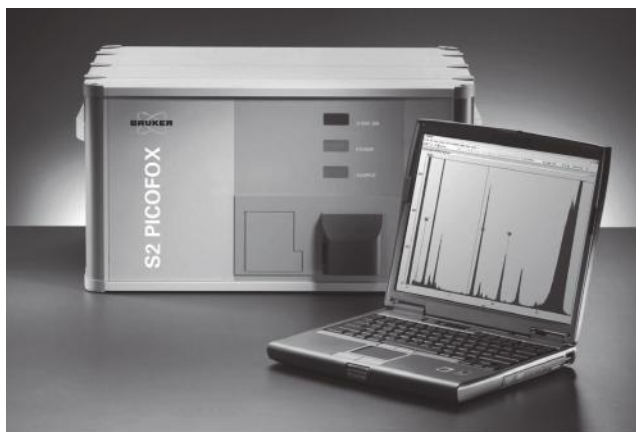


(b)

**Figure 8.17** (a) Schematic drawing of a TXRF system. From left to right is the X-ray source, the synthetic multilayer monochromator (Section 8.2.3.2), the thin sample on a support, the silicon drift detector (SDD) above the sample, and finally a beam stop. (b) A commercial TXRF spectrometer, the Bruker S2 PICOFOX with its laptop computer. The displayed spectrum shows the high S/N ratio. (© 2013 Bruker, Inc. www.bruker.com. Used with permission.)

micropowder, will exhibit a very low background and thus an excellent signal-to-noise ratio. These systems are quite compact, as seen in Figure 8.17b.

#### *8.2.2.1 Excitation Source*

Most tubes in EDXRF systems are end-window or transmission target designs. For secondary target and mobile XRF units, side-window tubes are used. Tube voltage and excitation is limited to usually 50 or 60 kV for handheld, portable, and benchtop devices. High voltages (≥100 kV) require more shielding and therefore require large floor units.

#### *8.2.2.2 Primary Beam Modifiers*

Primary beam filters, beam masks, and other devices are used to modify the excitation from the source. One of the problems with using an X-ray tube is that both continuum and characteristic line radiation are generated at certain operating voltages, as seen in Figure 8.3. For many analytical uses, only one type of radiation is desired. Filters of various materials can be used to absorb unwanted radiation but permit radiation of the desired wavelength to pass by placing the filter between the X-ray source and the sample.

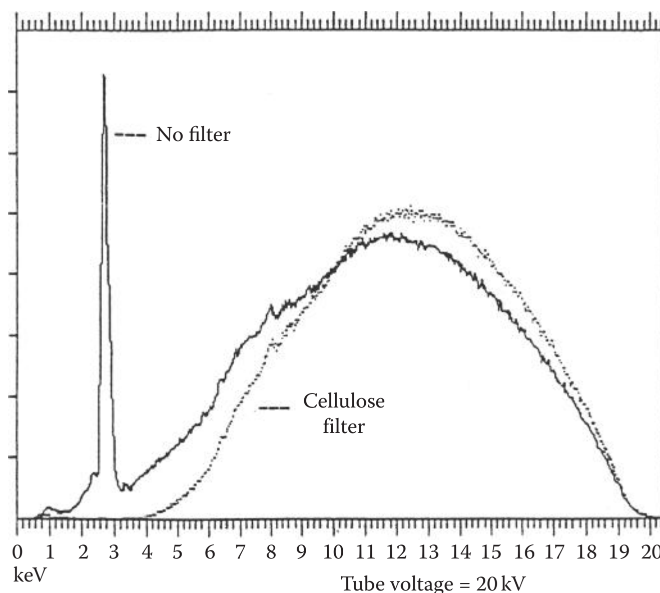


**Figure 8.18** The use of a filter to remove unwanted radiation from entering the spectrometer is demonstrated. A cellulose filter placed between a Rh X-ray tube and the sample removes the Rh $L_\alpha$ line at 2.69 keV and allows only the continuum radiation to excite the sample. (© Thermo Fisher Scientific. www.thermofisher.com. Used with permission.)

Primary beam filters are used to modify the excitation spectra by making use of characteristic, selective absorption. The nature of the material and thickness of the material are the parameters used to tune the primary excitation. Filters are customized based upon the target material and application. Manual filters are inserted by the user into the beam path whereas automatic filters are generally arranged in a wheel-like fashion and controlled by the instrument software (see Figure 8.15).

A simple example of how a filter is used is shown in Figure 8.18. The solid line spectrum is the output of a Rh tube operated at 20 kV with no filter between the tube and the detector. The Rh $L_\alpha$ line at 2.69 keV is seen, along with a broad continuum of X-rays from 4 to 19 keV. If the Rh $L_\alpha$ line gets scattered into the detector, as it can from a crystalline sample, it can be mistaken for an element in the sample or may overlap another line, causing spectral interference. Placing a cellulose filter over the tube window causes the low-energy Rh characteristic line to be absorbed; only the continuum radiation reaches the detector, as shown by the dotted line spectrum.

Alternatively, when monochromatic radiation is desired, a filter is chosen with its absorption edge between the $K_\alpha$ and the $K_\beta$ emission lines of the target element or between the continuum and the characteristic emission lines of the target. Using an Al filter in front of a silver X-ray tube removes most of the continuum radiation (Bremsstrahlung) between 5 and 15 keV; the light reaching the sample is essentially the characteristic line or lines of the target (Figure 8.19a). As seen in Figure 8.19b, using the correct filter greatly improves the signal-to-background ratio of the sample spectrum, which will reduce uncertainty in the measurement of these lines and improve quantitative analysis.

Filters are commonly thin metal foils, usually pure elements, but some alloys such as brass and materials like cellulose are used. Varying the foil thickness of a filter is used to optimize peak-to-background ratios. Commonly used filters for various targets are listed in Tables 8.5 and 8.6.

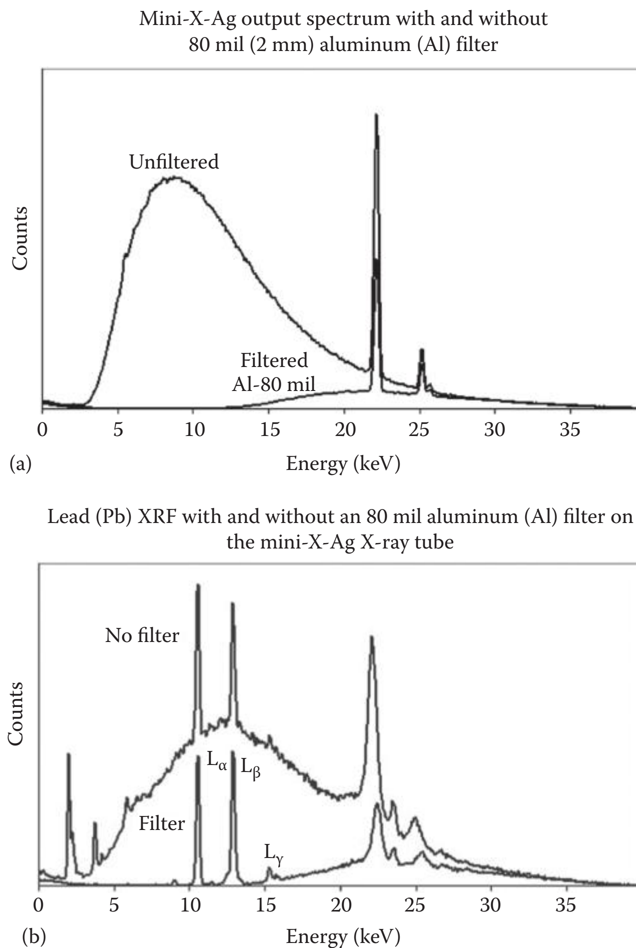


**Figure 8.19** (a) Output spectra of the mini-X silver X-ray tube at 40 kV unfiltered and filtered with 2 mm Al. The filter removes the majority of the continuum radiation. (b) A Pb sample analyzed with and without a filter on the Ag X-ray tube. With no filter, the Pb characteristic X-rays are superimposed on a large background of scattered X-rays. With the Al filter, the signal-to-background ratio for Pb is greatly improved. Note that the Pb $L_\gamma$ is much more visible in the filtered spectrum. (Courtesy of Amptek, Inc. www.amptek.com.)

Applications of primary beam filters include

- Attenuation or suppression of the characteristic tube lines (e.g., Rh $K_\alpha$) to enable analysis for the target element or neighboring elements (Cd, Ag)
- Attenuation of elemental ranges (e.g., removal of all energies below 10 kV)
- Optimization of signal-to-noise (signal-to-background) levels
- Use as “secondary” targets to emit the target radiation in addition to the nonabsorbed source radiation

In addition, the primary beam filter units can be equipped with a beam-reducing device referred to as a mask or pinhole collimator. The device is based on the complete absorption of the primary beam except what passes through the opening. The smaller the reduced beam diameter, the more signal is being eliminated, thus reducing the signal from the sample. Units with small spot capability therefore are usually higher power (e.g., 50 W) to compensate for the decreased signal.

**Table 8.5 Filters for Commonly Available X-Ray Tubes**

| Target | Target $K_\alpha$ (Å) | Target $K_\beta$ (Å) | Filter Element | Filter K Edge (Å) | Foil Thickness (μm) | % $K_\beta$ Absorbed |
|---|---|---|---|---|---|---|
| Cr | 2.289 | 2.085 | V | 2.269 | 15.3 | 99.0 |
| Fe | 1.936 | 1.757 | Mn | 1.896 | 12.1 | 98.7 |
| Co | 1.789 | 1.621 | Fe | 1.743 | 14.7 | 98.9 |
| Ni | 1.658 | 1.500 | Co | 1.608 | 14.3 | 98.4 |
| Cu | 1.541 | 1.393 | Ni | 1.488 | 15.8 | 97.9 |
| Mo | 0.709 | 0.632 | Zr | 0.689 | 63.0 | 96.3 |
| Ag | 0.559 | 0.497 | Pd | 0.509 | 41.3 | 94.6 |
| W | 0.209 | 0.185 | | | | |

*Source:* From Parsons, M.L., X-ray methods, in Ewing, G.W. (ed.), *Analytical Instrumentation Handbook*, 2nd edn., Marcel Dekker, Inc., New York, 1997. Used with permission.
*Note:* No suitable filter is available for tungsten.

**Table 8.6 Typical Primary Beam Filters and Range of Use in EDXRF Systems**

| Filter | Thickness (μm) | X-Ray Tube Range (kV) | Elements | Comments |
|---|---|---|---|---|
| None | | 4–50 | Na–Ca | Optimum for light elements, 4–8 kV excitation[a] |
| Cellulose | | 5–10 | Si–Ti | Suppresses tube L lines (see Figure 8.16)[a] |
| Al, thin | 25–75 | 8–12 | S–V | Removes tube L lines[a] |
| Al, thick | 75–200 | 10–20 | Ca–Cu | Used for transition elements |
| Anode element, thin | 25–75 | 25–40 | Ca–Mo | Good for trace analysis[b] |
| Anode element, thick | 100–150 | 40–50 | Cu–Mo | Trace analysis with heavy element L lines[b] |
| Cu | 200–500 | 50 | >Fe | Suppresses tube K lines |

*Source:* Modified from Ellis, A.T., in Van Griekin, R.E.; Markowicz, A.A. (eds.), *Handbook of X-Ray Spectrometry*, 2nd edn., Marcel Dekker, Inc.: New York, 2002. With permission.
[a] He purge or vacuum path needed to avoid attenuation of low-energy lines.
[b] Serves as a secondary fluorescence source, also called a monochromatizing filter; preferentially transmits tube K lines.

Beam restrictors and concentrators using capillary optics concentrate the beam on a small spot without the loss of signal from masks. Commercial units can achieve spot sizes of 25 μm with suitable intensity. Masks and beam restrictors are used to observe microscopic regions within a sample and, using raster techniques, can provide elemental image maps of samples that are heterogeneous.

#### *8.2.2.3 Sample Holders*

XRF is used for the analysis of solid and liquid samples, and similar sample holders and autosamplers are used for both EDXRF and WDXRF. Sample preparation and other considerations will be discussed in the applications section. For quantitative analysis, the surface of the sample must be as flat as possible, as will be discussed in the applications section. There are two classes of sample holders: cassettes for bulk solid samples and cells for loose powders, small drillings, and liquids. A typical cassette for a flat bulk solid such as a polished metal disk, a pressed powder disk, and a glass or polymer flat is shown in Figure 8.20a. The cassette is a metal cylinder, with a

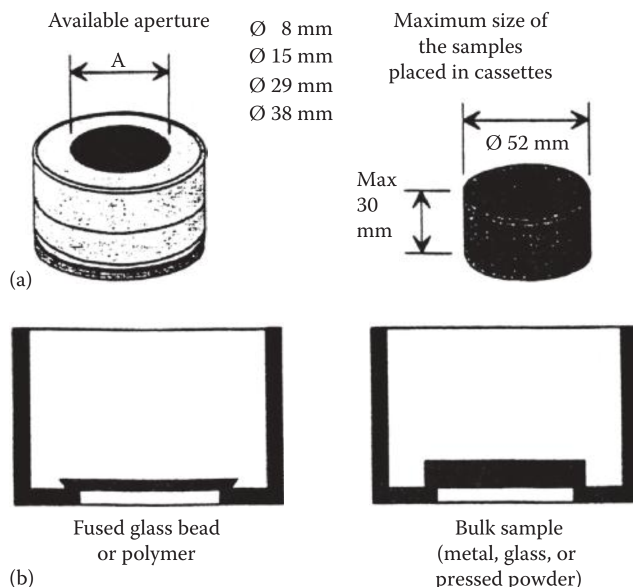


**Figure 8.20** (a) Sample cassette for bulk solid samples. (b) Position of a bulk solid in the facedown configuration used in many spectrometers. (© Thermo Fisher Scientific. www.thermofisher.com. Used with permission.)

screw top and a circular opening or aperture, where the sample will be exposed to the X-ray beam. The maximum size for a bulk sample is shown. The sample is placed in the cassette. For a system where the sample is analyzed facedown, the cassette is placed with the opening down and the bulk sample sits in the holder held in position by gravity, as shown in Figure 8.20b. If the system requires the sample faceup, the body of the cassette must be filled with an inert support (often a block of wood) to press the sample surface against the opening. These cassettes are available with a variety of apertures, usually from 8 to 38 mm in diameter, to accommodate samples of different diameters. Other types of solid samples, such coatings on a solid substrate, can be placed directly in this type of cassette.

The analysis of liquids, loose powders, or small pieces requires a different holder. The cells for these types of samples are multipart plastic holders, shown in Figure 8.21a, and require squares or circles of thin polymer film to hold the sample in the cell. The body of the cell is a cylinder open on both ends. One end of the cylinder is covered with the plastic film (or even clear plastic adhesive tape), and the film or tape is clamped into place by a plastic ring. The cell is placed with the film down, and the sample of liquid, powder, or filings is added. The film surface should be completely covered, as uniformly as possible. A plastic disk that just fits into the cell is inserted and pressed against the sample to obtain as flat a surface as possible, and a top cap is screwed or pressed on. For liquid samples, a vented top is used to avoid pressure buildup from heating of the sample by the X-ray beam. This assembled cell may be used "as is" or may be inserted into a standard cassette, as shown in Figure 8.21b in a facedown configuration. As you can imagine, if the thin polymer film breaks, samples of loose powder, chips, or liquid will spill into the interior of the spectrometer, contaminating the system and possibly breaking the Be window of the X-ray tube, if the tube is below the sample. It is for this reason that liquid sample cells are vented and a vacuum not used. This is the main disadvantage of the facedown configuration; for anything other than bulk samples, there is a risk of contaminating the instrument if the film covering the sample ruptures. Figure 8.21b shows that in the facedown configuration, a liquid

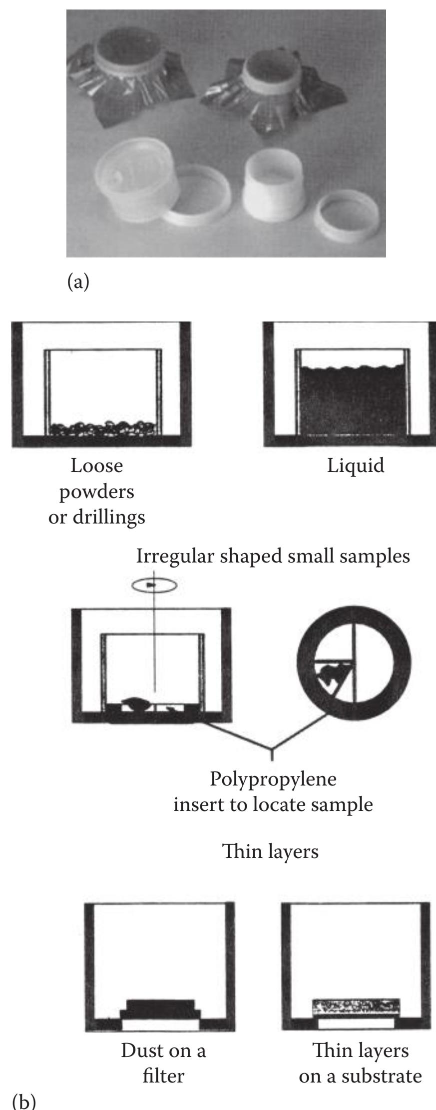


**Figure 8.21** Cells for liquid samples, loose powders, and chips. (a) Two types of disposable polyethylene sample cups for liquids and loose samples, consisting of a cup and snap ring to hold the polymer film cover. The cells with polymer film in place are shown at the top of the photograph. The disassembled cup and ring pieces are shown at the bottom of the photograph. (Courtesy of SPEX Certiprep, Inc. Metuchen, NJ. www.spexcsp.com.) (b) Liquid and other loose samples in cells such as those shown in the photo, and then inserted into a sample cassette of the type shown in (a) for a facedown configuration spectrometer. As shown, dust sampled on impact filters or thin-layer samples may be inserted directly into the sample cassette. (© Thermo Fisher Scientific, www.thermofisher.com. Used with permission.)

naturally assumes a flat surface. Imagine what the liquid sample would look like faceup. An air bubble will form at the film surface if a sealed cell is used and not filled completely. A bubble may form at the surface by heating of the sample in the X-ray beam if the cell is filled completely. If this occurs, the intensity of XRF from the sample will drop dramatically, and the possibility of film rupture as the pressure in the cell builds increases dramatically. So, if liquid samples

must be analyzed, the facedown configuration gives better quantitative results, even at the risk of contaminating the spectrometer.

The sample cassette is moved into position, either manually or with an automatic sample changer. In position, the sample is spun, generally at about 30 rpm, to homogenize the surface presented to the X-ray beam.

Polymer films used to cover the cell opening must be low in trace element impurities, strong enough to hold the sample without breaking, thermally stable, and chemically inert. They certainly must not be soluble in any liquid samples to be analyzed. Films of polyester (Mylar®), polyimide (Kapton®), polycarbonate, polypropylene, and fluoropolymer (Teflon®) are commonly used, with film thickness ranging about 3–8 μm. Films of different composition and thickness transmit X-rays to varying degrees (Figure 8.22), and the film chosen must transmit the wavelengths for the elements to be measured in the sample.

Manual XRF units are designed for the operator to place the sample into the measurement position, and this is done one sample at a time. Manual systems also include handheld XRF (HH XRF) analyzers, where the sample is pressed against the unit's "nose," with no sample holder (or preparation). The sample position and beam path from source to sample and detector accommodate different atmospheres, including vacuum, helium, nitrogen, and air.

Portable and handheld units can accommodate either vacuum or helium purges in their instrument nose. Sample changers or autosamplers are used to enable units to operate unattended, and the number of samples in the autosampler varies with instrument make and model.

Random access sample changers are more complex than standard autosamplers and allow the operator to add and remove samples while the unit is analyzing another sample in the measurement position. Batch sample changers are usually based on a circular tray or a conveyer belt with multiple sample positions. Samples are rotated or moved over the measurement position. This design does not allow a sample change while the measurement sequence is started since it is connected to an interlock and/or purged with the user-selected atmosphere. This design though is technically less complex and can be used for small units.

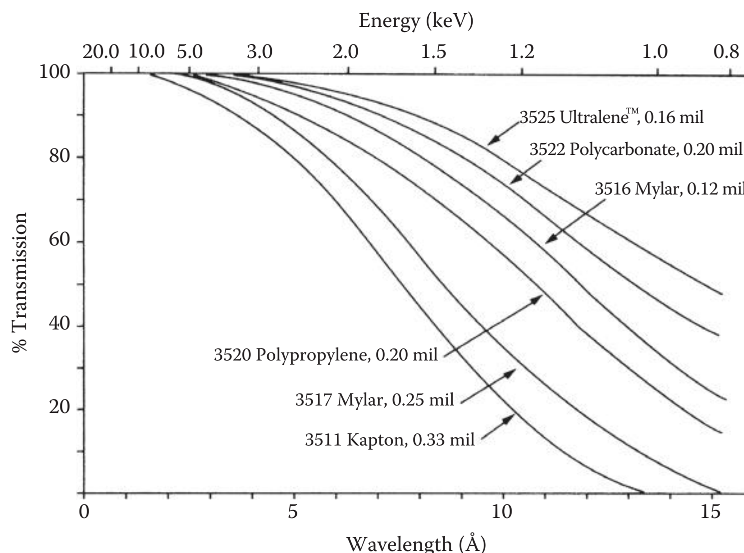


**Figure 8.22** The X-ray transmission characteristics of some thin polymer films used as sample holder covers for liquid, loose powder, and similar samples. (Courtesy of SPEX Certiprep, Inc., Metuchen, NJ. www.spexcsp.com.)

### 8.2.2.4 EDXRF Detectors

The detector is the most crucial component of the EDXRF unit since it detects and sorts the incoming photons originating from the sample. The detector type and associated electronics determine the performance with respect to count rate, resolution, and detection efficiency.

The count rate is the total of *all* photons detected and counted by the detector over the energy range being detected.

Two type of detectors are used in commercially available units: proportional detectors and semiconductor detectors such as silicon PIN, Si(Li), Ge(Li), and silicon drift detectors. The detectors used in EDXRF have very high intrinsic energy resolution. In these systems, the detector resolves the spectrum. The signal pulses are collected, integrated, and displayed by a multichannel analyzer (MCA).

*Semiconductor detectors*. When an X-ray falls on a solid-state semiconductor, it generates an electron ($e^-$) and a hole ($e^+$). Based on this phenomenon, semiconductor detectors have been developed and are now of prime importance in EDXRF and scanning electron microscopy. The total ionization caused by an X-ray photon striking the detector is proportional to the energy of the incident photon. A formerly common semiconductor detector for laboratory EDXRF systems was the *lithium-drifted silicon diode*, represented as Si(Li) and called a "silly" detector. A schematic diagram of a silicon lithium-drifted detector is shown in Figure 8.23.

A cylindrical piece of pure, single-crystal silicon is used. The size of this piece is 4–19 mm in diameter and 3–5 mm thick. The density of free electrons in the silicon is very low, constituting a p-type semiconductor. If the density of free electrons is high in a semiconductor, then we have an n-type semiconductor. Semiconductor diode detectors always operate with a combination of these two types.

The diode is made by plating lithium onto one end of the silicon. The lithium is drifted into, that is diffused into, the silicon crystal by an applied voltage. The high concentration of Li at the one end creates an n-type region. In the diffusion process, all electron acceptors are neutralized in the bulk of the crystal, which becomes highly nonconducting. This is the *intrinsic* material. The lithium drifting is stopped before reaching the other end of the silicon crystal, leaving a region of pure Si (p-type), as shown in Figure 8.23. Submicron gold layers are applied at each end as electrical contacts. The detector is reverse-biased, removing any free charge carriers from the intrinsic region. Under this condition, no current should flow since there are no charge carriers in the intrinsic region. However, the bandgap between the valence band and the conduction band is small, only 1.1 eV for Si(Li). At room temperature, thermally generated charge carriers cross this barrier easily and become conductive even with no X-ray photons striking the detector. This causes a high noise level. To decrease this noise and increase the sensitivity of the detector, the temperature of the system must be decreased significantly. This is accomplished by cooling the detector to 77 K with liquid nitrogen, which must be replenished regularly. Peltier effect-based electronic cooling is used with temperatures of as low as −90°C on benchtop EDXRF units. A Peltier cooling device, also known as a thermoelectric cooling device, uses the Peltier effect to create a heat flux between the junction of two different materials. A Peltier cooler is a solid-state heat pump, which transfers heat from one side of the device to the other, depending on the direction of the electric current. The solid-state nature of the cooler means no moving parts, compact size, and no maintenance. These devices are commonly used to cool electronic components.

In exactly the same fashion, germanium, also in group IV of the periodic table, can be used instead of silicon, making a Ge(Li)-drifted detector. (You might guess this is called a "jelly" detector.) The Ge(Li) detector also requires liquid nitrogen or electronic cooling, since its bandgap is only 0.66 eV.

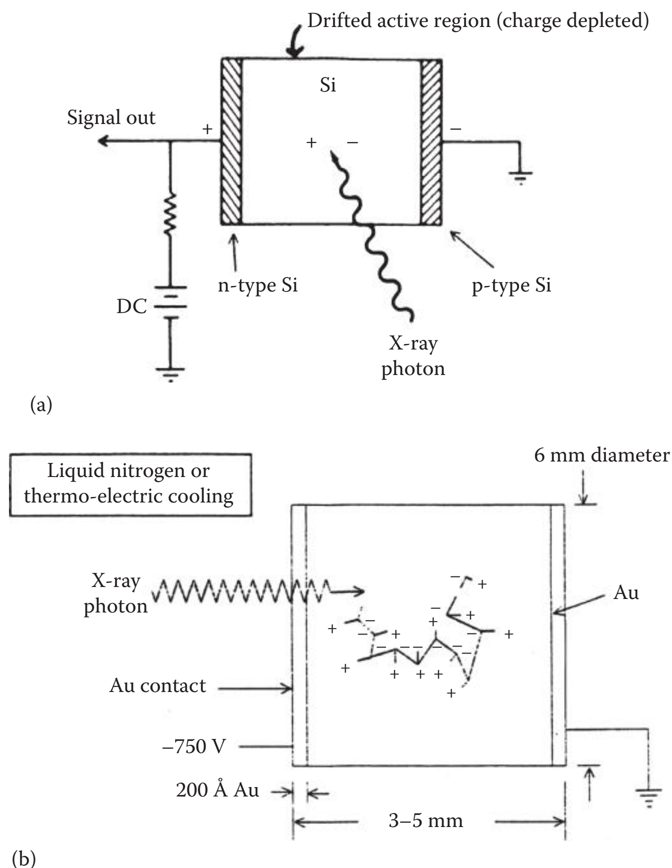


**Figure 8.23** The Si(Li) semiconductor detector. (a) Schematic shows the n-type Si region on one end of the Si crystal, a central charge-depleted intrinsic region and p-type Si on the other end. (b) The actual detector has 200 Å layers of gold as electric contacts on each end of the crystal. An X-ray photon striking the intrinsic region generates electron–hole pairs within the diode. (b: © Thermo Fisher Scientific. www.thermofisher.com. Used with permission.)

An X-ray photon striking the detector produces multiple electron–hole pairs in the intrinsic region (Figure 8.23b). The number of electron–hole pairs produced is proportional to the photon energy. The energy required to make an electron–hole pair is 3.86 eV in Si(Li), so the number of electron–hole pairs formed is approximately

$$n = \frac{E}{\varepsilon} = \frac{E}{3.65\ \text{eV}} \tag{8.16}$$

where

$n$ is the number of electron–hole pairs
$E$ is the energy of the incident X-ray photon (eV)
$\varepsilon$ is the energy to form an electron–hole pair (eV)

For a similar Ge lithium-drifted detector, the energy required for ionization is 2.96 eV. This is much less than the energy required for ionization in a proportional counter or a NaI(Tl) scintillation detector.

Under the influence of an applied voltage, the electrons move toward the positive end and the holes toward the negative end of the detector. The total charge collected at the positive contact is

$$Q = nq_e \tag{8.17}$$

where
$Q$ is the total charge in coulombs (C)
$n$ is the number of electron–hole pairs = $E/\varepsilon$
$q_e$ is the charge on one electron = $1.69 \times 10^{-19}$ C/electron

The collection of charge results in a voltage pulse. Since the total charge is proportional to the energy of the incident photon, the amplitude of the voltage pulse produced is also directly proportional to the energy of the incident photon. The voltage pulses are amplified and "shaped" electronically and sent to a *multichannel pulse height analyzer* (Section 8.2.2.5) to be sorted by pulse height and counted.

*Silicon PIN diode detectors*. These consist essentially of a couple of mm thick silicon junction type p-i-n diode with a bias of 1000 V across it. The heavily doped central part forms the nonconducting i-layer (intrinsic layer), where the doping compensates the residual acceptors that would otherwise make the layer p-type. When an X-ray photon passes through, it causes a swarm of electron–hole pairs to form, and this causes a voltage pulse. To obtain sufficiently low conductivity, the detector must be maintained at low temperature with a Peltier device. Continuous improvement of the pulse processing results in resolution as low as 125 eV. Count rate and resolution are strongly correlated; the resolution is best at a low count rate. The yield of this detector for higher energies is good although less than the Si(Li) detector (Figure 8.24).

*Silicon drift detector*. Commercially available silicon drift detectors (SDDs) are based on the drift chamber principle. The detector crystal is moderately cooled by vibration-free thermoelectric coolers. A monolithically integrated on-chip field effect transistor (FET) acts as a signal amplifier and controls energy resolution. The sideward depletion of the active detector volume in connection with the integrated drift structure provides an extremely small detector capacitance that enables the use of fast signal processing techniques, thus enabling high count rate processing. The processing electronics enable high count rate and the lowest possible resolution (Figure 8.25).

The unique property of this type of detector is the extremely small value of the anode capacitance, allowing the FET to be either integrated on the chip or connected to it by a short metal strip.

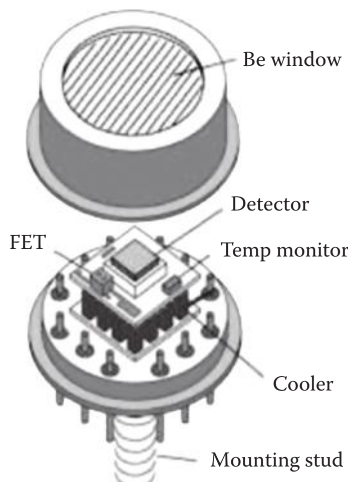


**Figure 8.24** Schematic of a silicon PIN detector. (Courtesy of Amptek, Inc. www.amptek.com.)

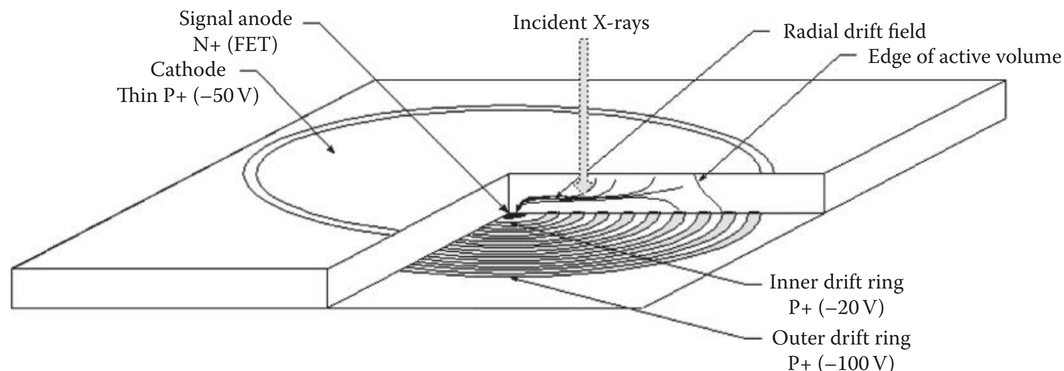


**Figure 8.25** Schematic of an SDD. (Courtesy of Amptek, Inc. www.amptek.com.)

Using very elaborate and proprietary processing technology in the fabrication reduces the leakage current level to such low levels that the detector can be operated with moderate cooling. This cooling can be readily achieved by Peltier cooling and is in the vicinity of −15 to −20°C.

#### *8.2.2.5 Multichannel Pulse Height Analyzer*

A multichannel pulse height analyzer, also called a multichannel analyzer (MCA) or digital pulse processor, collects, integrates, and displays the signal pulses from the detector. The operation of an MCA can be modeled in a simple fashion. Assume we have a handful of coins of different denominations and a coin-sorting device to put each coin into a separate stack (Figure 8.26a). The stacks will have different heights, depending on the number of coins of each type (Figure 8.26b, second plot from the bottom). We can plot "counts" or number of coins versus the height of the stack. An MCA does the same thing with photons of different energies. Assume that we have a pulse height analyzer of a given total voltage range with the ability to change the voltage in small increments. As an example, the total voltage range is 10 V, and the interval of change is 0.1 V. X-rays of short wavelengths (high energies) must be separated from X-rays of long wavelengths (low energies). That is what a pulse height analyzer does; it rejects energy signals that are higher or lower than a selected energy window. If the analyzer window can be changed in small energy increments, only photons with that energy will pass through. Those photons are counted and stored in that energy window location in the analyzer memory. Each energy window location is called a *channel*. Then the energy window (voltage) is changed by 0.1 V, and only photons corresponding to the new energy window will pass through and be counted and stored in a second channel. Sweeping the voltage range in steps of 0.1 V permits us to distinguish between X-rays of various energies. If the X-ray photons are counted by energy, we can obtain $I$, the X-ray intensity at given energy. This permits us to plot $I$ versus wavelength (energy), which gives us an energy spectrum of the XRF from the sample. An EDXRF spectrum is in the form of a histogram, usually plotted as "counts" on the $y$-axis, where counts means the number of photons counted in a given channel, versus energy on the $x$-axis. In practice, an EDXRF is equipped with a pulse height analyzer with many channels and complicated signal processing circuitry. A typical multichannel pulse height analyzer may have 2048 channels, each corresponding to a different energy interval.

Resolution in a semiconductor detector EDXRF system is a function of both the detector characteristics and the electronic pulse processing. The energy resolution of semiconductor detectors is much better than either proportional counters or scintillation counters (SCs). Their excellent resolution is what makes it possible to eliminate the physical dispersion of the X-ray beam; without the energy resolution of semiconductor detectors, EDXRF would not be possible. Resolution is generally defined as the smallest energy difference observable between peaks. In EDXRF, the energy resolution is defined

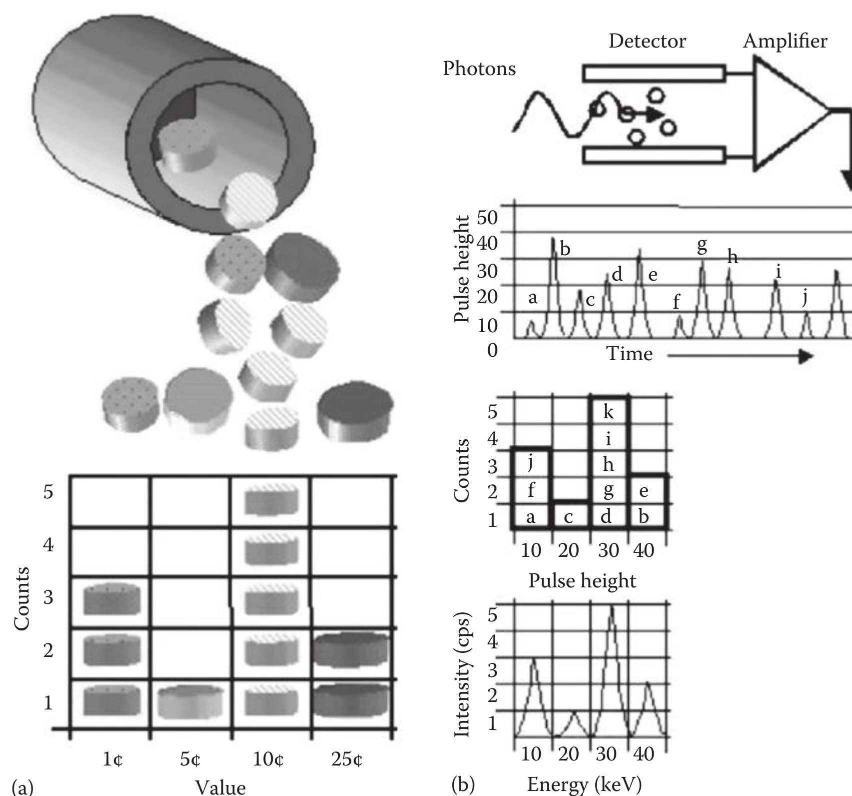


**Figure 8.26** Schematic of the pulse processing of an MCA. (a) The "coins" (photons) are separated by denomination and binned. (b) second from the bottom: The number of coins gives a "stack height" (counts). The typical EDXRF output is the lower-right plot of counts per second versus energy.

as the FWHM of the Mn K emission peak. Resolution is dependent on the energy of the detected photon and due to the pulse processing also depends on the total number of photons counted (total input count rate). The area of the detector as well as the electronic parameters of the pulse processor affect resolution as well and need to be included in a complete system comparison.

The most common detectors in benchtop EDXRF units are SDDs of <10 mm$^2$ area with a resolution of <150 eV for the Mn K line at 100,000 counts/s.

In handheld or portable instrumentation, Si-PIN detectors of <10 mm$^2$ area are common, with a resolution of <170 eV at 40,000 cps. For the detection of light elements (Mg to S), SDDs are more suitable and achieve a resolution of <190 eV at 90,000 cps with detector areas of ≥25 mm$^2$.

#### *8.2.2.6 Detector Artifact Escape Peaks and Sum Peaks*

Spectrum artifacts may appear in the energy-dispersive (ED) spectrum. These are peaks that are not from elements in the sample, but are caused by interaction between the sample and the detector material. For example, when measuring pure iron or steel, some of the Fe photon energy is transferred to the Si detector atoms; the amount of energy absorbed by a Si atom has *escaped* from the Fe photon. This type of peak, which may appear in the spectrum, is called an escape peak. The Si escape peak, from the Si $K_\alpha$ line, results in an artifact peak 1.74 keV lower than the parent peak when any silicon-based detector is used. Similar escape peaks at different energies appear for Ge if a Ge detector is used. Table 8.A.2 in the appendix gives the keV values for the K and L lines of all the elements and can be used to calculate where an escape peak might appear in the spectrum.

Sum peaks in the EDXRF spectrum occur when two high-intensity photons arrive so close in time that the signal processing electronics cannot separate them. A single peak is registered at an energy that is the sum of the two peaks. Sum peaks can be avoided by reducing the current and thus the signal on the detector. Major elements in the sample, such as Fe in steel, are generally the source of the sum peaks. Most EDXRF systems come with software that automatically can correct for escape peaks and some also for sum peaks. Figure 8.27 shows some examples of these artifact peaks in EDXRF spectra. Table 8.A.2 in the appendix can help with identification of these artifacts. In Figure 8.27a, the instrument software "marks" a peak and identifies it as the element francium. In reality, the peak at 2.77 keV is the Ti $K_\alpha$ escape peak. Note the position of the marker line—it is not at the center of the emission peak, and francium is not a very likely element in most samples. Also check Table 8.A.2. The peak energy does not match Fr. This should alert the analyst to an artifact in the spectrum.

For the major elements in a sample at high count rates, it is possible that two photons are detected at the same time. These two photons are "summed" in the detector output. Figure 8.27b shows the Fe emission spectrum on the left with three observed sum peaks, calculated as follows: 6.40 keV + 6.40 keV = 12.8 keV; 6.40 keV + 7.05 keV = 13.4 keV; and 7.05 keV + 7.05 keV = 14.1 keV.

Figure 8.27c is the spectrum of pure iron, measured with a Si(Li) detector, which shows both escape peaks and sum peaks.

### 8.2.3 Instrumentation for Wavelength-Dispersive X-Ray Spectrometry

There are three types of WDXRF instruments: **sequential spectrometers**, which use a **goniometer** and sequentially measure the elements by scanning the wavelength; **simultaneous spectrometers**, which use multiple channels, with each channel having its own crystal/detector combination optimized for a specific element or background measurement; and **hybrid spectrometers**, which combine sequential goniometers or scanners with fixed channels as well as XRD channels and goniometers. Hybrid instruments will be discussed in Section 8.4 with XRD instruments.

A WDXRF spectrometer can be generally divided into four major components based on their functionality: the generator, spectrometer, electronic pulse processing unit, and sample changer. The **generator** supplies the current and high voltage for the X-ray tube to produce the tube radiation (primary X-rays). The generators available today can provide a maximum output of around 4 kW with a maximum voltage of up to 70 kV and up to 170 mA current.

The **spectrometer** contains the X-ray tube, primary beam filters, collimators, analyzing crystals, and detectors. Parts of the spectrometer and the sample measurement position are generally under vacuum, but other atmospheres (purge gases) can be used based on the desired application. X-ray tubes and primary beam filters have been discussed earlier. Most commercially available WDXRF units today use end-window X-ray tubes, which are water-cooled. The window thickness is around 75 μm or less (see Figure 8.10).

The primary beam filter wheel is equipped with a selection of absorbing foils, commonly Al and Cu foils of various thicknesses. It is located between the tube and the sample, filtering out undesirable or interfering components of the tube radiation to increase the peak-to-background ratio.

#### *8.2.3.1 Collimators*

The X-rays emitted by the anode in an X-ray tube are radially directed. As a result, they form a hemisphere with the target at the center. In WDXRF spectroscopy or XRD structural determination, the spectrometer's analyzing crystal or the crystalline substance undergoing structure determination requires a nearly parallel beam of radiation to function properly. A narrow, nearly parallel beam of X-rays can be made by using two sets of closely packed metal plates or blades separated by small gaps. This arrangement absorbs all the radiation except the narrow beam that passes between the gaps (Figure 8.28).

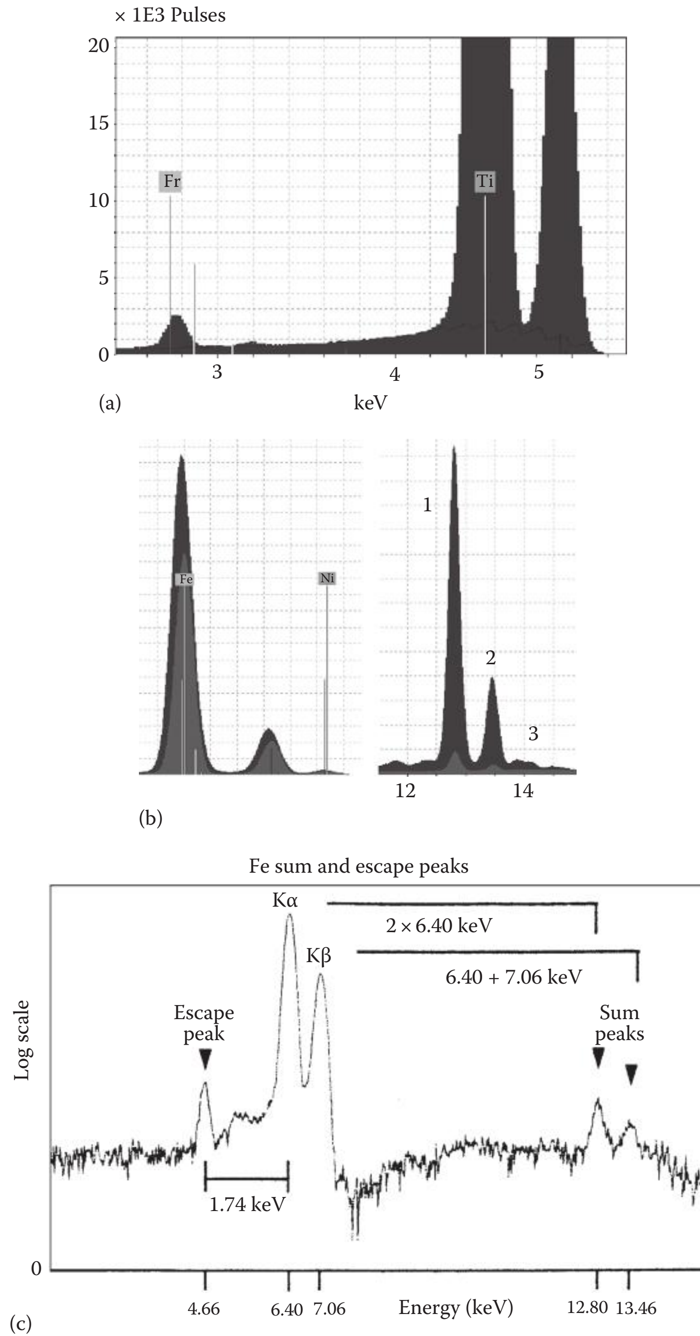


**Figure 8.27** (a) The peak at 2.77 keV with the Fr emission line marker shown is in reality the Ti Ka escape peak: 4.51 keV (Ti Ka) – 1.74 (Si Ka) = 2.77 keV. (b) Fe emission shown on the left (Ka at 6.40 keV); sum peaks shown on the right as described earlier. (a and b: Data courtesy of Bruker Elemental © 2013 Bruker, Inc. www.bruker.com. Used with permission.) (c) Iron spectrum showing both escape and sum peaks. The escape peak is lower in energy than the Fe $K_\alpha$ peak by an amount exactly equal to the energy of the Si $K_\alpha$ line. Sum peaks also appear in EDXRF spectra when two intense photons arrive at the detector simultaneously. A sum peak from two $K_\alpha$ photons is shown along with a sum peak from one $K_\alpha$ and one $K_\beta$ photon. (c: © Thermo Fisher Scientific. www.thermofisher.com. Used with permission.)

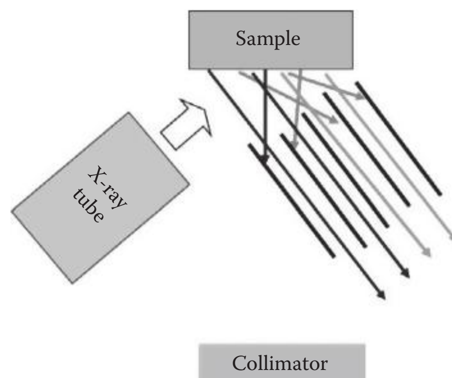


**Figure 8.28** The function of a collimator is shown. All radiation is absorbed except for the photons passing through the gaps, forming a narrow, nearly parallel beam of X-rays. (© 2013 Bruker, Inc. www.bruker.com. Used with permission.)

Decreasing the distance between the plates or increasing the total length of the gaps decreases the divergence of the beam of X-rays (i.e., it collimates or renders them parallel). The use of a collimator increases the wavelength resolution of a spectrometer's analyzing crystal, cuts down on stray X-ray emission, and reduces background (Figure 8.29).

Commercial instruments use multiple tube or multiple slit collimator arrangements, often both before the analyzing crystal (the primary collimator) and before the detector (the secondary collimator). The collimator positions in a sequential WDXRF spectrometer are shown schematically in Figure 8.30. In many wavelength-dispersive (WD) instruments, two detectors are used in tandem, and a third auxiliary collimator may be required. Such an arrangement is shown in Figure 8.31.

Collimators are not needed for curved crystal spectrometers where slits or pinholes are used instead nor are they needed for ED spectrometers. **Collimator masks** are situated between the

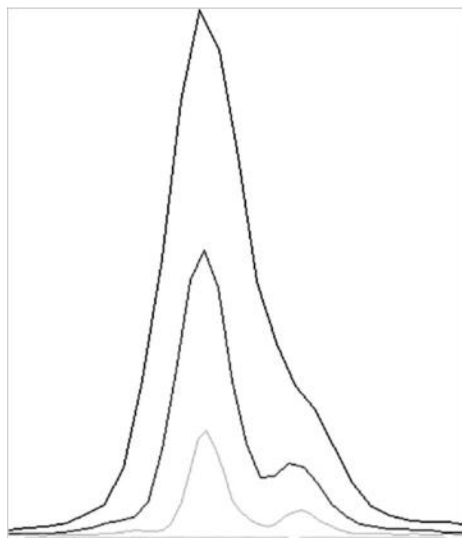

**Figure 8.29** Peak resolution and intensity as a function of finer and finer divergence (blade spacing). Finer divergence increases resolution but decreases intensity. (© 2013 Bruker, Inc. www.bruker.com. Used with permission.)

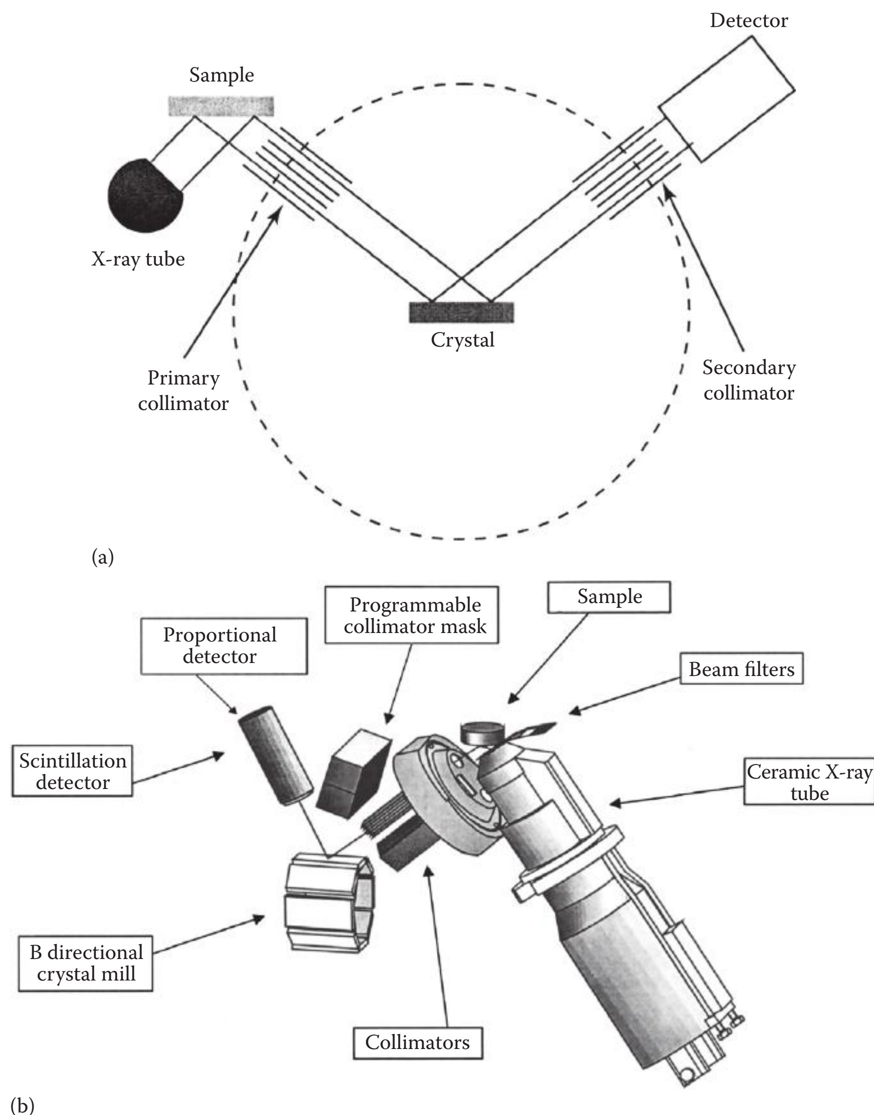


**Figure 8.30** (a) Schematic of the optical path in a WD sequential spectrometer, showing the positions of the collimators. (b) Schematic layout of a commercial sequential WDXRF system. (Courtesy of PANalytical, Inc., The Netherlands. www.panalytical.com.)

sample and collimator and serve the purpose of cutting out the radiation coming from the edge of sample cup aperture (Figure 8.32).

### *8.2.3.2 Analyzing Crystals*

The analyzing crystals are the "heart" of a WDXRF spectrometer. As we have discussed, a crystal is made up of layers of ions, atoms, or molecules arranged in a well-ordered system or lattice. If the spacing between the layers of atoms is about the same as the wavelength of the radiation, an impinging beam of X-rays is reflected at each layer in the crystal (Figure 8.8).

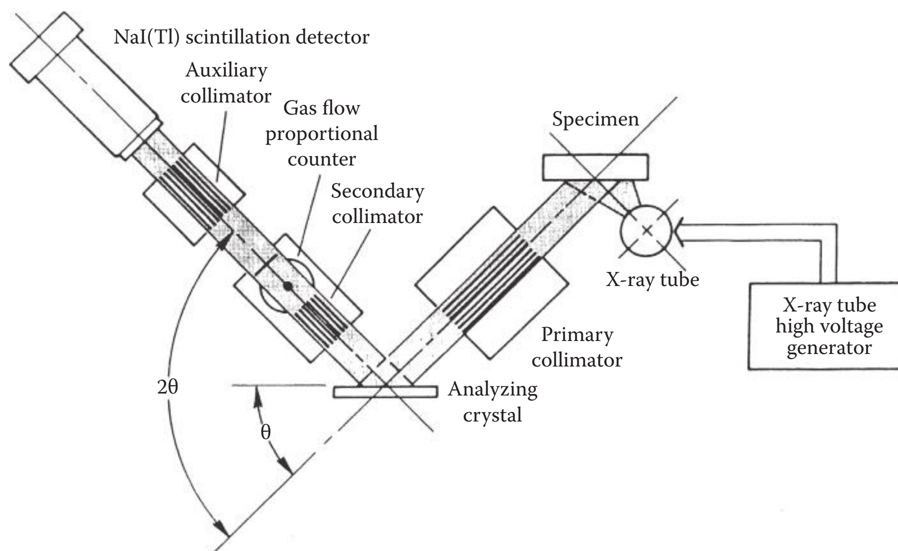


**Figure 8.31** A sequential spectrometer with two tandem detectors, showing the placement of the collimators in the optical path. (From Jenkins, R. et al., *Quantitative X-Ray Spectrometry*, Marcel Dekker, Inc., New York, 1981. Used with permission.)

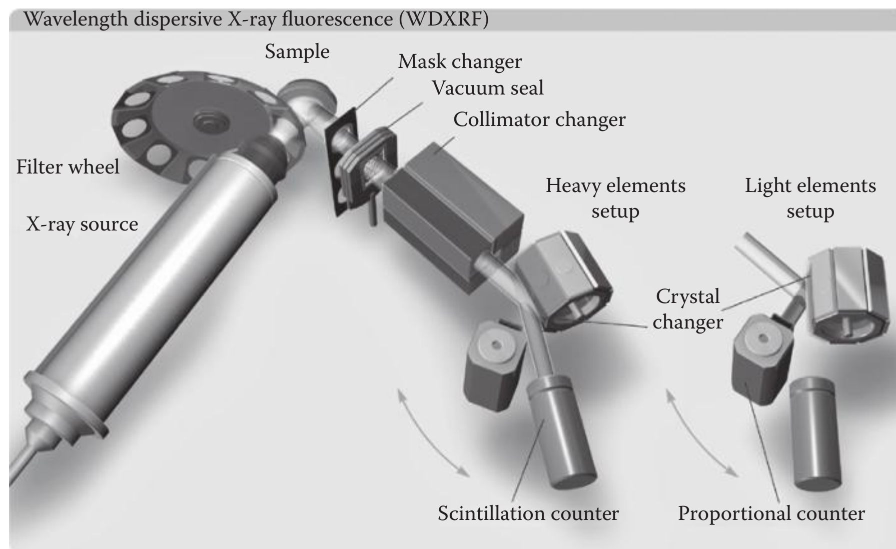


**Figure 8.32** Schematic commercial WDXRF system showing the position of a collimator mask changer, as well as the layout of X-ray tube, filter wheel, sample, collimator, analyzing crystal changer, and detector. (© 2013 Bruker, Inc. www.bruker.com. Used with permission.)

Bragg's Law (Equation 8.15) indicates that at any particular angle of incidence θ, only X-rays of a particular wavelength fulfill the requirement of staying in phase and being reinforced, and are therefore diffracted by the crystal. If an X-ray beam consisting of a range of wavelengths falls on the crystal, the diffracted beams of different wavelengths emerge at different angles. The incident beam is thus split up by the crystal into its component X-ray wavelengths, just as a prism or

grating splits up white light into a spectrum of its component colors. The analyzing crystal is an X-ray monochromator, with the small lattice distances found in natural or synthetic crystals acting exactly like the ruled diffraction gratings used in the UV/visible (VIS) region. Because X-ray wavelengths are so small, it is not possible to mechanically rule a grating for use in the X-ray region. The crystal separates X-rays of different wavelengths by diffracting them at different angles. Bragg's law fixes the spectral range of a given crystal. Since the maximum value of sinθ is 1.00, the upper spectral limit $\lambda_{max} = 2d$. The diffraction efficiency and the resolution depend on the purity and perfection of the crystal lattice. The crystal should be as perfect as possible, so that the *d*-spacing for a given plane will be constant in all parts of the crystal. The principle is illustrated in Figure 8.33a. Figure 8.33a shows schematically that two detectors placed at the proper locations could detect two diffracted wavelengths simultaneously. Alternatively, the detector or analyzing crystal could move, allowing each wavelength to be detected sequentially. Both types of spectrometers are commercially available. Some crystals in common use for dispersion of X-rays in commercial XRF spectrometers are listed in Table 8.7. Most crystals are natural inorganic or organic compounds. A serious limitation in XRF was the lack of natural crystals with *d*-spacings large enough to diffract the low-energy X-rays from low atomic number elements. That limitation has been overcome by the synthesis of multilayer "pseudocrystals." The desired lattice plane *d*-spacing is produced from alternating layers of materials with high and low optical densities, such as Si and W or Ni and BN, deposited on a silicon or quartz flat. Figure 8.33b shows how such a synthetic multilayer crystal functions. The PX-3 multilayer is made from $B_4C$ alternating with Mo, for example. These engineered multilayers are stable and commercially available and have revolutionized the determination of light elements, permitting elements as light as Be to be detected.

When applying Bragg's law, the *d*-spacing of a specific analyzing crystal limits its detectable element range. The shorter the *d*-spacing of a crystal, the better the separation of two adjacent or overlapping peaks. For example, looking at vanadium (V) and chromium (Cr), the V $K_{\alpha_1}$ and Cr $K_{\alpha_1}$ lines are farther apart when measured with LiF-220 ($2d = 0.2848$ nm) than when measured with LiF-200 crystal ($2d = 0.4028$).

As is clear from Table 8.7, different crystals are needed to measure different elements. Commercial sequential XRF systems have a computer-controlled multiple-crystal holder inside the spectrometer, with positions for as many as 8–10 crystals in some instruments, as seen in Figure 8.32.

The analyzing crystal is mounted on a turntable that can be rotated through θ degrees (see the arrow marked θ on the lower left side of Figure 8.31). The detector(s) are connected to the crystal turntable so that when the analyzing crystal rotates by θ degrees, the detector rotates

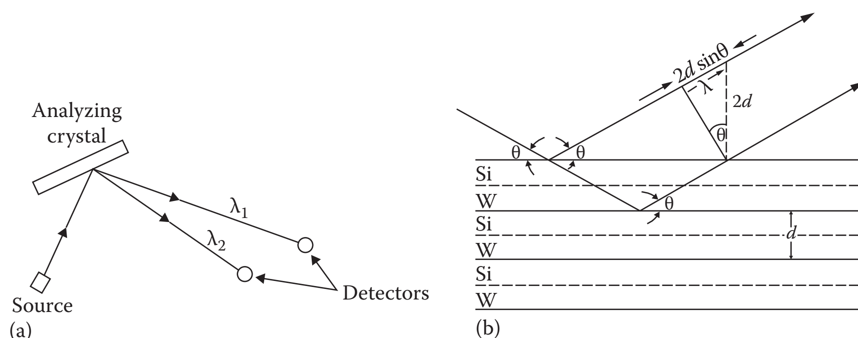


**Figure 8.33** (a) The analyzing crystal as a monochromator. (b) A synthetic crystal made from multiple alternating layers of Si and W, showing the *d*-spacing and the ability to diffract X-rays. (b: © 2013 Bruker, Inc., www.bruker.com. Used with permission.)

**Table 8.7 Analyzing Crystals Used in Modern X-Ray Spectrometers**

| Crystal | Name and Orientation (Miller Indices) | 2*d*-Spacing (nm) | Element Range |
|---|---|---|---|
| LiF-420 | Lithium fluoride (420) | 0.1891 | $\geq NiK_{\alpha_1}$ |
| LiF-220 | Lithium fluoride (220) | 0.2848 | $\geq VK_{\alpha_1}$ |
| LiF-200 | Lithium fluoride (200) | 0.4028 | $\geq KK_{\alpha_1}$ |
| Ge | Germanium (111) | 0.6530 | P, S, Cl |
| InSb | Indium antimonide (111) | 0.7481 | Si |
| PET[a] | Pentaerythritol (002) | 0.8740 | Al–Ti, Kr–Xe, Hf–Bi |
| ADP | Ammonium dihydrogen phosphate | 1.064 | Mg |
| TlAP[b] | Thallium acid phthalate (100) (Thallium hydrogen phthalate) | 2.576 | Fe–Na |
| XS55, OV055, AX06, PX-1, PX-3, and others | Multilayered synthetic crystal[c] | 5.0–19 | Light elements from Be to N, N–Al, Ca–Br depending on the *d*-spacing |

[a] The most heat-sensitive crystal.
[b] Toxic.
[c] The designations for these multilayered synthetic crystals are commercial trade names from different instrument manufacturers.

through 2θ degrees, as shown by the marked arrow. Therefore, the detector is always in the correct position (at the Bragg angle) to detect the dispersed and diffracted fluorescence. This crystal positioning system is called a **goniometer**. Figure 8.34 shows the turntable and the concentric circles made by the crystal and the detector. In most systems, the maximum diffraction angle attainable is 75° θ (or 150° 2θ).

In some systems, the rotation of the crystal and the detector is mechanically coupled with gears. Other systems have no mechanical coupling but use computer-controlled stepper motors for the

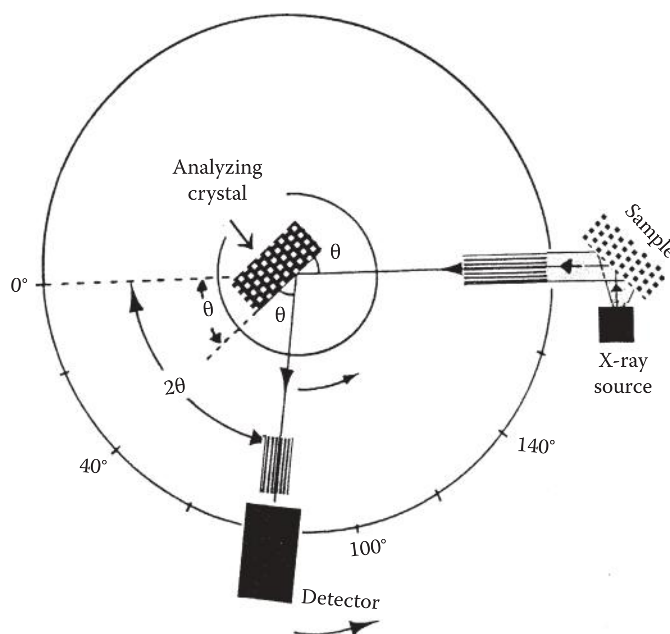


**Figure 8.34** Goniometer layout for a sequential XRF spectrometer.

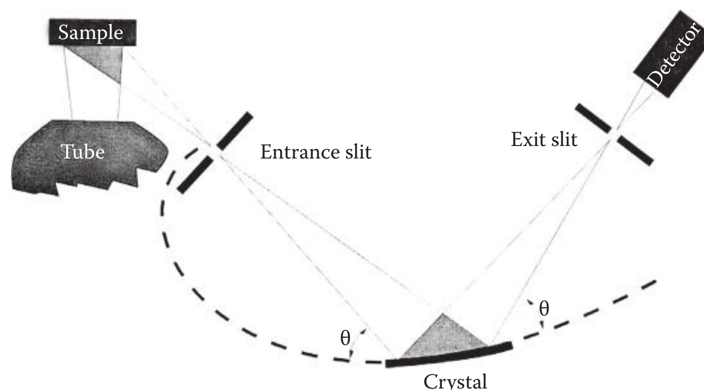


**Figure 8.35** Schematic of the optical path in a curved crystal spectrometer. (Courtesy of PANalytical, Inc., The Netherlands. www.panalytical.com.)

crystal and the detector. The newest systems use optical position control by optical sensors or optical encoding devices. Optical position control permits very high angular precision and accuracy and very fast scanning speeds.

The analyzing crystals are interchanged by rotation of the crystal holder, but the same goniometer is used to select the diffraction angle, meaning that only one wavelength can be measured at a time with a sequential system.

The analyzing crystal(s) shown schematically in Figures 8.30 through 8.32 have a flat surface. Flat crystals are used in scanning (sequential) spectrometers. Curved crystals, both natural and synthetic multilayers, are used in simultaneous spectrometers, electron microprobes, and for synchrotron X-ray spectrometry. The advantage to a curved crystal is that the X-rays are focused and the collimators replaced by slits, resulting in much higher intensities at the detector than with flat crystal geometry. This makes curved crystals excellent for analysis of very small samples. The use of a curved crystal and slits in a simultaneous spectrometer is illustrated schematically in Figure 8.35. The curved crystal spectrometer geometry should remind you of the Rowland circle geometry for optical emission spectrometers discussed in Chapter 7. Curved crystals are used in the "fixed" channel design of most simultaneous (multichannel) spectrometers.

#### *8.2.3.3 Detectors*

X-ray detectors transform photon energy into electrical pulses. The pulses (and therefore, the photons) are counted over a period of time. The *count rate*, usually expressed as counts per second, is a measure of the intensity of the X-ray beam. Operating the detector as a photon counter is particularly useful with low-intensity sources, as is often the case with X-radiation.

There are three major classes of X-ray detectors in commercial use: gas-filled detectors, scintillation detectors, and semiconductor detectors. Semiconductor detectors are used in EDXRF and handheld systems and were discussed earlier with EDXRF instrumentation. Both WDXRF and EDXRF detection make use of a signal processor called a pulse height analyzer or selector in conjunction with the detector.

WDXRF systems commonly use one or more of the following detectors: gas flow proportional counter (flow counter [FC]), sealed gas-proportional counter, and scintillation counters (SC).

*Gas-filled detectors*. Suppose we take a metal cylinder, fit it with X-ray transparent windows, place in its center a positively charged wire, fill it with inert filler gas, such as helium, argon, or xenon, and seal it. If an X-ray photon enters the cylinder, it will collide with and ionize a molecule of the filler gas by ejecting an *outer shell electron*, creating a *primary ion pair*. With helium as a

filler gas, the ion pair would be $He^+$ and a photoelectron $e^-$. A sealed gas-filled detector of this type is illustrated in Figure 8.36. The interaction

$$h\nu + \text{He} \rightarrow \text{He}^+ + e^- + h\nu$$

takes place inside the tube. The electron is attracted to the center wire by the applied potential on the wire. The positive charge causes the wire to act as the anode, while the positive ion, $He^+$ in this case, migrates to the metal body (the cathode). The ejected photoelectron has a very high kinetic energy. It loses energy by colliding with and ionizing many additional gas molecules as it moves to the center wire. A plot of the number of electrons reaching the wire versus the applied potential is given in Figure 8.37.

With no voltage applied, the electron and the positive ion ($He^+$) recombine and no current flows. As the voltage is slowly increased, an increasing number of electrons reach the anode, but not all of them; recombination still occurs. This is the sloping region marked A in Figure 8.37. At the plateau marked B in Figure 8.37, all the electrons released by a single photon reach the anode and the current is independent of small changes in the voltage. A detector operating under these voltage conditions is known as an *ionization counter*. Ionization counters are not used in X-ray spectrometers because of their lack of sensitivity.

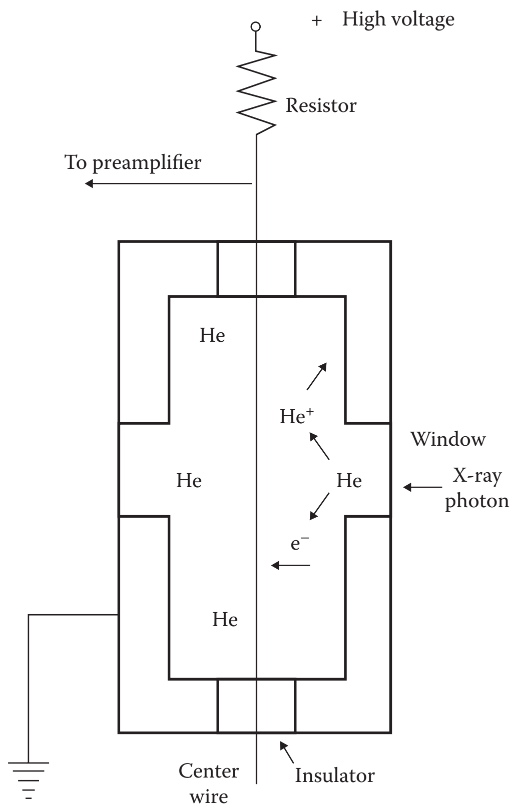


**Figure 8.36** Schematic diagram of a gas-filled X-ray detector tube. He filler gas is ionized by X-ray photons to produce $He^+$ ions and electrons, $e^-$. The electrons move to the positively charged center wire and are detected. (Modified from Parsons, M.L., X-ray methods, in Ewing, G.W. (ed.), *Analytical Instrumentation Handbook*, 2nd edn., Marcel Dekker, Inc., New York, 1997. Used with permission.)

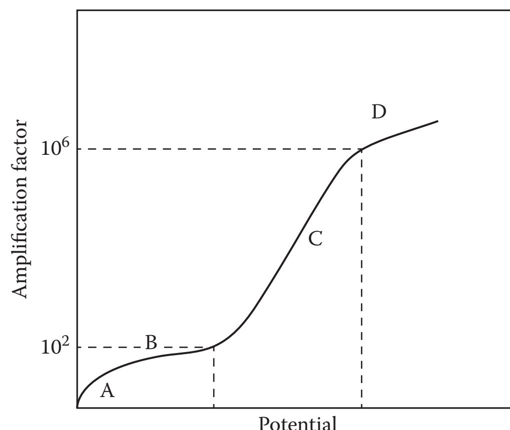


**Figure 8.37** Gas-filled detector response versus potential. A detector operating at the plateau marked B is an ionization counter. A proportional counter operates in the sloping region marked C where the response is proportional to the energy of the incoming photon. The plateau marked D represents the response of a Geiger counter. (Modified from Helsen, L.A. and Kuczumow, A., in Van Griekin, R.E.; Markowicz, A.A. (eds.), *Handbook of X-Ray Spectrometry*, 2nd edn., Marcel Dekker, Inc., New York, 2002. Used with permission.)

As the voltage increases further, the electrons moving toward the center wire are increasingly accelerated. More and more electrons reach the detector as a result of an avalanche of secondary ion pairs being formed, and the signal is greatly amplified. In the region marked C in Figure 8.37, the current pulse is proportional to the energy of the incoming X-ray photon. This is the basis of a *proportional counter*. In X-ray spectrometry, gas-filled detectors are used exclusively in this range, that is, as proportional counters. The amplification factor is a complex function that depends on the ionization potential of the filler gas, the anode potential, the mean free path of the photoelectrons, and other factors. It is critical that the applied potential, filler gas pressure, and other factors be kept constant to produce accurate pulse amplitude measurements. There are two main types of proportional counter: flow proportional counters and sealed proportional counters.

As shown in Figure 8.37, if the voltage is further increased, electrons formed in primary and secondary ion pairs are accelerated sufficiently to cause the formation of more ion pairs. This results in huge amplification in electrons reaching the center wire from each X-ray photon falling on the detector. The signal becomes independent of the energy of the photons and results in another plateau, marked D. This is called the Geiger–Müller plateau; a detector operated in this potential range is the basis of the *Geiger counter* or *Geiger–Müller* tube. It should be noted that a Geiger counter gives the highest signal for an X-ray beam without regard to the photon energy. However, it suffers from a long *dead time*. The dead time is the amount of time the detector does not respond to incoming X-rays. It occurs because the positive ions move more slowly than the electrons in the ionized gas, creating a *space charge*; this stops the flow of electrons until the positive ions have migrated to the tube walls. The dead time in a Geiger counter is on the order of 100 μs, about 1000 times longer than the dead time in a proportional counter. Due to the long dead time compared with other detectors, Geiger counters are not used for quantitative X-ray spectrometry. They are, however, very important portable detectors for indicating the presence or absence of X-rays. Portable radiation detectors equipped with Geiger counters are used to monitor the operation of equipment that creates or uses ionizing radiation to check for leaks in the shielding.

As was the case with EDXRF, escape peaks that are detector artifacts occur in WDXRF gas-filled detectors. Ionization of the filler gas by an X-ray photon usually results in the ejection of an outer shell electron. However, it is possible for ionization to occur by ejection of an inner

shell electron. When this happens, the incoming X-ray photon is absorbed, and the filler gas emits its characteristic K or L lines. This will result in peaks appearing at an energy $E'$ equal to

$$E' = E\,(\text{incoming X-ray}) - E\,(\text{filler gas characteristic X-ray}) \quad (8.18)$$

As an example, if the detector filler gas is Ar, the Ar K line has energy of about 3 keV (or a wavelength of 3.87 Å). If an incoming X-ray has a wavelength shorter than 3.87 Å, it can eject an argon K electron. Assuming that the incoming X-ray is the Fe $K_\alpha$ line at 6.3 keV, a peak will appear at (6.4 – 3) keV or about 3.4 keV. This peak at 3.4 keV is called an **escape peak** and can be called either the Fe $K_\alpha$ escape peak or the argon escape peak. An escape peak appears at a constant distance from the parent fluorescence X-ray (in this case, Fe $K_\alpha$) on the low-energy side. Escape peaks can often be very intense and can be useful in identifying elements.

*FC*. This detector consists of a metallic cylinder with a thin (counting) wire mounted in the middle (Figure 8.38).

The cylinder is filled with continuous flow of P-10 gas (10% methane [$CH_4$] and 90% Ar). A high positive voltage (+1400 to +1900 V) is applied to the thin wire. The cylinder is sealed with a

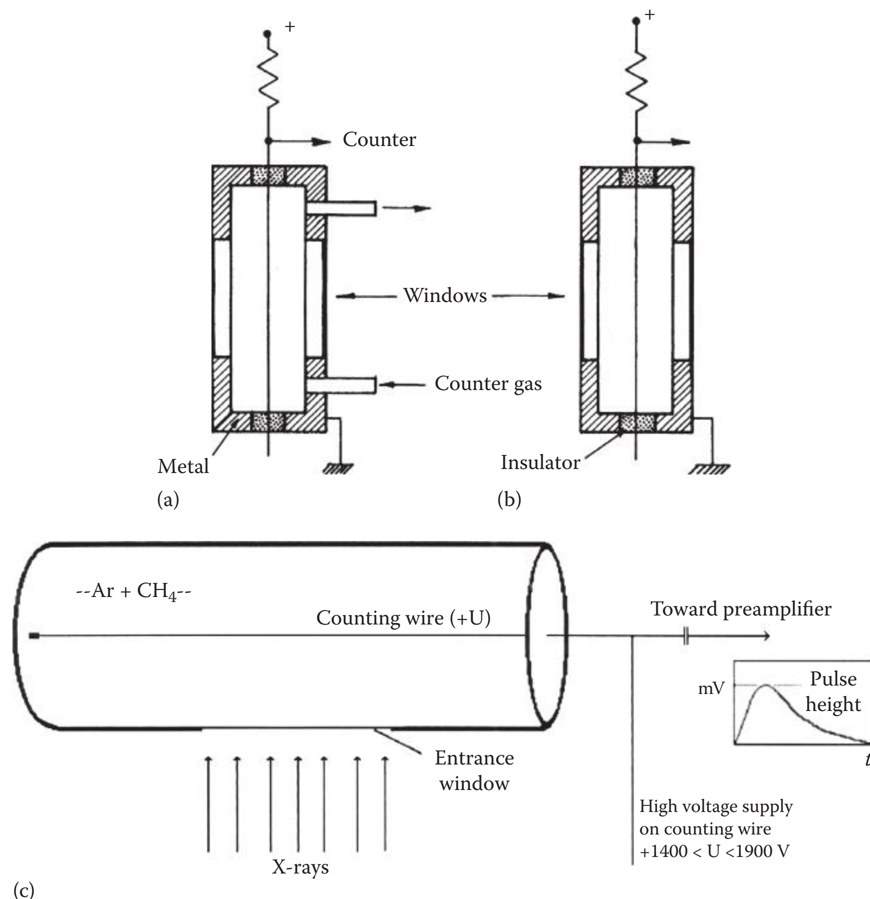


**Figure 8.38** Schematics of (a) a flow proportional counter and (b) a sealed proportional counter. (From Helsen, L.A. and Kuczumow, A., in Van Griekin, R.E.; Markowicz, A.A. (eds.), *Handbook of X-Ray Spectrometry*, 2nd edn., Marcel Dekker, Inc., New York, 2002. Used with permission.) (c) Schematic view of a flow proportional counter.

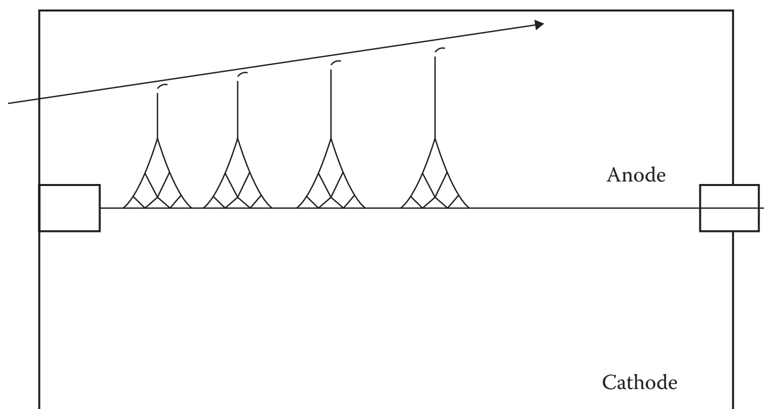


**Figure 8.39** Four primary ions pairs produce four “avalanches,” all of which contribute to a single pulse. (Copyright Oak Ridge Associated Universities, www.orau.org.)

0.3–1 μm very thin foil window permeable to X-ray photons with low energies and is thus suitable for measuring light elements, with Z < 27. The thin windows allow the filler gas to leak out; therefore, a supply of filler gas is constantly provided to the detector through the inlet as shown in Figure 8.38a. The pressure, flow, and temperature of the gas must be precisely controlled for accurate detector response.

X-ray photons interact with the inert gas in the detector by ionizing it. This ionization is based on the ejection of an outer shell electron and creates a primary ion pair. When argon is used, we will observe both an $Ar^+$ ion and an electron ($e^-$). The electron is attracted to the wire, which is positively charged, and the $Ar^+$ will be attracted and migrate to the metallic body. Each primary ion pair produces 10–10,000 electrons due to an “avalanche” of secondary pairs produced as the initial electrons are accelerated toward the wire (Figure 8.39). The principle of operation is that the number of electron–ion pairs created is proportional to the energy of X-rays that entered the detector. The pulse voltage as recorded by the counting electronics is proportional to the energy of the “counted” photon.

*Sealed gas-proportional counter*. This detector is a sealed or closed system with a fixed volume of filler gas (Figure 3.38b). The filler gas used in a sealed proportional counter may be Ne, Kr, or Xe. The detector is sealed with thicker windows than those used in the FC and therefore do not leak. Window materials include polymers, mica, aluminum, and beryllium. The window thickness generally prevents the sealed proportional counter from being used for the measurement of light elements from Be to Na. It is used for analyzing elements from Al to Ti.

Multiple proportional counters are used in simultaneous X-ray spectrometers, described later, while one proportional counter is often used in tandem with an SC in a sequential system. It is for this reason that the detector has two windows as shown in Figure 8.38. X-ray photons pass through the proportional counter to the SC located behind it, as illustrated in Figure 8.31, and signals are obtained from both detectors. It should be noted that this tandem arrangement does not permit independent optimization of both detectors. There are sequential spectrometer systems available with independent proportional and scintillation detectors.

*SC*. Photomultiplier detectors, discussed in Chapter 5, are very sensitive to visible and UV light, but not to X-rays, to which they are transparent. In a *scintillation detector*, the X-radiation falls on a compound that absorbs X-rays and emits visible light as a result. This phenomenon is called *scintillation*. A PMT can detect the visible light scintillations. The scintillating compound or phosphor can be an inorganic crystal, an organic crystal, or an organic compound dissolved in solvent.

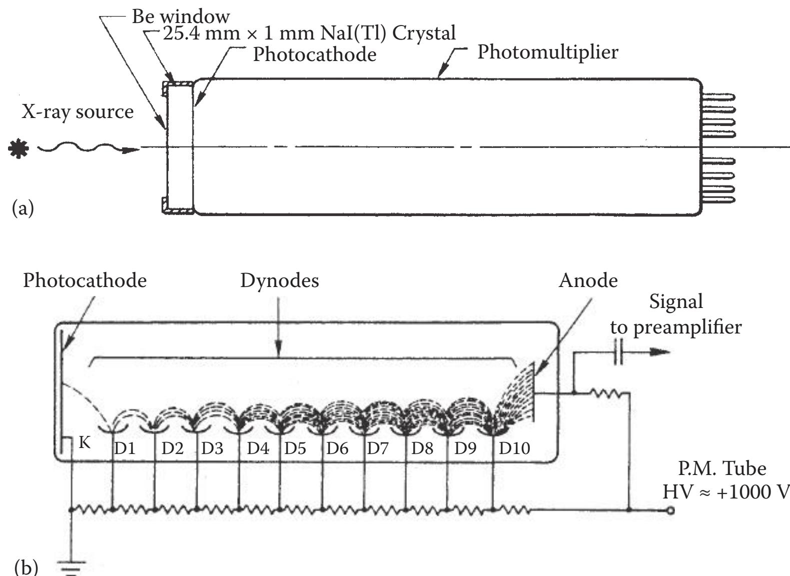


**Figure 8.40** Schematic NaI(Tl) scintillation detector. (a) The assembled detector. (b) Schematic representation of the photomultiplier and its circuitry. (Courtesy of ORTEC (Ametek). www. ortec-online. com; From Jenkins, R. et al., *Quantitative X-Ray Spectrometry*, Marcel Dekker, Inc., New York, 1981. Used with permission.)

The most commonly used commercial scintillation detector has a thallium-doped sodium iodide crystal, NaI(Tl), as the scintillating material. A single crystal of NaI containing a small amount of homogeneously distributed Tl in the crystal lattice is coupled to a PMT, shown in Figure 8.40.

When an X-ray photon enters the crystal, it causes the interaction

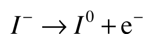

$$I^- \rightarrow I^0 + e^-$$

and the ejection of photoelectrons, as in the gas-filled detector. The ejected photoelectrons cause excited electronic states to form in the crystal by promotion of valence band electrons. When these excited electrons drop back to the ground state, flashes of visible light (scintillations) are emitted. The excited state lies about 3 eV above the ground state, so the emitted light has a wavelength of 410 nm. The intensity of the emitted light pulse from the crystal is proportional to the number of electrons excited by the X-ray photon. The number of electrons excited is proportional to the energy of the X-ray photon; therefore, the scintillation intensity is proportional to the energy of the X-ray.

The scintillations (visible light photons) from the crystal fall on the cathode of the PMT, which is made of a photoemissive material such as indium antimonide. Photoemissive materials release electrons when struck by photons. Electrons ejected from the cathode are accelerated to the first dynode, generating a larger number of electrons. The electron multiplication process occurs at each successive dynode, resulting in approximately $10^6$ electrons reaching the anode for every electron that strikes the cathode. The amplitude of the current pulse from the photomultiplier is proportional to the energy of the X-ray photon causing the ionization in the crystal.

To summarize, the scintillation detector works by (1) formation of a photoelectron in the NaI(Tl) crystal after an X-ray photon hits the crystal, (2) emission of visible light photons from an excited state in the crystal, (3) production of photoelectrons from the cathode in the photomultiplier, and (4) electron multiplication.

The NaI(Tl) scintillation detector is most useful for short-wavelength X-rays, <2 Å ($Z > 27$), so it complements the proportional counter. It also has the potential for escape peaks caused by the iodine K line (about 30 keV or 0.374 Å). Incoming X-rays with wavelengths less than 0.374 Å will result in escape peaks about 30 keV lower in energy than the true energy. The major disadvantage of the NaI(Tl) detector is that its resolution is much worse than that of the proportional counter. This is due to the wider pulse height distribution that occurs in the output pulse because of the multiple steps involved in the operation of this detector.

### *8.2.3.4 Electronic Pulse Processing Units*

In the detector, a photon generates a number of ion pairs, that is, a current pulse with a certain magnitude or pulse height. The pulse height (voltage) in an XRF detector depends on the energy of the photon. Unfortunately, the height of the current pulse that results is not exactly the same for photons of the same energy. Formation of ion pairs and secondary ion pairs is a statistically random process, so a Gaussian distribution of pulse heights centered on the most probable value results.

A series of pulses and their heights is shown in Figure 8.41. On the left side, this figure shows a series of current pulses from photons of two different energies counted over a period of time. If the pulses are plotted by height (amplitude), the result is a Gaussian **pulse height distribution**, shown on the right side of the figure. Two Gaussian pulse height distributions are seen since we had two photons of different energies reaching the detector. The width of the distribution is measured at half of the maximum height; this is called the FWHM. The FWHM is a measure of the energy resolution of a detector. Energy resolution is best in semiconductor detectors and worst in scintillation detectors, with gas-filled proportional counters in the middle.

In a WD instrument, the analyzing crystal separates the wavelengths falling on it, but as Bragg's law tells us, it is possible for higher-order ($n > 1$) lines of other elements to reach the detector. A higher-order line from a different element will have a very different energy and will result in a second pulse height distribution centered at a different energy reaching the detector. This would result in an error, since the signal would be misinterpreted as coming from just one element. This problem is eliminated by the use of a **pulse height discriminator**. The pulse height discriminator sets a lower and an upper pulse height threshold. Only the pulse heights that lie within these limits are counted. It thus reduces the background noise from the electronics and eliminates the interference of higher-order reflections. **A sine amplifier** ensures that a discriminator window, once set for a crystal, will be applicable for all detectable energies.

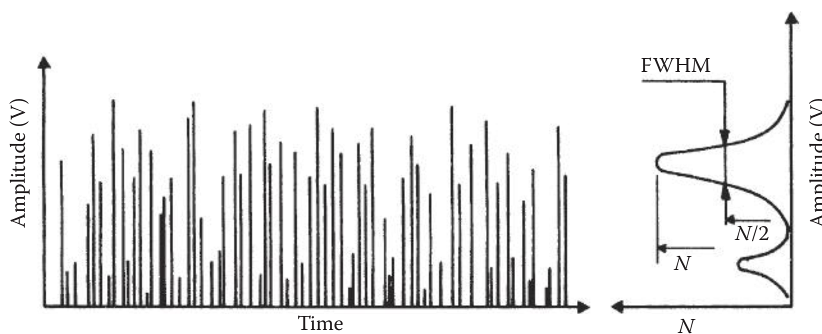


**Figure 8.41** Amplitude or pulse height and time record of signals from the detector is on the left. Transformation of the data into a pulse height distribution is shown on the right. The FWHM measurement is shown for the higher peak. (From Helsen, L.A. and Kuczumow, A., in Van Griekin, R.E.; Markowicz, A.A. (eds.), *Handbook of X-Ray Spectrometry*, 2nd edn., Marcel Dekker, Inc., New York, 2002. Used with permission.)

Pulse processing also incorporates **dead time correction**. Dead time results from the inability of the detector electronics to process the pulses fast enough to match the volume of input signals. Therefore, the greater the incident intensity, the greater the losses would be during measurement. Dead time is typically 300–400 ns for modern spectrometers.

#### *8.2.3.5 Sample Changers*

Commercial instruments are equipped with automatic sample changers. These are of various types and sizes, permitting either controlled loading of samples with sequential access or X–Y random access.

### 8.2.4 Simultaneous WDXRF Spectrometers

A simultaneous WDXRF system, also called a multichannel system, uses multiple channels, optimized for a specific element or background measurement. Each individual channel consists of a crystal, detector, and electronics module and is dedicated to a specific wavelength. Instruments with as many as 38 fixed crystal/detector channels or as few as two are available. These systems are designed for specific applications, such as the analysis of steel in a production facility where hundreds of samples must be analyzed very quickly (e.g., in less than 60 s) for the same suite of elements every day.

It is difficult to arrange a large number of channels in close proximity to the sample. Therefore, curved crystal monochromators with slit optics are used (Figure 8.42). Two commonly used curvatures are those that follow a logarithmic spiral, shown in Figure 8.42, and the Johansson curvature, which results in a Rowland circle monochromator (Figure 8.43) with the curve of the crystal matching the curve of the Rowland circle. The curvature of the crystal is selected so that the X-ray entrance slit is focused by the crystal onto the exit slit. This allows for higher intensities in a space-saving geometric arrangement.

As seen in Figure 8.42, the X-ray beam is applied from above the sample in these systems. He detector is located behind the exit slit. Scintillation or gas-proportional counters are used depending

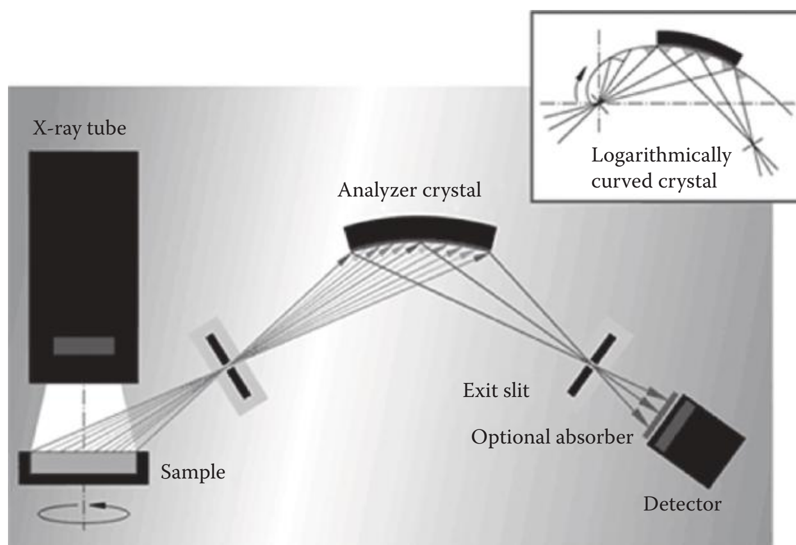


**Figure 8.42** Monochromator schematic with a logarithmic spiral curved crystal. (© 2013 Bruker, Inc. www.bruker.com. Used with permission.)

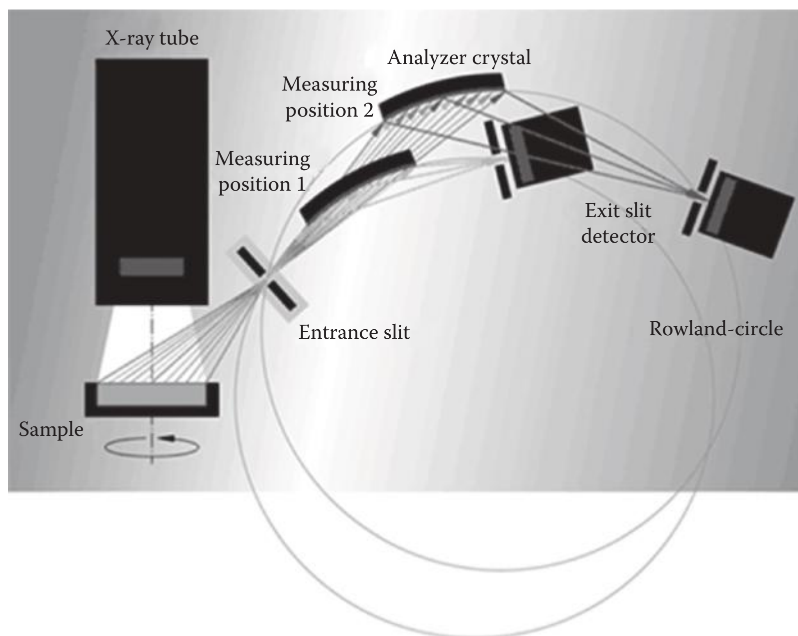


**Figure 8.43** Rowland circle type monochromator schematic with a Johansson curved crystal used as a scanning channel. (© 2013 Bruker, Inc. www.bruker.com. Used with permission.)

on the wavelength. All the monochromators are located in a large vacuum chamber. All channels are measured simultaneously, so the generator setting must provide the best compromise for all of the elements measured. The measurement time depends on the statistical accuracy requirements of the element with the lowest intensity; the time is typically 20–60 s.

When measuring trace and major elements simultaneously, the generator is normally set so that the trace elements can be measured with the highest possible intensity. Absorbers or attenuators are then needed for the major element channels to reduce their intensities so that they are in the operational range of the detectors.

While the fixed channels are used exclusively for quantitative analysis, a scanner or movable channel may be installed in the vacuum chamber to provide qualitative analysis ability and some flexibility in what is otherwise a system with a fixed suite of elements.

A single crystal, usually LiF200 or pentaerythritol (PET), is used, and the scanner's 2θ angular range is limited to 30°–120°. Therefore, some elements must be measured in second order. The scanner works on the principle of the Rowland circle, in which the crystal and the detector move in such a way that the entrance slit, exit slit, and crystal lie on a fixed radius circle that changes in position, as shown in Figure 8.43. A typical commercial instrument is shown in Figure 8.44.

### 8.2.5 Micro-XRF Instrumentation

Classically, XRF has been considered a "bulk" analysis technique because standard EDXRF and WDXRF systems have analysis spot sizes with a diameter in the mm–cm range, depending on the system. This requires a relative large volume of sample, with inhomogeneous materials requiring a great deal of sample preparation, discussed in Section 8.2.7. Developments in X-ray optics now permit the analysis of discrete microscopic particles, and the creation of elemental maps of a sample with high spatial resolution. The systems are variously called micro-XRF spectrometers, μ-XRF

(a) (b)

**Figure 8.44** (a) The S8 TIGER, a floor-mounted commercial WDXRF system. (b) The sample compartment of the S8 TIGER, showing the multiposition autosampler with typical samples such as polished metal flats on the left and pressed pellets on the right. (The namesake operator shown is not standard! Geaux Tigers!) (© 2013 Bruker, Inc. www.bruker.com. Used with permission.)

systems, X-ray analytical microscopes (not to be confused with electron microscopes equipped with EDS detectors discussed in Section 8.5.1), and X-ray microanalyzers.

### *8.2.5.1 Micro-X-Ray Beam Optics*

In order to decrease the analysis spot size, it is necessary to generate an intense, narrow X-ray beam of the necessary diameter. One way to do this is to pass the X-ray beam through an aperture (in effect, a small collimator) with diameters of a few mm to a few hundreds of micrometers. In 1984, Russian scientist Muradin Kumakhov discovered that X-rays were efficiently reflected from glass surfaces when the angle of incidence is low. This total external reflection from a smooth solid surface could be used to focus, collimate, and guide X-ray beams and has led to a new generation of micro-X-ray optics. The production of carefully shaped glass capillary optics allows X-ray beam diameters of 10 μm to 1 mm. A monocapillary optic is shown in Figure 8.45a. The solid angle from the X-ray source to the capillary is relatively large, which allows efficient coupling. Very-high-intensity X-rays can be channeled into the capillary, and high-intensity microbeams as small as 10 μm in diameter are formed by total external reflection.

Capillary optics can also be bundled together to form polycapillary optics, also called Kumakhov lenses. These lenses can be bundles of several thousand capillaries or a monolithic polycapillary structure. Beams produced using polycapillary optics (Figure 8.46) are highly intense and strongly focused. In comparison to a pinhole collimator, the fluorescence intensity of a polycapillary lens is increased by a factor of more than 1000. Focused beam diameters of 40–50 μm are possible. Table 8.8 shows how rapidly these X-ray optics have evolved.

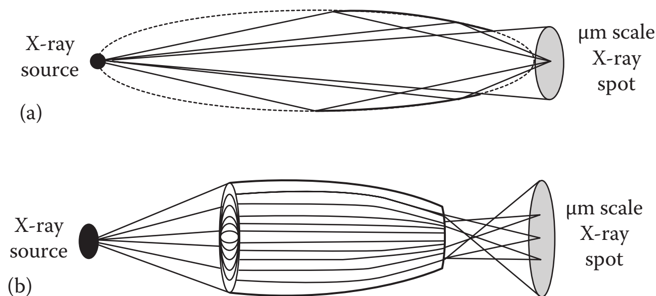


**Figure 8.45** (a) Schematic of a monocapillary X-ray optic for producing microbeams of X-rays. (b) Schematic of polycapillary X-ray optics for producing microbeams of X-rays. (© 2013 HORIBA, Ltd. www.horiba.com. All rights reserved.)

**Figure 8.46** A micro-XRF system with a large sample chamber, the SPECTRO MIDEX. This is used for analysis of large objects, such as the complete circuit board shown to the left of the analyst. (© AMETEK, Inc. www.ametek.com. Used with permission.)

**Table 8.8 Evolution of Kumakhov Capillary X-Ray Optics**

| Lens Parameter | 1985 | 2003 |
|---|---|---|
| Channel size | 1 mm | <1 μm |
| Lens length | 1000 mm | 10 mm |
| No. of channels | Max. 1000 | >1,000,000 |
| Lens diameter | 100 mm | 1 mm |
| Focal distance | Min. 50 mm | ≤1 mm |
| Spot size | 500 μm | 3 μm |

*Source:* © 2013 Unisantis Europe GmbH. All rights reserved.

### *8.2.5.2 Micro-XRF System Components*

Commercial systems consist of an optical microscope for observation of the sample area and an ED-based XRF system with a low-power, microfocused X-ray source using Kumakhov optics, a filter wheel, and a detector (Si[Li], Si-PIN, SDD). The X-ray source is generally air-cooled, and

some systems allow a choice of beam diameters. Systems are available that enable He purge gas for light elements, atmospheric pressure analysis, and low- or high-vacuum analysis.

Systems generally have large sample chambers allowing for analysis of complete circuit boards, for example, Figure 8.46, and open beam systems are available to bring the measurement head anywhere, permitting investigation of very large samples as well as uneven or structured surfaces. The chamber contains an automated motor-driven sample stage that allows the sample to be moved in the *x*-, *y*-, and *z*-directions for single-point, raster, or mapping analyses. A laser beam is used for reproducible sample positioning.

Many systems have proprietary mapping software and a charge-coupled device (CCD) camera for visual observation of the area being measured. Applications of micro-XRF spectroscopy will be discussed in Section 8.2.8.

### 8.2.6 Total Reflection XRF

Total reflection (or reflectance) XRF (TXRF) is a technique that looks at thin film samples or thin-layer samples with the ability to detect elements from Na to U. A schematic TXRF spectrometer and a commercial system can be seen in Figure 8.17a and b. The Bruker S2 PICOFOX consists of an air-cooled Mo anode metal–ceramic X-ray tube, a multilayer monochromator, and an XFlash® SDD and can be equipped with a 25 position autosampler.

The beam incident on the sample is at a very shallow angle, close to 0°, while the fluorescent radiation is detected at 90° from the sample disk, as seen in Figure 8.17a. Because the samples are very thin, matrix effects are negligible. Elemental composition can be quantified using an internal standard (IS).

Samples for TXRF must be prepared on a reflective medium. Polished quartz, glass, or polyacrylic glass disks are used. The samples must be in the form of a thin layer, thin film, or microparticulates. Sample sizes are on the order of microliters for liquids and milligrams for solids. Liquid samples are pipetted directly onto the disk and then dried using heat or vacuum. Solid samples can be analyzed directly if thin enough or prepared by suspension. Solid materials are ground to a fine particle size, weighed, and transferred to a test tube. The sample powder is suspended in a detergent solution, an IS is added, and the suspension is homogenized. An aliquot is pipetted onto the disk, dried under heat or vacuum, and is ready for analysis. TXRF is suitable for the analysis of clinical chemistry samples for trace elements, biological tissues, fluids, plant material, and the like. Other applications can be found at www.bruker-axs.com.

### 8.2.7 Comparison between EDXRF and WDXRF

The major difference between EDXRF and WDXRF is in the achievable energy (spectral) resolution, shown in Figure 8.47. WDXRF systems can routinely provide working resolutions between 5 and 20 eV, while EDXRF systems typically provide resolutions of 150–300 eV, depending on the type of detector used.

The higher resolution of WDXRF provides several advantages: reduced spectral overlaps, allowing complex sample matrices to be more accurately characterized, and reduced background, which improves detection limits (DLs). However, the additional optical components of a WDXRF instrument, including the collimators and analyzing crystals, reduce the efficiency of the instrument. This can be compensated for by the use of high-power X-ray sources, but the increased complexity of the instrument and the requirements for water-cooling, counting gases, and the like increase the cost of the instrument. WDXRF systems are larger (often floor mounted such as the system in Figure 8.44) and more expensive than EDXRF systems.

Another significant difference is in spectral acquisition. With an EDXRF system, the entire spectrum is acquired simultaneously within a few seconds. In a WDXRF system, the spectrum is acquired point by point, which requires more time. The alternative, a simultaneous WD system such as has been described, is very expensive.

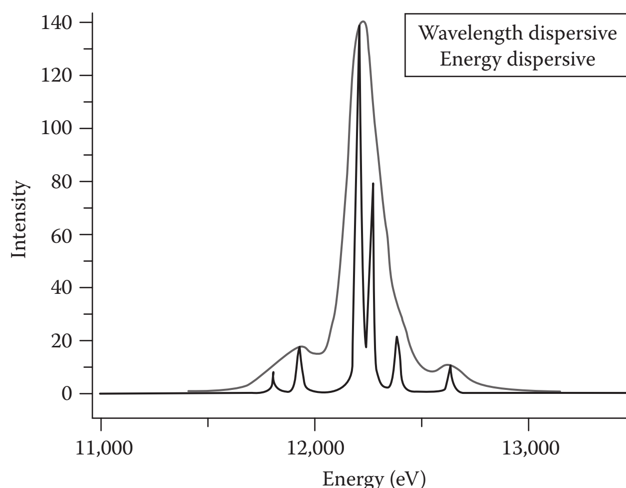


**Figure 8.47** Comparison of the resolution of EDXRF and WDXRF systems. WDXRF provides higher resolution than EDXRF. (© 2013 HORIBA, Ltd. www.horiba.com. All rights reserved.)

### 8.2.8 XRF Applications

When a sample is placed in a beam of X-rays, atoms in the sample are excited by the X-rays and emit X-rays of *characteristic* wavelengths/energies from the elements in the sample. This process is called *XRF*. Since the wavelength (energy) of the fluorescence is characteristic of the element being excited, measurement of this *wavelength or energy* enables us to *identify* the fluorescing element. Tables of X-ray lines are given in the appendices of this chapter. The *intensity* of the fluorescence depends on *how much* of that element is in the sample. For most laboratory XRF equipment, the energy of the emitted X-ray is independent of the chemical state of the element; therefore, XRF is generally considered to be an elemental analysis method. Solid and liquid samples can be analyzed directly.

Modern WDXRF instruments permit the determination of all elements from fluorine ($Z = 9$) to uranium ($Z = 92$). Some WDXRF systems allow measurement of elements from Be to U. Benchtop EDXRF instruments can determine elements from sodium ($Z = 11$) to uranium ($Z = 92$); with a special SDD detector, it is possible to measure from fluorine to uranium. Handheld EDXRF units with SDD detectors can measure from magnesium ($Z = 12$) to uranium, and Si-PIN units can do the same with vacuum or He purge.

Elements with atomic numbers between Mg ($Z = 12$) and U ($Z = 92$) can be analyzed in air. Elements with atomic numbers 3 (beryllium) through 11 (sodium) fluoresce at long wavelengths (low energy), and air absorbs the fluorescence. Analysis of this group must be carried out in a vacuum or in a helium atmosphere.

WDXRF units usually operate primarily under vacuum and use a helium atmosphere for loose powder samples and liquid samples. Benchtop EDXRF and micro-XRF systems can operate under vacuum, helium, or air, based on the configuration. Handheld or portable units generally operate in air at atmospheric pressure.

The DLs are in the ppm range for most elements with a wide linear working range. XRF thus permits multielement analysis of alloys and other materials for major, minor, and trace elements. Sensitivity is poorest for the low Z elements and best for the high Z elements. XRF capabilities are dependent on the technique (ED or WD used) as well as the power and other design variables of the actual instrument employed.

### *8.2.8.1 Analyzed Layer*

Both solid and liquid samples can be analyzed by XRF as described earlier in the chapter. With the exception of micro-XRF, XRF is considered to be a “bulk” analysis technique. This means that the analysis represents the elemental composition of the entire sample, assuming the sample is homogeneous. The term “bulk” analysis is used to distinguish such techniques from “surface analysis” techniques (Chapter 14), which look at only a very thin layer at the sample surface. But there are conditions that must be considered in XRF in order to obtain accurate results. The limiting factor for direct XRF analysis or the analysis of prepared samples is that the signal of the characteristic radiation from the sample originates from different layers within the sample.

The excited radiation inside the sample will need to travel out of the sample before it can be detected by the detector. Assuming a constant density for the sample, lower-energy characteristic radiation will only exit from relatively close to the surface, whereas higher-energy radiation will be detectable from increasingly deeper layers of the sample. Figure 8.48 illustrates the concept.

XRF is a *surface-sensitive* technique because the depth of penetration and the thickness of the analyzed layer depend on the exciting radiation and the sample composition (atomic number).

The analyzed layer is a function of the characteristic energy of the emission line being measured as well as the density and composition of the sample. The effect is based on absorption of the excited radiation. The effective analyzed layer is also dependent on the geometry of the instrument. The effective analyzed layer is usually defined as the layer from which either 50% or 90% of the signal originates.

To better understand the implications for accurate XRF determinations of composition, Table 8.9 shows selected characteristic $K_{\alpha}$ emission lines and shows the analyzed layer depth (90% signal) for various matrices, which increase in density from the left to the right. Note that the table uses a typical “shortcut” for line notation: KA1 instead of $K_{\alpha_1}$ and the energies of the lines are expressed in keV. Some examples of the use of this table are presented.

Considering the S $K_a$ emission line, in a graphite matrix, the emission is detectable from a depth of 116 μm in the sample, but that depth is reduced to 14.8 μm in a silicate glass matrix and reduced even more in the dense matrices of iron and lead. This means that if the sulfur in the glass sample

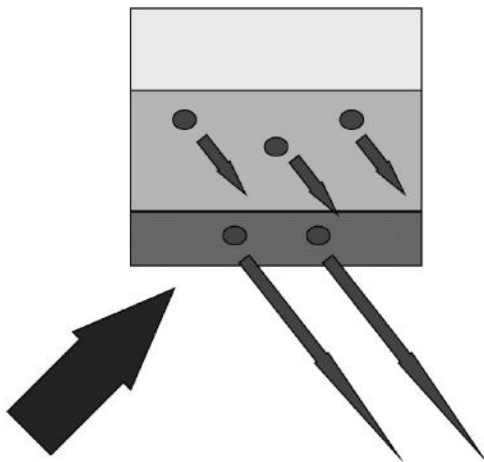

**Figure 8.48** Illustration of the analyzed layer from the sample: The incoming primary radiation excites the lower and middle parts of the sample as shown but does not excite the upper part since the sample is infinitely thick for the primary radiation. The excited characteristic radiation from the element in the middle part is reabsorbed within the sample. Only the signal from the layer near the surface is able to be detected by the detector.

**Table 8.9 X-Ray Emission Lines and Depth of the Analyzed Layer in Various Matrices**

| Line | Energy | Graphite | Glass | Iron | Lead |
|---|---|---|---|---|---|
| Cd KA1 | 23.17 keV | 14.46 cm | 8.20 mm | 0.70 mm | 77.30 μm |
| Mo KA1 | 17.48 | 6.06 | 3.60 | 0.31 | 36.70 |
| Cu KA1 | 8.05 | 5.51 mm | 0.38 | 36.40 μm | 20.00 |
| Ni KA1 | 7.48 | 4.39 | 0.31 | 29.80 | 16.60 |
| Fe KA1 | 6.40 | 2.72 | 0.20 | | 11.10 |
| Cr KA1 | 5.41 | 1.62 | 0.12 | 104.00 | 7.23 |
| S KA1 | 2.31 | 116.0 μm | 14.80 μm | 10.10 | 4.83 |
| Mg KA1 | 1.25 | 20.00 | 7.08 | 1.92 | 1.13 |
| F KA1 | 0.68 | 3.70 | 1.71 | 0.36 | 0.26 |
| N KA1 | 0.39 | 0.83 | 1.11 | 0.08 | 0.07 |
| C KA1 | 0.28 | | 0.42 | 0.03 | 0.03 |
| B KA1 | 0.18 | 4.19 | 0.13 | 0.01 | 0.01 |

lies much deeper than 14.8 μm from the surface of the sample, it will not be detected because the radiation cannot escape from the matrix. Conversely, this means that to measure sulfur in glass accurately, the top 14.8 μm of the sample must be homogeneous and representative of the sulfur concentration throughout the glass; in graphite, the top 116 μm of the sample must be homogeneous. The XRF analyst needs to ensure that the analyzed layer is *representative* of the entire sample. This might require intensive sample preparation to ensure that in a powdered sample, the "grain" or particle size is well below the size of the analyzed layer. Table 8.10 shows this issue for a limestone sample with no binder.

The preparation of the sample needs to be designed to ensure that the analyzed layer is representative of the sample. This has implications mainly for solid samples such as minerals where the sample needs to be pulverized to be made homogeneous with the resulting grain size less than the analyzed layer of the lightest element to be determined. As can be seen in Table 8.10, the magnesium emission originates from a depth of only 7 μm. To grind a sample to particle diameters substantially below 7 μm while keeping the sample homogeneous is extremely difficult.

A coal sample (which we can approximate by using the graphite data in Table 8.9) would need to be about 14.5 cm thick to measure 90% of the Cd $K_\alpha$ signal. Since most benchtop or laboratory

**Table 8.10 Analyzed Layer Thickness of NIST 88B Dolomite Sample for Various Elements**

| Compound | Line | Concentration (%) | Energy (keV) | Layer Thickness (μm) |
|---|---|---|---|---|
| $Fe_2O_3$ | Fe KA1 | 0.722 | 6.40 | 174 |
| MnO | Mn KA1 | 0.016 | 5.89 | 139 |
| $TiO_2$ | Ti KA1 | 0.016 | 4.51 | 66 |
| CaO | Ca KA1 | 30.12 | 3.69 | 104 |
| $K_2O$ | K KA1 | 0.103 | 3.31 | 77 |
| $SO_3$ | S KA1 | 0.000 | 2.31 | 27 |
| $P_2O_5$ | P KA1 | 0.004 | 2.01 | 19 |
| $SiO_2$ | Si KA1 | 1.130 | 1.74 | 13 |
| $Al_2O_3$ | Al KA1 | 0.277 | 1.49 | 8 |
| MgO | Mg KA1 | 21.03 | 1.25 | 7 |
| $Na_2O$ | Na KA1 | 0.029 | 1.04 | 4 |
| $CO_2$ | | 46.37 | | |

units can only load samples with a maximum thickness of 5 cm, one has to ensure that all samples, standards, and reference samples are prepared with identical thickness.

#### *8.2.8.2 Sample Preparation Considerations for XRF*

While general sample preparation approaches were covered in Chapter 1, as seen from the examples earlier, XRF sample preparation requires some thought as well as an understanding of the chemical and physical properties of the sample material. Samples must be representative of the material to be analyzed. They must fit the sample holder being used and completely cover the opening in the sample holder or be larger than the measurement spot size being used.

Very flat surfaces are required for quantitative analysis, as discussed subsequently. Liquid samples flow naturally into flat surfaces, but cannot be run under vacuum. Liquid samples are usually run in a polymer cup with a sleeve or ring to hold a polymer film in place over the liquid. The film needs to be mechanically stable, chemically inert, and as thin as possible to allow transmission of radiation, especially for the low Z elements. Elements with atomic numbers less than Na cannot be detected through polymer films. As discussed in Section 8.2.2.3, liquid samples and loose powders are best run in a facedown configuration for greatest accuracy, that is, the source should be below the sample. The best solvents for samples that must be dissolved for analysis are $H_2O$, $HNO_3$, hydrocarbons, and oxygenated carbon compounds, because these compounds contain only low atomic number elements. Solvents such as HCl, $H_2SO_4$, $CS_2$, and $CCl_4$ are undesirable because they contain elements with higher atomic numbers; they may reabsorb the fluorescence from lower Z elements and will also give characteristic lines for Cl or S. This will preclude identification of these elements in the sample. Organic solvents must not dissolve or react with the film used to cover the sample.

Solid samples may be prepared using several techniques. Solid samples that can be cut and polished to give a flat surface can be analyzed after polishing. Care must be taken not to contaminate the sample with the cutting tool or polishing compound. For example, cutting a flat piece of polymer with a steel razor blade can result in iron being detected in the polymer sample. Other solids should be ground to a powder, preferably using a ball mill or similar device to pulverize the sample. Again, the grinding tools must not contaminate the sample, so boron carbide is often used to contain and grind samples. The sample powder may be pressed "as is" or mixed with lithium borate salt, borax, wax, or other suitable "binder" and formed into a briquette or disk. This procedure provides a sample that can be easily handled and has the advantage that the borate salts and hydrocarbon binders provide a standard matrix for the sample. Furthermore, the matrix is composed of low atomic weight elements, which interact only slightly with the X-ray beam. In addition, the disks or pellets are pressed to a uniform thickness, as is required for accurate analysis. Figure 8.49 presents a summary of the various sample preparation techniques used for XRF analysis and shows some types of sample holders used.

Minerals in particular present challenges to grinding and achieving a uniform grain size due to the complex composition of mineral samples, a problem known as the mineralogical effect.

It may not be possible to grind a sample to achieve ideal grain size. The next best approach is to ensure that the grinding process results in a repeatable grain size in the samples to be analyzed. The sample grain size must be similar to the grain size in standards and reference materials used in the analysis. This may require different grinding procedures for different materials. Integrating over a larger sample by spinning the sample over the beam or making multiple measurements enables the analyst to average the analyzed layer and obtain more repeatable data. These approaches will create methods that work but may limit the accuracy of the measurement and applicability of the method.

The ultimate preparation is to remove the "grains" from the sample to enable accurate and efficient analysis of multiple types of materials. The best approach is to mix the sample and salts

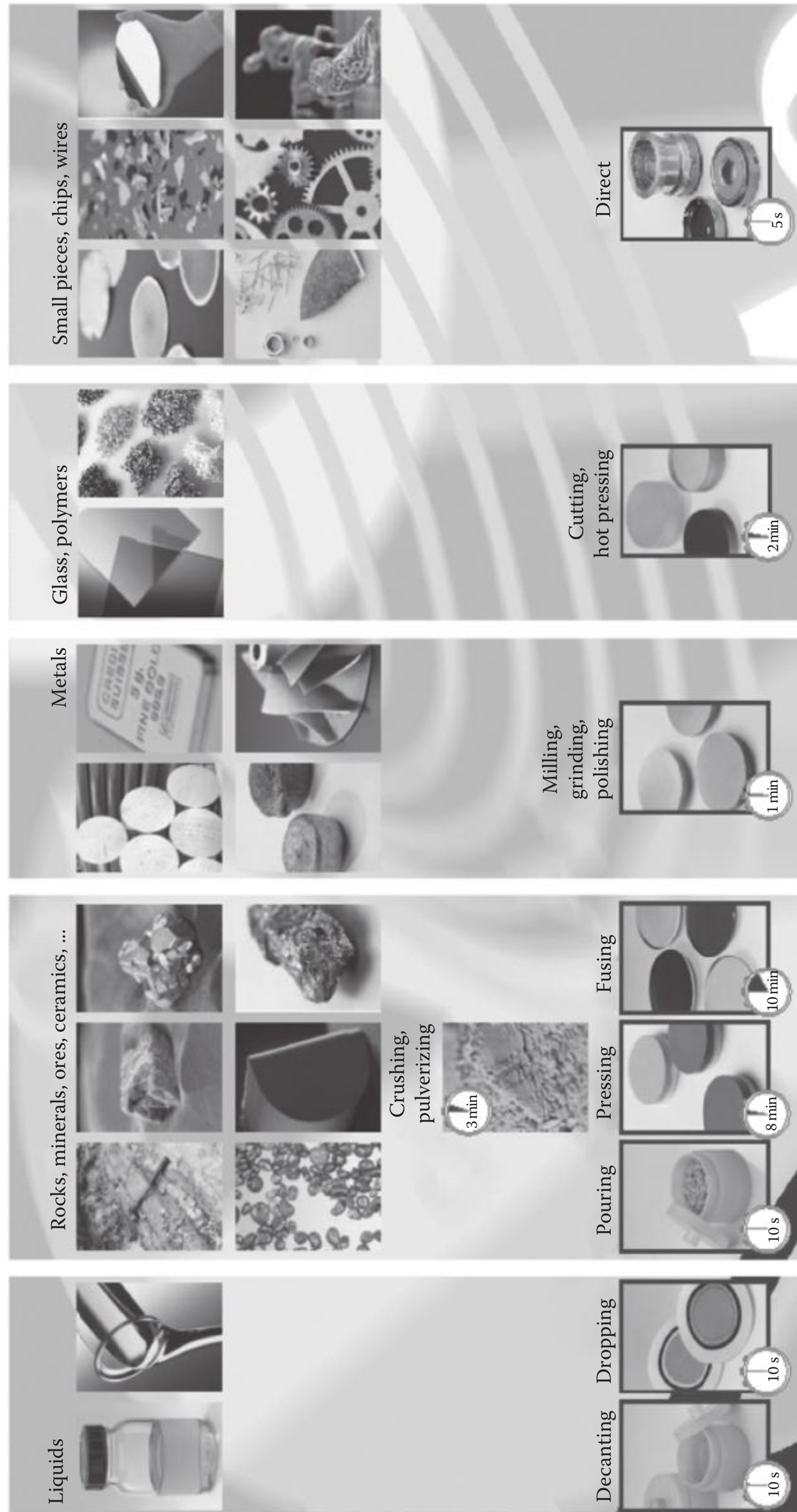


**Figure 8.49** Sample preparation techniques and sample holders for XRF analysis.

such as lithium metaborate or lithium tetraborate and heat the mixture in a Pt crucible over high heat. The process is called fusion and is shown in the photographs in Figure 8.50a through c. The heat melts the sample and salt, and the molten mixture is poured into a Pt/Au mold with a flat bottom. When the melt is allowed to cool, a glassy flat "fused bead" is formed, suitable for quantitative XRF analysis with the advantage that the matrix and sample thickness is now the same for all samples. Fusion is usually required for analysis of geological samples to eliminate mineralogical effects, for example. Calibration standards are prepared by fusing known amounts of the analyte with the borate salt and casting standard beads. Automated fusion devices, called fluxers, are available, as are a wide variety of devices for grinding and powdering samples. A handbook of XRF sample preparation methods and equipment, with pictures of the various fluxers, crucibles, molds, and grinders, is available from Spex Certiprep at www.spexcsp.com. Videos and links to online sample preparation resources from Claisse® (www.claisse.com) are available on their website. A short video of automatic sample fusion using the Claisse M4 fluxer can be seen at: http://www.youtube.com/watch?v=pSMAbFMZ1Ko. The use of 6 position commercial fluxers allows the preparation of 20–30 fusion beads/h, faster and more accurately than the manual method shown in Figure 8.50.

Since the physics of X-ray emission is governed by the sample and not by the instrumentation, special care needs to be applied to the use of handheld and portable XRF in the direct analysis of field samples that have not been "prepared." Especially for the low Z elements, one needs to understand that these only emit from very close to the sample surface. The calibration of the analyzer must be tuned to the preparation or presentation of the sample. If not done correctly (or not done at all), the values obtained from the analyzer will be incorrect.

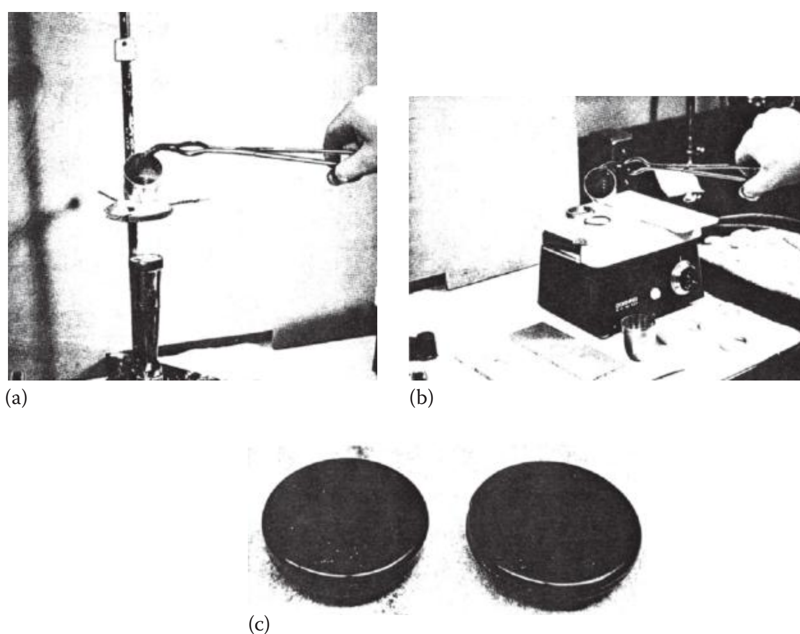


**Figure 8.50** Preparing a fusion bead for analysis. (a) The sample and a salt such as lithium tetraborate are heated until liquid in a Pt crucible over a burner. The crucible tongs are tipped with Pt to avoid contamination of the crucible. (b) The molten mixture is poured into a mold, in this case, a ring placed on a smooth marble slab. (c) Cooled beads removed from the molds. The flat bottom surface, shown turned up, is the side used for analysis. (From Jenkins, R. et al., *Quantitative X-Ray Spectrometry*, Marcel Dekker, Inc., New York, 1981. Used with permission.)

#### *8.2.8.3 Qualitative Analysis by XRF*

Each element fluoresces at its own characteristic wavelengths (energies); the fluorescing element can be identified from a table of wavelengths (energies) such as those in Appendix 8.A. An example of qualitative analysis is shown in Figure 8.51. The EDXRF spectrum is that of a zinc-coated iron washer. The spectra are much simpler than those from atomic emission spectrometry. Fe gives hundreds of strong emission lines in an inductively coupled plasma (ICP) or direct current (DC) arc emission experiment; here, only two lines are seen for Fe in this XRF spectrum. The coated washer also shows Zn, which is fully resolved.

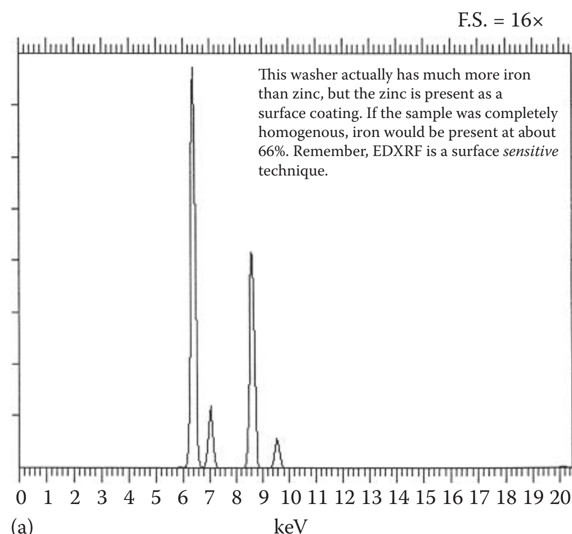


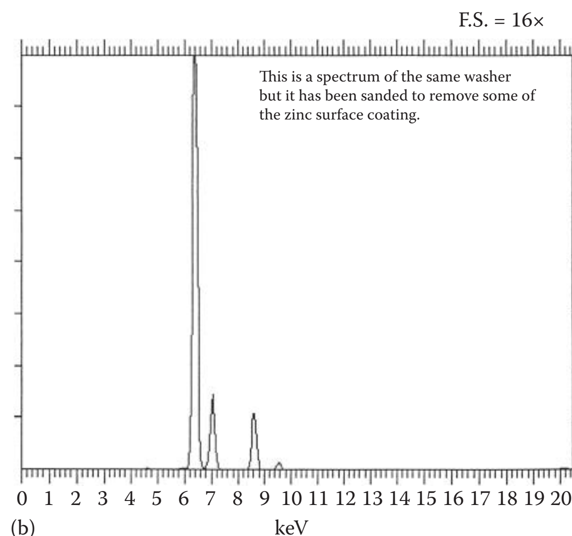


**Figure 8.51** Qualitative EDXRF spectrum of a zinc-coated iron washer. (a) The coated washer. The peaks present are, from left to right, Fe $K_\alpha$, Fe $K_\beta$, Zn $K_\alpha$, and Zn $K_\beta$. (Confirm these peaks by looking in Table 8.A.2.) (b) The same washer, but after sanding to remove some of the surface. Note the decrease in the intensity of the Zn peaks and the increase in the Fe peaks. These spectra were collected for 50 s with an Rh tube at 30 kV and 0.01 mA, under vacuum, using a filter to remove the X-ray tube lines. (© Thermo Fisher Scientific. www.thermofisher.com. Used with permission.)

Even with the relatively simple spectra, spectral interference does occur in XRF. The major sources of spectral interference are scattered radiation from the tube, higher-order lines diffracted in a WD system, and L lines of higher atomic number elements overlapping K lines of lower atomic number elements. Two examples are given in Figure 8.52. The peaks in each spectrum are labeled, but you should use the tables in Appendix 8.A to confirm that they have been labeled correctly and to give yourself some practice in figuring out what elements are present from the energy positions of the peaks. The top spectrum shows the overlap of the spectral lines from pure Fe and pure Mn; the spectral interference occurs between the Fe $K_\alpha$ and Mn $K_\beta$ peaks. The peak maxima are not at exactly the same energy, so in a mixture or alloy of the two elements, the Fe $K_\alpha$ line can be identified, and if the Mn content of a mixture or alloy were high, the Mn $K_\beta$ peak might appear as a shoulder on the Fe $K_\alpha$ peak. The overlap is not critical in a two-component system; as you can see, the unobstructed Mn $K_\alpha$, the strong Fe $K_\alpha$, and the unobstructed Fe $K_\beta$ peaks can easily identify the presence of both elements.

The ratio between the $K_\alpha$ and $K_\beta$ line of an emission is fixed and tabulated for every element. A $K_\beta$ emission is *always* accompanied by a $K_\alpha$ emission. Similarly, an $L_\beta$ emission is always accompanied by an $L_\alpha$ emission. Keep these facts in mind when examining an XRF spectrum.

The bottom spectrum in Figure 8.52 is that of a more complex alloy containing Cr, Mn, Fe, Co, Ni, and W. Qualitatively, it is easy to see that Cr, Fe, W, and Co are present. Cr and W have unobstructed lines that tell us they are in the alloy. Fe is clearly present, because if there is any Mn, it must be in low concentration compared to the Cr and Fe. The Mn $K_\alpha$ peak overlaps the Cr $K_\beta$ peak; we know there is Cr present from its $K_\alpha$ peak, so some (at least) of the intensity of the small peak

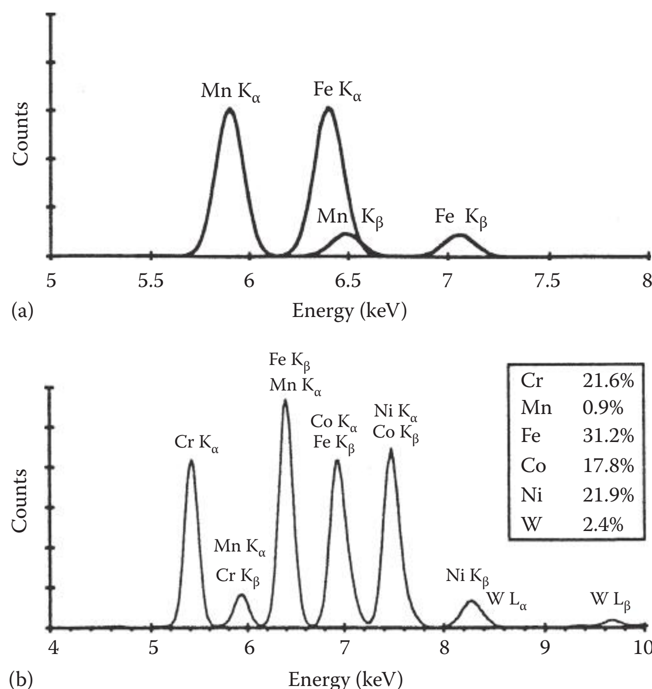


**Figure 8.52** Spectral overlap in EDXRF spectra. (a) A simple overlap demonstrated by overlaying the spectra of pure Fe and pure Mn. There is overlap of the Fe $K_\alpha$ line with the Mn $K_\beta$ line. (b) The spectrum of a multielement alloy showing multiple spectral interferences due to line overlaps. Despite the overlaps, knowledge of the relative line intensities permits qualitative identification of most of the elements present.

at 5.8 keV is due to Cr. If Mn is present but in low concentration, then most of the intensity at about 6.4 keV is from Fe, since the Mn $K_\beta$ peak is much smaller than its $K_\alpha$ peak, as seen in the top spectrum. Looking at the peak to the right of the Fe $K_\alpha$ peak, we see a much bigger peak than would be expected from Fe $K_\beta$ alone. (Compare the Fe peak heights in the top spectrum.) Therefore, most of the peak at about 6.9 keV must be from Co $K_\alpha$. That indicates that Co is present in the alloy. From the Mn and Fe peak ratios in the top spectrum, it is reasonable to assume that the Co $K_\beta$ peak is less intense than the Co $K_\alpha$ peak. But the peak at approximately 7.5 keV, about where we would expect the Co $K_\beta$ peak, is actually more intense than the Co $K_\alpha$ peak (and the "Co $K_\alpha$" peak intensity also includes some interfering Fe $K_\beta$ intensity). Therefore, the high intensity of the 7.5 keV peak tells us we have another element, Ni, in the alloy. The one element that is not clearly present is Mn; the intensity ratio for the two Cr lines needs to be ascertained. If the "Cr $K_\beta$" peak is too high relative to the $K_\alpha$ peak, then Mn is probably in the alloy as well. So even though only two elements, Cr and W, have lines with no spectral interference, knowledge of the relative intensities of lines allows us to state with certainty that Fe, Co, and Ni are present, and that Mn may be present in low concentration. We will come back to this spectrum in the discussion of quantitative analysis by XRF. Modern instrument software generally displays the position and relative heights of the lines of each element, superimposed on the collected spectrum.

The spectrum shown in Figure 8.53 is a more complex spectrum of a duplex steel sample, containing Cr, Mn, Fe, Cu, Ni, and Mo. Note that the instrument software automatically shows element line positions and identity. The emission line from the Rh tube can be seen in the spectrum. There is also an emission line from argon. (Look at the figure caption. Can you suggest where the argon comes from?)

To analyze a spectrum to determine what elements are present, identify the strongest (most intense) line first and then continue with the next most intense lines. Look for the tube emission line and any lines that may come from air. Lines that do not match an element line may be scatter lines from the tube, an escape peak, or a sum peak.

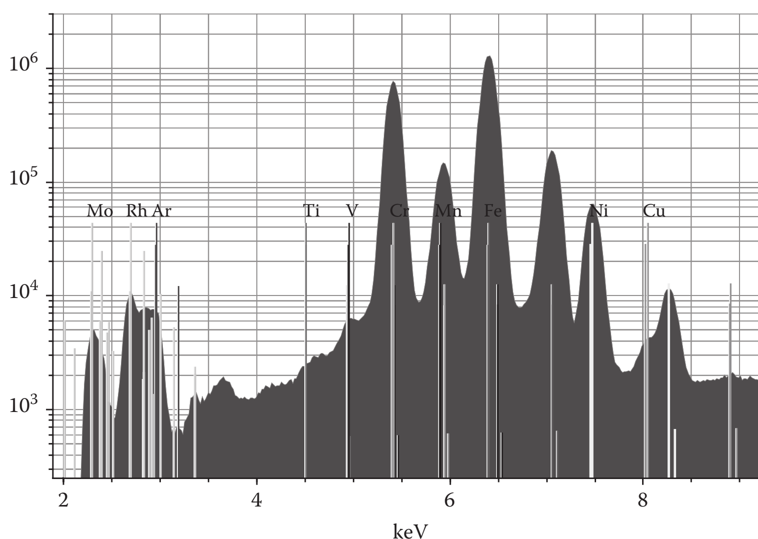


**Figure 8.53** XRF spectrum of a duplex steel sample. Handheld XRF (HH XRF) measurement under air, 15 s, using a Rh tube at 15 kV. (Courtesy of Bruker Elemental, © 2013 Bruker, Inc. www.bruker.com. Used with permission.)

The XRF method is nondestructive, an important feature when the sample is available in limited amounts or when it is valuable or even irreplaceable, as in the case with works of art, antiques, rocks from the moon, or forensic samples. The nondestructive nature of XRF coupled with the fact that sample preparation may not be required means that direct multielement analysis can be performed *in situ*. Portable HH XRF analyzers are used in the field by geologists to study soil and minerals, to sort metal scrap, glass, and plastics at recycling centers, for quality control in steel plants, and to check incoming lots of material before unloading a ship or a truck (Figure 8.54).

Another large handheld application segment is in positive material identification (PMI) where, similar to scrap sorting, the sample is identified as a specific alloy or material. PMI ensures that, for example, the repair of a crucial pipe in a hazardous material-containing process is only performed using the correct and certified material. After a catastrophic accident in a Texas refinery, PMI inspection of components carrying hazardous products was made mandatory. This mandate is easily accomplished on site using HH XRF instrumentation.

Antiques, jewelry, gems, and art objects can be characterized. Original art and copies of masterpieces can be distinguished from each other based on elemental composition and layering of pigments. Natural gems can be distinguished from synthetic gems in many cases, because the laboratory synthesis often adds specific elements not usually found in the natural gems or may even produce gems with fewer trace elements than real gems. Plated jewelry can be distinguished from solid gold or solid silver jewelry. Museums rely heavily on this method for examining works of art. The sample

**Figure 8.54** Scrap metal sorting using the TITAN, an HH XRF analyzer, to identify elemental composition. (Courtesy of Bruker Elemental, © 2013 Bruker, Inc. www.bruker.com. Used with permission.)

is usually unaffected physically or chemically by the analytical process. Usually low-power EDXRF or micro-XRF units are used for this application, and some units have dedicated software for particular applications. It is possible for some sensitive materials like paper or plastics to turn yellow or brown upon prolonged exposure to X-rays, so low power and short analytical times are used for these materials.

Forensic samples are often very small and inhomogeneous. As discussed later, it is difficult to perform quantitative analysis on such samples. However, it is possible to use qualitative XRF to good advantage. Using the spectral "fingerprint" of a sample does not require exact concentrations to be determined. By proving that a spectrum of soil found in a shoe matches the spectrum of soil from the location of a crime scene, it is possible to place the object at that scene.

Examples of the use of nondestructive spatial investigation of element distribution of artworks, archeological items, pharmaceutical products, and other samples using micro-XRF are available on several instrument companies' websites, including Bruker, Horiba Scientific, SPECTRO, and Unisantis. A few examples will be discussed.

An altarpiece from 1424 AD, the Göttingen Barfüßer altarpiece, was examined using a Bruker ARTAX® μ-XRF spectrometer (Bruker Nano GmbH, www.bruker.com). Thin layers of gold and silver approximately 1 μm thick were examined by single-point measurements with a W target tube and a 0.65 mm collimator. Layers of pure silver, historical gold alloys like "green gold" containing 30% Cu, and layers of Au and Ag hammered together ("Zwischgold") were identified. Studies of two colored copperplate engraving copies of a famous work by Albrecht Dürer using the ARTAX® μ-XRF system showed that the pigments used in one copy were consistent with it being painted in the sixteenth century, while the second copy contained pigments that were not in use until the 1800s (Gross; Hahn et al.). With the same system equipped with a Mo source and polycapillary lens, 2D mapping of a $2 \times 2.5$ mm piece of fabric with gunshot residue permitted identification of particles $\geq 10$ μm in diameter. The particle distribution pattern across the fabric allowed the determination of the angle of incidence of the gun shot.

A key area that benefits from micro-XRF is the pharmaceutical industry where tablet imaging can determine active pharmaceutical ingredient (API) distribution, mixing uniformity, contamination and interbatch concentration fluctuations. The ability to pinpoint single microscopic particles and identify them is very important in ocular and intravenous (IV) formulations, which must meet stringent particulate concentration limits. An example of the use of micro-XRF in mapping a pharmaceutical tablet is shown in Figure 8.55.

Other pharmaceutical applications for micro-XRF can be found at www.horiba.com/scientific/products/X-ray-fluorescence-analysis/applications/pharmaceutics/.

The Unisantis XMF-104 X-ray microanalyzer (Unisantis S.A., www.unisantis.com) was used by researchers at the Institute for Roentgen Optics, Moscow, Russian Federation, to examine nondestructively the composition of ancient coins from the fourth century BC through the second century AD. The fourth century BC coins were found to be an alloy of 82% Ag/18% Cu, but areas of pure Ag showed the inhomogeneity of the alloy. A drachma coin depicting Alexander was composed of 99% Ag/1% Cu. The XMF-104 system had a 50 W Mo tube, a 2-stage Peltier-cooled compact Si-PIN detector and polycapillary focused X-ray beam with a 50–250 μm focal spot. Spectra, images of the coins, and details are available at www.unisantis.com, application note 605.

#### *8.2.8.4 Quantitative Analysis by XRF*

Quantitative analysis can be carried out by measuring the intensity of fluorescence at the wavelength characteristic of the element being determined. The method has wide application to most of the elements in the periodic table, both metals and nonmetals and many types of sample matrices. It is comparable in precision and accuracy to most atomic spectroscopic instrumental techniques. The sensitivity limits are on the order of 1–10 ppm, although sub-ppm DLs can be obtained for the

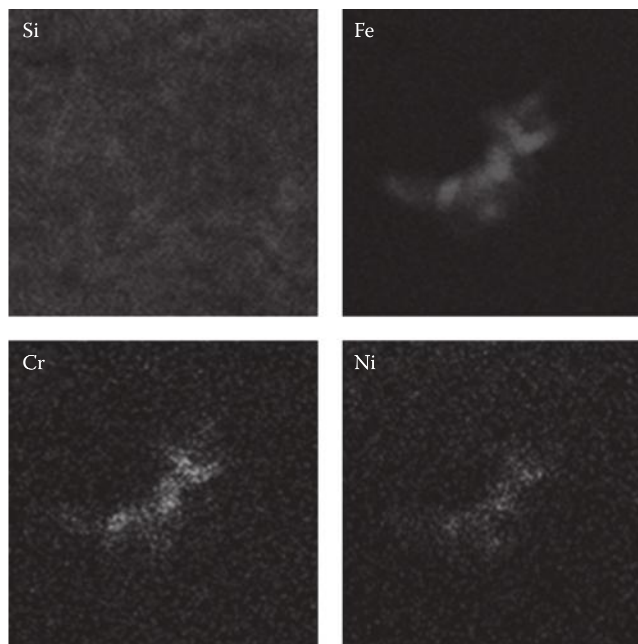


**Figure 8.55** Mapping across a pharmaceutical tablet allows a buried steel particle to be visualized and identified. Contaminants such as this can be introduced from the manufacturing process and are typically caused by wear debris from mechanical mixing/compressing equipment. (© 2013 HORIBA Scientific. www.horiba.com/scientific. All rights reserved.)

heavier Z elements under appropriate conditions. Accuracy depends on a thorough understanding of the sample heterogeneity, the sample matrix, and the absorption and fluorescence processes.

X-rays only penetrate a certain distance into a sample, and the fluorescing X-rays can only escape from a relatively shallow depth (otherwise, they would be reabsorbed by the sample) as we have seen. While XRF is considered a "bulk" analysis technique, the X-rays measured are usually from no deeper than 1000 Å from the surface. True surface analysis techniques such as Auger spectroscopy only measure a few angstroms into the sample, so in that respect, XRF does measure the bulk sample, but only if the surface is homogeneous and representative of the entire sample composition.

The relationship between the measured X-ray intensity for a given peak and the concentration of the element can be written

$$C = K(I)(M)(S) \tag{8.19}$$

where $C$ is the concentration of the element. The factor $K$ is a function of the spectrometer and the operating conditions. $I$, the intensity of the measured signal, is the net intensity after subtraction of the background. $M$ represents interelement effects such as absorption and enhancement effects. Interelement effects must be corrected for or minimized to obtain accurate concentration values. $S$ is the sample preparation term (also called the sample homogeneity term) and describes the difference between the reference sample with which $K$ was obtained and the sample being measured. The classical approach to quantitative analysis is to use an external calibration curve. A set of standards at various concentrations is prepared in a manner similar to the sample preparation, intensity is carefully measured for all standards and samples using the same instrumental conditions, and a plot of $C$ versus $I$ is made. $M$ and $S$ are considered to be constant (a good assumption only if the standards reflect the matrix and particle size distribution of the samples). Precision depends only on

careful measurement of intensity; accuracy depends on the elimination or evaluation of *M*, the interelement effects, and the elimination of *S* by using the same preparation of standards and unknowns.

Peak and background intensities are measured by counting photons at the appropriate wavelengths/energies. The net intensity is obtained via background correction. The process of background correction differs between EDXRF and WDXRF. In WDXRF, a fixed position close to the emission line to be measured needs to be identified. This position needs to be free of other emission lines, which could occur in the sample. It is usual to perform a scan where the signal as a function of diffraction angle 2θ is obtained. From this scan (spectrum), a background is mathematically obtained by fitting a numerical function (e.g., a polynomial) using a user-defined minimization based on least squares. Once the background is determined, the remainder of the spectrum is the net intensity from the sample. In EDXRF, the area of the peak is used for quantification; in WDXRF, the peak height is used. In ED systems, background subtraction is usually performed. The background is very matrix dependent in XRF, so background correction is more difficult than in other types of spectroscopy.

Calibration methods include the use of external standards and may include the use of ISs to improve precision. The IS may be an added element or elements not present in the sample, but this is a very time-consuming endeavor, both in making the standards and samples and in measuring all the lines. Frequently, the scattered radiation from the X-ray tube is used as an IS; this is a reasonable approach because the scattered radiation (background) is very dependent on the sample matrix. The ratio of analyte line to scattered radiation results in better precision than the measurement of the analyte line alone. XRF calibration used to require a set of accurate standards, as well as certified reference materials (CRMs) for verification of the accuracy and precision of the analysis. Depending on the range of materials that require analysis, laboratories can spend a great deal of money on the highly pure elements, compounds, and reference materials required for calibration and sample preparation.

A variety of mathematical approaches to the correction of absorption-enhancement effects and calibration is now in use, due to the availability of inexpensive, powerful computers and powerful software programs. One approach is the **fundamental parameters (FP) method**.

Using a set of pure element samples or well-certified multielement reference materials, the *M* factor for each element (Equation 8.19) can be calculated using the fundamental parameters describing the primary spectral distribution (tube spectrum), effective mass absorption of the primary and secondary radiation, and the fluorescent yield for each element. The *M* factor represents the effect the "other" elements have on the analyte element. The parameters used assume that the sample has a planar surface and is homogeneous and infinitely thick (no transmission of X-rays through the sample). This approach enables wide ranging "universal" calibrations to be established for metals and alloys, such as a FeCrNiCo base curve for WDXRF or dedicated calibrations for cement, glass, and so on.

These universal calibrations or standardless calibrations can now be found on any commercial XRF. They are still based on a calibration of a larger set of samples, but this is usually performed at the instrument manufacturer's factory and the calibration transferred to the unit. From the user's point of view, quantitative analysis is standardless since no calibration standards or standard reference materials (SRMs) are required. These calibrations allow for good accuracy if the samples are homogeneous, flat and infinitely thick, or described in terms of thickness and weight to allow for corrections. Universal calibrations will fail when the sample is inhomogeneous. Results become more "semiquantitative" as samples become smaller and less homogeneous. Forensic samples and failure analysis samples may be small, nonplanar, and not particularly homogeneous. For forensic analysis, one does not compare concentrations but the ratio of the net signal, or one tries to match the spectral "fingerprint."

Most commercial XRF systems have a fundamentals parameters software program as part of their data processing package. The advantage to the FP approach is that many industrial materials do not have readily available matrix-matched calibration standards commercially available. Preparation of good, stable calibration standards takes a lot of time and money even when it is possible to make

such standards. Even when well-defined standards are available commercially, as they are for steels, brasses, bronzes, nickel-based superalloys, and many other types of alloys, as well as some glasses and ceramics, the standards are expensive and must be handled carefully to avoid scratching or contaminating their surfaces. Sources for prepared XRF standards include government standards agencies such as NIST in the United States, as well as commercial firms. Although this standardless software approach has improved dramatically in accuracy over the years, the analyst should, when possible, verify the accuracy of any mathematical approach with known materials that reflect the samples being analyzed. More information on these approaches can be found in several of the introductory XRF texts (e.g., those by Bertin, Jenkins et al., and Herglotz and Birks listed in the bibliography).

Modern WDXRF systems can measure the entire periodic table in less than 20 min and calculate the composition of a complete unknown using an FP program. Using a “fast scan” approach, a semiquantitative analysis can be obtained in less than 2 min of measurement time. Handheld EDXRF systems with SDD detector technology require less than 5 s to identify a standard alloy and about 20–30 s to identify an aluminum or magnesium alloy.

When quantitative analysis is needed on complex samples with peak overlaps, a method of extracting the individual intensities of each element is needed. These mathematical corrections are now performed in instrument data processing software and may include overlap corrections, interelement corrections, matrix corrections, corrections for non-Gaussian peak shapes, and different statistical fitting routines. A combination of these corrections was used to determine the concentration of the elements in the alloy shown in Figure 8.53. The HH measurement of a 2205 type duplex steel sample took less than 15 s.

#### *8.2.8.5 Applications of Quantitative XRF*

Quantitative XRF is used in virtually every industry for almost any type of liquid or solid sample. XRF is used daily to analyze minerals, metals, paper, textiles, ceramics, cement, polymers, wood, environmental samples, food, forensic samples, cosmetics and personal care products, and more. Only a few examples will be given here.

The petroleum industry uses XRF to measure sulfur in fuels, the elemental composition of catalysts used to “crack” petroleum hydrocarbons, and lubricating oil additives. The sulfur in oil or fuel application is driven by the US federal government clean air regulations. Diesel fuel, for example, is required to contain less than 15 ppm S. Refineries, pipeline operators, and commercial and government labs need to be able to certify sulfur content to ensure fuel classification and compliance. There are procedures published by American Society for Testing and Materials (ASTM) to ensure minimum performance for accuracy and precision: ASTM D2622 for WDXRF, ASTM D4294 for direct excitation EDXRF, and D7220 for polarized (3D) EDXRF. The performance and DLs for the methods are different, but all enable the user to be able to comply with the regulatory requirements. Refineries often choose WDXRF due to the higher accuracy and precision achieved in about 3 min of measurement when compared to EDXRF.

Petroleum hydrocarbon cracking catalysts usually contain more than 12 elements, including transition metals, rare earth elements (REEs), and alkali and alkaline earth elements at concentrations varying from 0.005 to 35 wt%. The composition of the catalyst can be determined accurately after fusion into borate beads; the total analysis takes up to 1 h. The procedure and approach is described in ASTM D7085. Lubrication oil blenders use EDXRF to check their blends and ensure that control samples from “lube” shops are what the products claim to be (ASTM D6481 outlines the procedure).

Used engine oil used to be monitored routinely for metal content, since the metal content indicated how parts of the engine were wearing away in use. The wear metals analysis indicated what parts needed to be replaced during maintenance. Analysis also enables extension of the oil life by verifying that there is still enough P, Ca, or Zn in the oil to function correctly. This analysis could be performed by XRF or by atomic emission spectrometry (e.g., ICP or DC plasma (DCP) emission).

However, filters in modern engines are now so efficient at trapping wear metal particles that the analysis of oil is no longer a good indicator of engine wear. Micro-XRF is now used to measure the metals on the filters themselves to predict engine failure and part replacement by quantifying and analyzing the individual particles from the filter.

In metallurgy, alloy composition can be rapidly determined and unknown samples identified rapidly. XRF has an advantage over wet chemistry in that all the components can be measured due to the wide dynamic range of XRF. For example, in the analysis of nickel alloys, a wet chemical approach would measure all the other elements and calculate the Ni content as the balance. With XRF, the major element, nickel, as well as the minor and trace components can be measured accurately. For high-grade steel and alloys with multiple major components, WDXRF achieves better accuracy and repeatability than optical emission spectroscopy (OES).

A limitation for XRF in a metallurgical application is the measurement of carbon in steel. The problem with carbon in this application is due to the small analyzed layer and the inhomogeneous distribution of carbon in steel. To ID the correct steel grade for low carbon steels, OES or combustion analysis is required.

The areas of restricted/prohibited elements and consumer product safety have major applications where XRF can be used successfully. Inspection of consumer goods for regulated elements such as Br (from flame retardants), Hg, Pb, Cr, and Cd as part of government regulations such as restriction of the use of hazardous substances (RoHS), waste electrical and electronic equipment (WEEE), and the Consumer Protection and Safety Improvement Act 2008 (CPSIA) use XRF (especially portable, handheld, and stationary microspot XRF) as screening tools. This is achieved by factory calibrations, which adjust and switch automatically for common matrices: high-density (HD) and low-density (LD) polymers and polyvinyl chloride (PVC) and metals. These matrices are the ones found in toys and jewelry. Controlled elements can be measured rapidly using such "dedicated" systems. Pb concentrations as low as 10 ppm can be determined in soil samples with a portable HH XRF system. XRF is used to measure the amount of phosphorus-based flame retardant in textiles and the amount of antimony-based flame retardant in plastics. For textiles, a piece of fabric is cut into a square piece and stretched across a standard sample cup and held in place by the sample container ring. This results in a flat specimen for analysis. Phosphorus levels in the range of 0.3%–3% P can be measured in a sample in as little as 30 s. (Details of the method are available from SPECTRO Analytical Instruments [www.spectro-ai.com].)

The ceramics industry routinely measures 6–12 elements quantitatively in both pressed pellet and fusion bead form for quality control using either WD or ED XRF. The elements (reported as oxides) vary in concentration from 0.01 to 70 wt%. Using a modern WDXRF spectrometer, aluminum (reported as $Al_2O_3$) can be determined at the 1 wt% level in a magnesium oxide-based ceramic with a standard deviation of 0.006 and a DL of about 8 ppm.

The cement industry requires the close monitoring of at least 10 major elements as oxides ($Na_2O$, MgO, $Al_2O_3$, $SiO_2$, $SO_3$, $P_2O_5$, $K_2O$, CaO, $MnO_2$, and $Fe_2O_3$) and determination of adverse trace elements (Zn, Cr, Cl). Based on the requirements of time to result, either WDXRF (simultaneous or sequential) or benchtop EDXRF can be used.

Most mining companies use XRF for the analysis of their process streams and monitor the "separation" of metals from the ore. XRF is faster than any wet or atomic spectroscopy technique since it can measure the sample as a solid. Trace elements in soil and sediment can be measured to collect geological, agricultural, and environmental data both in the lab and in the field, using portable or benchtop EDXRF analyzers.

Online XRF analyzers are available for monitoring process streams for metals in plating baths, metals in hydrocarbons, silicon in adhesive coatings on paper, acid leaching solutions, effluent discharge monitoring, and similar applications. The thickness of coatings can be measured on a wide variety of materials, such as paint on steel for the automotive industry and silicone release coating on paper (the shiny nonstick backing paper you peel adhesive labels from is coated with a silicone polymer called a "release coating"). Solar panels are routinely checked with XRF either online or at line.

Due to the extremely high current price for gold, many jewelers, pawnshops, and the like are buying scrap gold and old jewelry. Handheld or portable systems with dedicated software to determine % Au and carat weight, silver and other precious metals are now available for accurate evaluation of the content of scrap jewelry, such as the Thermo Fisher Scientific Niton DXL precious metal analyzer. This is a countertop unit that delivers fast XRF analysis for all precious metals and has an integrated program called AuDIT™, which automatically identifies gold-plated items, based on the thickness of the Au layer. Units with dedicated software for determining plating thickness of other metal coatings on substrates are also common.

XRF can be superior to atomic spectroscopy when calibration and consumable costs are compared, assuming the DLs are comparable. XRF units are calibrated usually either at the factory or on site when the source is changed; calibration is adjusted or checked with a set of solid check samples. Consumables for XRF are limited to those for sample preparation (fusion fluxes, disposable sample holders, polymer film) and helium, when liquid samples are measured. A significant advantage for XRF over atomic spectroscopy is the ability to measure major, minor, and trace elements simultaneously and directly in the solid or liquid; for most atomic spectroscopy techniques, major and minor components require serial dilutions and multiple analyses. Most solid samples for atomic spectroscopy must be dissolved for analysis. AAS, atomic emission systems, and ICP-mass spectrometry (MS) systems need to be calibrated daily before use and when sample introduction systems are changed, and when parts are cleaned or replaced. They all require large amounts of gases, calibration standards for each element, large volumes of high-purity acids, disposable autosampler cups or tubes, graphite furnace (GF) components, torches, nebulizers, disposable pump tubing, and so on.

## 8.3 X-RAY ABSORPTION

If the wavelength of an X-ray beam is short enough (high energy), it will excite an atom that is in its path. In other words, the atom absorbs X-rays that have enough energy to cause it to become excited. As a rule of thumb, the X-rays emitted from a particular element will be absorbed by elements with a lower atomic number. The ability of each element to absorb increases with atomic number.

Beer's law states that

$$\log\left(\frac{P_0}{P_x}\right) = \mu_x t \tag{8.20}$$

where

$\mu_x$ is the linear absorption coefficient
$t$ is the path length through the absorbing material
$P_0$ is the X-ray power before entering sample
$P_x$ is the X-ray power leaving sample

However,

$$\left(\frac{\mu_x}{\rho}\right) = \mu_m \tag{8.21}$$

where

$\mu_m$ is the mass absorption coefficient
$\rho$ is the density

But

$$\mu_m = \left( \frac{CN_0 Z^4 \lambda^3}{A} \right) \tag{8.22}$$

where
- $C$ is a constant
- $N_0$ is Avogadro's number
- $Z$ is the atomic number
- $A$ is the atomic weight
- $\lambda$ is the wavelength of the radiation

It can be seen that at a given wavelength, $\mu_m$ is proportional to $Z^4$ divided by the atomic weight. This relationship is shown in Figure 8.56. The setup for X-ray absorption is slightly different than that for XRF, as seen in Figure 8.57. The sample is placed directly in line with the X-ray tube, in

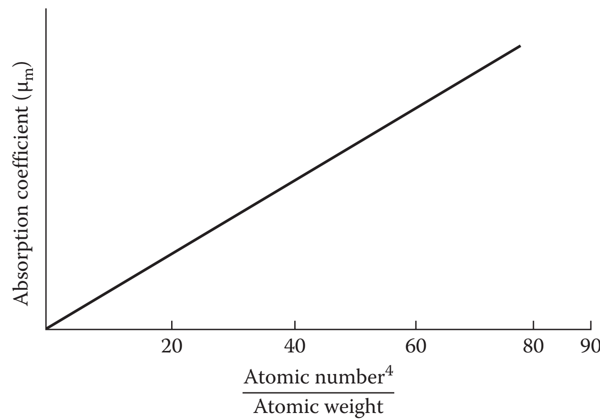


**Figure 8.56** Relationship between atomic number and X-ray absorption coefficient.

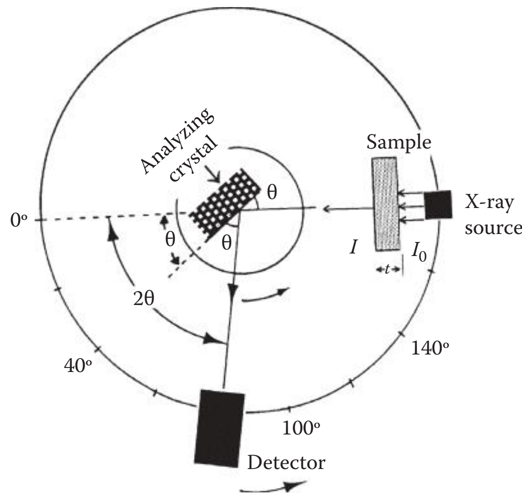


**Figure 8.57** X-ray absorption. The sample is placed between the X-ray tube and the detector. The intensity of the source is $I_0$. The intensity of light reaching the detector after passing through a sample of thickness $t$ is $I$. $I$ will be less than $I_0$ if absorption occurs.

a configuration very similar to UV/VIS absorption spectrometry. The parameter measured is the decrease in intensity of the incident beam after passing through the sample. The same detectors described for XRF may be used for X-ray absorption spectrometry. Older systems and some current medical systems use photographic film for detection (radiography).

The most familiar example (and the oldest use) of X-ray absorption does not provide chemical information, but rather physical information. That is the use of X-ray absorption in medical radiography, but it is based on the relationship between absorption coefficient and atomic number. For example, the human arm consists of flesh, blood, and bone. The flesh or muscle is made up primarily of carbon, nitrogen, oxygen, and hydrogen. These are all low atomic number elements, and their absorptive power is very low. Similarly, blood, which is primarily water, consists of hydrogen and oxygen, plus small quantities of sodium chloride and trace materials. Again, the absorptive power of blood is quite low. In contrast, bone contains large quantities of calcium and phosphorus, primarily as calcium phosphate. The atomic numbers of these elements are considerably higher than those in tissue and blood, and so the absorptive power is considerably higher. When an X-ray picture is taken of a hand (Figure

**Figure 8.58** X-ray photograph of a human hand.

8.58), the x-radiation penetrates the muscle tissue and blood quite readily, but is absorbed significantly by the bone. A photograph of this absorption indicates the location of the bones in the hand. The procedure is routinely used in medicine to detect broken bones, fractures, and arthritic changes in joints.

Another application of X-ray absorption in medicine is to define the shapes of arteries and capillaries. Normally, the blood absorbs only poorly; however, it is possible to inject a solution of strongly absorbing cesium iodide into the veins. The material is then swept along with the blood and follows the contours of the arteries. An X-ray video is recorded as the highly absorbing cesium iodide flows through the arteries, showing the contours of the arteries. This can be used to identify breaks in the veins or arteries that could cause internal bleeding. Such internal bleeding can be the cause of a stroke. The technique may also be used to indicate a buildup of coating (plaque) on the inside of the veins. This is particularly dangerous in the heart, where deposits of cholesterol restrict the flow of blood through the heart. If this is left unchecked, a heart attack will result. X-ray absorption can be used to diagnose this problem and to locate exactly the position of deposits. Surgery is made much easier by this technique. In a similar fashion, a barium-containing liquid ingested by a patient permits the detailed observation of the colon since barium, a high Z element, absorbs very strongly (Figure 8.59a through c).

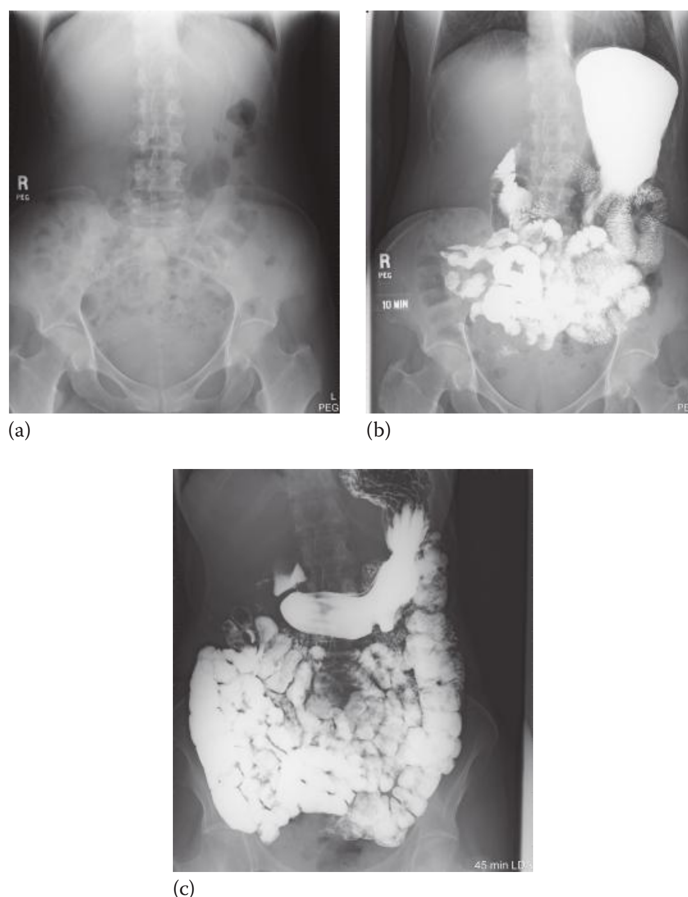


**Figure 8.59** X-ray photographs of a human colon before and after ingestion of a barium-containing liquid. (a) Before ingestion of the barium solution, the colon cannot be seen at all. (b) 10 min after ingestion, the highly absorbing barium has entered the colon. (c) After 45 min, the entire colon can be clearly seen.

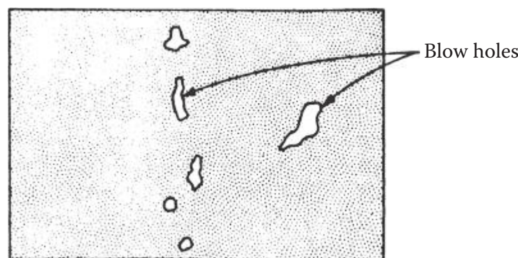


**Figure 8.60** Schematic X-ray absorption photograph of a mechanical weld.

In the field of metallurgy, applications of X-ray absorption include the detection of voids or the segregation of impurities, such as oxides, in welds and other joints. Figure 8.60 shows an idealized X-ray absorption photograph of a mechanical weld that contains voids or internal holes. Such holes indicate that the weld is mechanically weak and might break in use. If the weld is weak, it must be strengthened to form a sufficiently strong joint. This type of nondestructive testing is used to check the manufacturing quality of ships, aircraft, bridges, and buildings. It is also used to check these structures during routine maintenance. X-ray absorption is routinely used for measuring the thickness of thin metal films.

The technique of X-ray absorption can also be used to determine the levels of liquids in enclosed vessels or pipes without opening or breaking them. The same process can be used to detect metal supports or metal fillings inside constructed objects as diverse as buildings and small works of art. A major advantage is that X-ray techniques are usually nondestructive. Sometimes artists paint over old paintings, using the canvas for their own work and covering unrecognized masterpieces in the process. Using X-ray absorption, it is possible to reveal the covered painting without removing the top painting. When used to examine a metal horse sold for several million dollars as an ancient Greek art piece, X-ray absorption showed that the horse contained internal metal supports and was therefore a fake. This was done without destroying the art piece, in case it had been authentic.

For quantitative elemental analysis, X-ray absorption is not particularly useful except in the case of a single heavy element in a light matrix. As we saw in Equation 8.10, the mass absorption coefficient needed for Beer's law calculation (Equation 8.20) must be calculated from the weight fractions of elements present in the sample. The weight fractions are usually unknown. Quantitative analysis by X-ray absorption is usually only used for the determination of a high atomic number element in a matrix of lower atomic number elements. Examples include the determination of lead or sulfur in hydrocarbon fuels and the determination of Pt catalyst in polymers, where the difference in mass absorption coefficients between analyte and matrix is large. One approach to quantitative analysis using X-ray absorption is based on the measurement of the intensities of two or more monochromatic X-rays passed through the sample. This is called X-ray preferential absorption analysis or dual-energy transmission analysis. The analysis depends on the selective absorption of the transmitted X-rays by the analyte compared with absorption by the rest of the sample (the matrix). The sensitivity of the analysis also depends on the difference in mass absorption coefficients of the analyte and sample matrix for the transmitted X-rays; a big difference results in a more sensitive analysis. The analyte concentration calculation in any absorption method requires that the thickness and density of the sample be known and requires a homogeneous matrix for accurate quantitative results.

An example of the use of X-ray absorption (transmission) is the determination of sulfur in heavy hydrocarbon process streams. Accurate determination of sulfur is required for assaying and

**Table 8.11 Molar Absorptivities of Elements in Petroleum**

| Element | Molar Absorptivity ($cm^2/g$) at 21 keV |
|---|---|
| H | 0.37 |
| C | 0.41 |
| O | 0.79 |
| S | 5.82 |

*Source:* Courtesy of Applied Rigaku Technologies, Inc. www.rigakuedxrf.com.

blending of crude oil, marine oil, and bunker fuel. The term used by the petroleum industry is X-ray transmission (XRT) or absorption (XRA) gauging. XRT/XRA gauging involves measuring the attenuation of a monochromatic X-ray beam at 21 keV. This energy is chosen because at 21 keV, the molar absorptivity for S is 14 times larger than the molar absorptivity of the hydrocarbon matrix and 7 times larger than oxygen (Table 8.11).

As seen in Table 8.11, the absorptivities of C and H are almost identical. The method is therefore insensitive to changes in the C:H ratio and is sensitive only to the sulfur content. In practice, a process stream passes through a flow cell where sulfur in the hydrocarbon matrix absorbs X-rays transmitted between the source and detector (Figure 8.61a). The recorded X-ray intensity is inversely proportional to the sulfur concentration; that is, X-ray transmission decreases as sulfur concentration increases. The commercial process analyzer is shown in Figure 8.61b. The process analyzer can withstand pressures up to 1480 psig and temperatures to 200°C.

Transmission of X-rays through the flow cell is given by the following equation:

$$T = \frac{I}{I_0} = \exp - dt\left[\mu_{\mathrm{m}}(1 - C_{\mathrm{s}}) + \mu_{\mathrm{s}} C_{\mathrm{s}}\right] \tag{8.23}$$

where

$I$ is the measured X-ray intensity (after the flow cell) (photons/s)
$I_0$ is the initial X-ray intensity (before the flow cell) (photons/s)
$d$ is the density of the hydrocarbon stream
$t$ is the thickness of the flow cell (cm)
$\mu_m$ is the molar absorptivity of the hydrocarbon matrix at 21 keV ($cm^2/g$)
$\mu_s$ is the molar absorptivity of sulfur at 21 keV ($cm^2/g$)
$C_s$ is the weight fraction of sulfur (% wt/wt)

### 8.3.1 EXAFS

A recent development in the use of X-ray absorption is a technique called EXAFS, extended X-ray absorption fine structure spectroscopy. A sample is placed in a beam of X-rays, and the incident and transmitted intensities are measured as the energy of the X-ray beam is varied. A plot of the absorption versus energy gives us the position (energy) and exact shape of the absorption edge for the element being measured. The exact energy of the absorption edge and its shape, the "fine structure," does change slightly depending on the oxidation state of the element and the number and type of nearest neighbor atoms. This change in position of the absorption edge is analogous to the chemical shift seen in nuclear magnetic resonance (NMR). EXAFS does provide oxidation

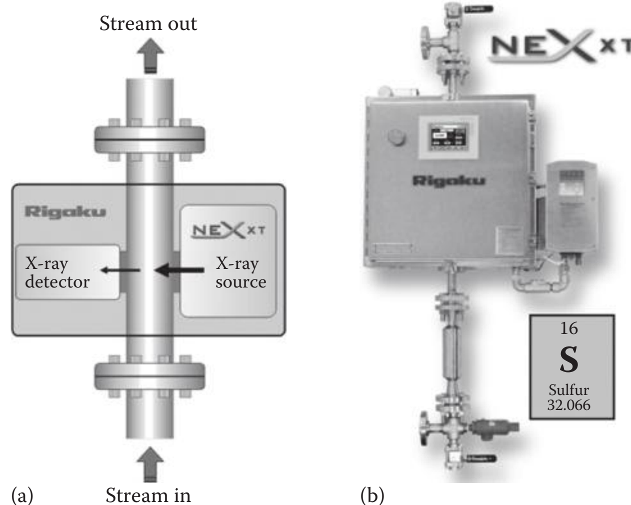


**Figure 8.61** (a) Schematic of the X-ray transmission NEX XT system showing the flow cell, source, and detector. (b) The Rigaku NEX XT on-line sulfur analyzer. (Courtesy of Applied Rigaku Technologies, Inc., TX. www.rigakuedxrf.com.)

state information and molecular structure information, unlike normal X-ray absorption or XRF, which are strictly elemental analysis techniques. Details of the spectral interpretation of EXAFS are beyond the scope of this book. The interested student can consult the text by Teo and Joy listed in the bibliography.

## 8.4 X-RAY DIFFRACTION

XRD is a technique that is useful for the analysis of solid crystalline or semicrystalline materials. Most organic and inorganic compounds, minerals, metals, and alloys, and many types of polymers form crystals and can be analyzed by XRD. XRD can provide the exact crystal structure of a pure single-crystal material. In addition, XRD can provide the qualitative and quantitative identification of the molecules present in pure crystalline powders or mixtures of crystalline powders.

The ions or molecules that make up a crystal are arranged in well-defined positions, called a crystal lattice. Figure 8.62 is an electron micrograph of the (110) plane of crystalline silicon. Three coordinates, called Miller indices, identify the plane in space; the Miller indices for this plane are 1,

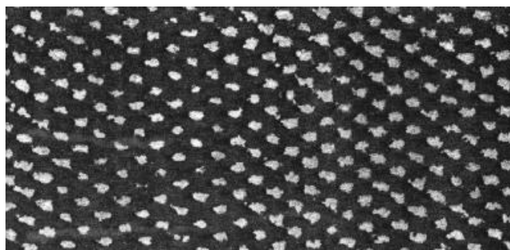

**Figure 8.62** An electron micrograph of the (110) plane in crystalline silicon.

1, and 0. The light spots are individual Si atoms. As can be seen, they are arranged in a very regular pattern in the 2D plane. The dark area is the empty space or interstitial space between the atoms in the lattice. A crystal is a 3D well-ordered array of atoms. An illustration of a typical crystal structure, greatly magnified, is shown in Figure 8.63a. As we examine the structure of the crystal, we see that the ions or atoms or molecules form planes in three dimensions. You can imagine stacking identical planes of Si atoms on top of each other to create a 3D crystal, for example.

The **unit cell**, shown in heavy outline in the lattice, can be moved in three dimensions to recreate the entire crystal lattice. The unit cell is the smallest volume that can be used to describe the entire lattice. A Cartesian coordinate system is used to locate points, directions, and planes in a crystal lattice. A unit cell has its origin at the intersection of the three axes and is designated by its edge lengths in the *x*-, *y*-, and *z*-directions and by three angles. An atom (molecule or ion) in the crystal lattice is a point, identified by its *x*, *y*, and *z* coordinates. A plane is identified by its Miller indices, the reciprocals of the intersection points of the plane with the *x*, *y*, and *z* axes. A triangular plane is shown within the unit cell. The plane intersects the *x*-axis at 1/2, the *y*-axis at 1/2, and the *z*-axis at 1; it has intercepts of 1/2, 1/2, and 1. The reciprocals are 2, 2, and 1, so the Miller indices for this plane are (221). A plane that is parallel to a given axis has an intercept of infinity; the reciprocal of infinity is 0. A crystal lattice will have many parallel planes, each uniformly spaced from each other. Such groups of planes are called families of planes and will have related Miller indices [e.g., the (110), (220), (330), and (440) planes are a family of planes]. These planes in a given family are all parallel,

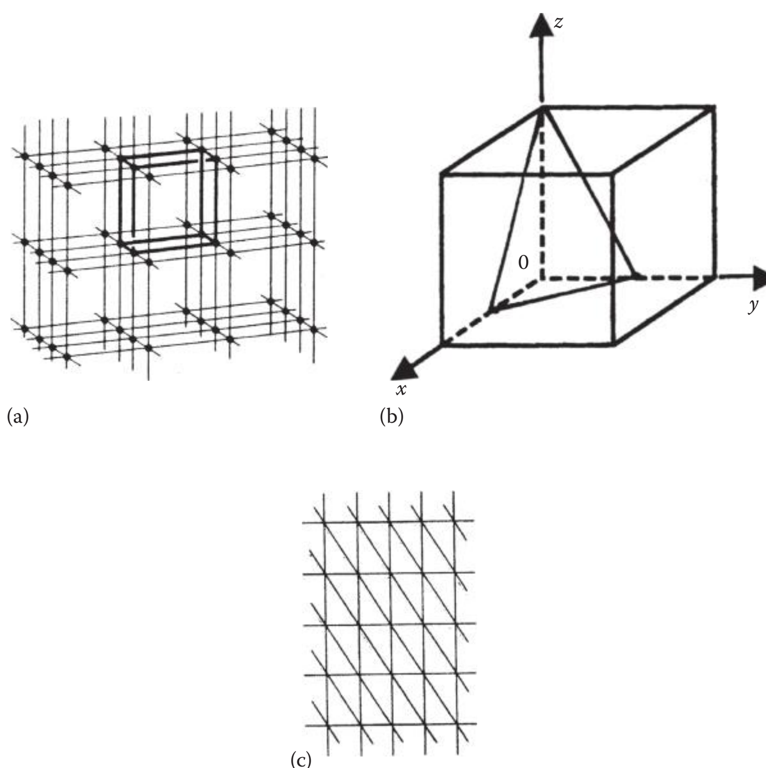


**Figure 8.63** (a) A portion of a 3D crystal lattice. The unit cell, or basic repeating unit, of the lattice is shown in heavy outline. The black dots represent the atoms or ions or molecules that make up the crystal. (b) A cubic unit cell, with the corners of the cell located at 1 unit from the origin (O). The triangular plane drawn within the unit cell intersects the *x*-axis at 1/2, the *y*-axis at 1/2, and the *z*-axis at 1. This plane has Miller indices of (221). (c) A family of planes shown in a 2D lattice.

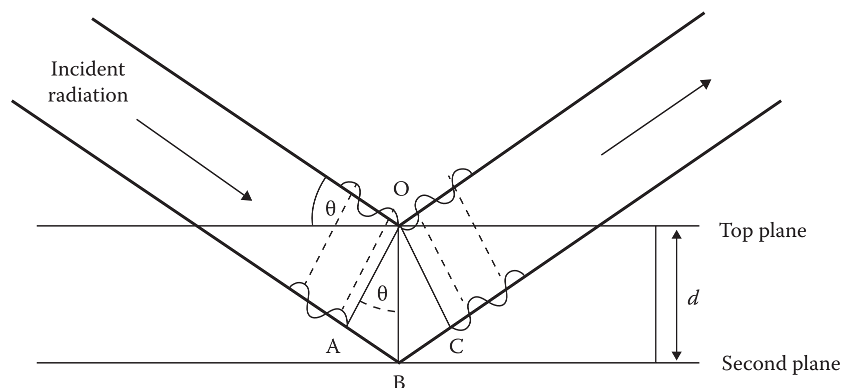


**Figure 8.64** Reinforcement of light diffracted from two crystal planes.

as shown in Figure 8.63c, just at different distances from the origin specified for the coordinate system. The (110) plane is the farthest from the origin, and the (440) plane is the closest to the origin of the set of planes (110), (220), (330), and (440). Miller indices for commonly used analyzing crystals were given in Table 8.7.

If a monochromatic X-ray beam falls on such a crystal, each atomic plane reflects the beam. Each separate reflected beam interacts with other reflected beams. If the beams are not in phase, they destroy each other and no beam emerges. Other beams reinforce each other and emerge from the crystal. The net result is a **diffraction pattern** of reinforced beams from many planes. It is the atomic planes that are important in XRD. It is of course possible to draw an infinite number of planes in three dimensions, but only those planes with electron density on them reflect X-rays.

In Figure 8.64, radiation from the source falls on the crystal, some on the top atomic plane and some on the second plane. Since the two beams are part of the same original beam, they are in phase on reaching the crystal. However, when they leave the crystal, the part leaving the second plane has traveled an extra distance ABC. If ABC is a whole number of wavelengths, the two beams leaving the crystal will be in phase and the light is coherent. If ABC is not a whole number of wavelengths, the two beams come together out of phase, and by destructive interference, the light is destroyed.

As we derived earlier, $n\lambda = 2d \sin\theta$. This is the Bragg equation, which states that coherence occurs when $n\lambda = 2d \sin\theta$. It can be used to measure $d$, the distance between planes of electron density in crystals, and is the basis of **X-ray crystallography**, the determination of the crystal structure of solid crystalline materials. Liquids, gases, and solids such as glasses and amorphous polymers have no well-ordered structure; therefore, they do not exhibit diffraction of X-rays.

For any given crystal, $d$ is constant for a given family of planes; hence, for any given angle θ and a given family of planes, $n\lambda$ is constant. Therefore, if $n$ varies, there must be a corresponding change in λ to satisfy the Bragg equation. For a given diffraction angle, a number of diffracted lines are possible from a given family of planes; $n$ is known as the **order** of diffraction. As an example, if $2d \sin\theta$ equals 0.60, each of the conditions of Table 8.12 will satisfy the Bragg equation. Radiation of wavelength 0.60, 0.30, 0.20, or 0.15 Å will diffract at the same angle θ in first, second, third, or fourth order, respectively, as seen in Figure 8.65. This is called order overlap and can create difficulty in interpretation of crystal diffraction data.

It should be noted that radiation of 0.30 Å would also be diffracted at a different angle in first order from the same family of planes (same $d$ value), as shown in Figure 8.65. Wavelengths

**Table 8.12 Order of Diffraction for Values of $n$, λ**

| $n$ | λ (Å) | $n$λ | Order |
|---|---|---|---|
| 1 | 0.60 | 0.60 | First |
| 2 | 0.30 | 0.60 | Second |
| 3 | 0.20 | 0.60 | Third |
| 4 | 0.15 | 0.60 | Fourth |

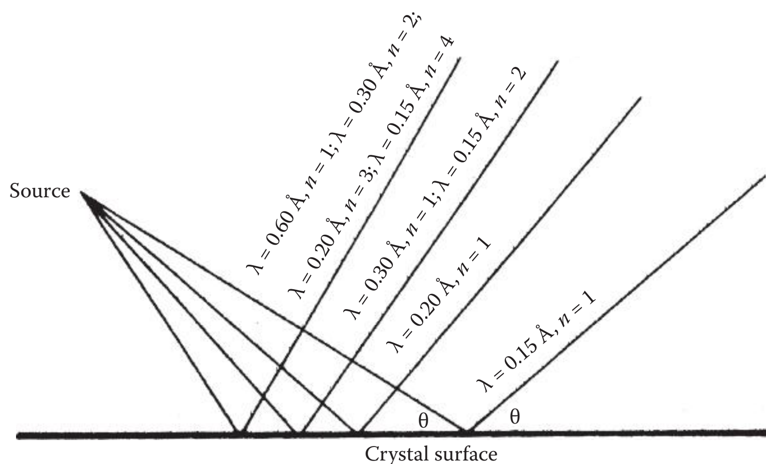


**Figure 8.65** Diffraction of radiation of different wavelengths. Overlap can occur when different orders are diffracted at the same angle.

corresponding to low orders such as first and second order give observable diffraction lines. Consequently, a single plane will generate several diffraction lines for each wavelength. Each of the planes in the three dimensions of the crystal will give diffraction lines. The sum total of these diffraction lines generates a diffraction pattern. From the diffraction pattern, it is possible to deduce the different distances between the planes as well as the angles between these planes in each of the three dimensions. Based on the diffraction pattern, the physical dimensions and arrangement of the atomic planes in the crystal can be identified.

### 8.4.1 Single-Crystal X-Ray Diffractometry

The schematic layout of a single-crystal diffractometer is given in Figure 8.66. This system uses an X-ray tube, a sample specimen, and a detector that rotates in an arc described by a Rowland circle. Note that the single-crystal sample takes the place of the analyzing crystal in a WDXRF analyzer. The goniometer mounting for a single-crystal diffractometer is very complex, because the crystal must be moved in three dimensions to collect data from many planes. A commercial benchtop single-crystal XRD instrument is shown in Figure 8.67.

For any given experiment, λ is the known wavelength of the monochromatic X-ray beam; θ is controlled and varied by the goniometer. From this information, $d$ can be calculated. By rotating the goniometer and examining various sides of the crystal, hundreds (or thousands) of diffracted X-rays are collected. This data is processed to identify the positions of the planes and atoms in the crystal in three dimensions. Modern single-crystal diffractometers use computers to control the goniometer and to process the data. The diffraction data is usually converted to a 2D electron density map by

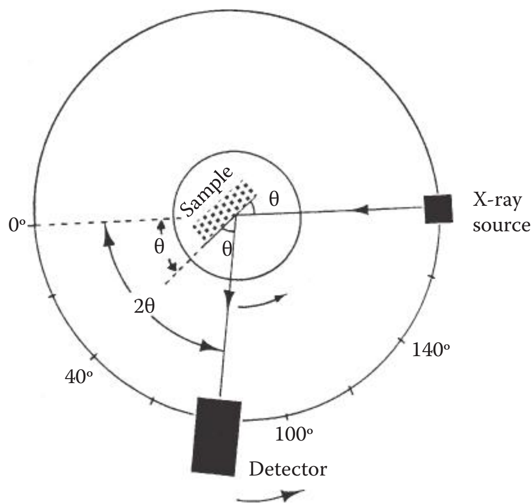


**Figure 8.66** Schematic layout of a single-crystal XRD.

(a)

(b)

**Figure 8.67** (a) A benchtop single-crystal XRD system, the Rigaku XtaLAB mini™. (b) Close-up of the goniometer, X-ray tube, and detector in the XtaLAB mini. The single-crystal sample is mounted at the tip of what looks like a sewing needle in the center of the photo. (Used by permission of Rigaku Corporation, www.rigaku.com.)

Fourier transformation. The electron density map shows the location of atoms. A 2D electron density map is produced for each angle. The computer program uses the 2D maps plus the rotation angle data to generate the 3D coordinates for atoms (molecules, ions) in the crystal. The mathematical treatment of the experimental data to produce a crystal structure from an unknown single-crystal diffraction pattern is complicated and beyond the scope of this text, but an example of the results will be shown in the following.

The diffraction pattern of a single crystal of an inorganic salt is shown in Figure 8.68; an actual diffraction pattern is shown in Figure 8.69. A given molecule always gives the same diffraction pattern, and from this pattern, we can determine the spacing between planes and the arrangement of planes in the crystal. Also, qualitative identification can be obtained by matching this pattern to previously identified patterns. Modern instruments are equipped with 2D imaging detectors such as CCDs.

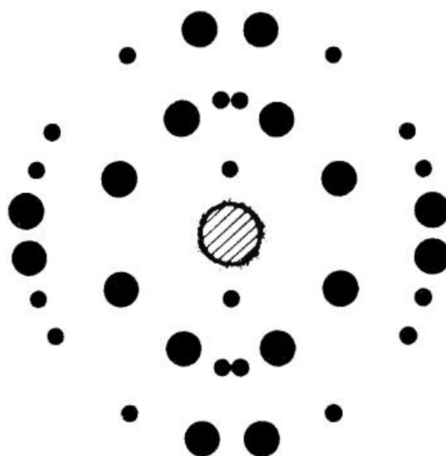

**Figure 8.68** Diffraction pattern in two dimensions of a single crystal of an inorganic salt.

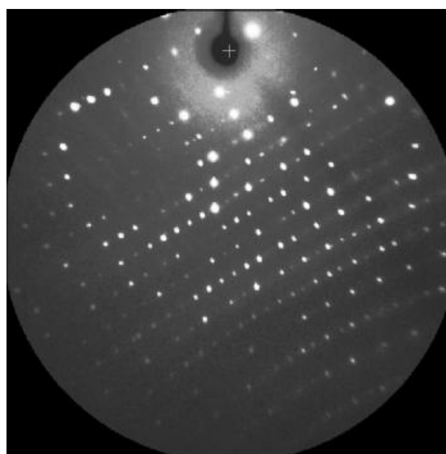

**Figure 8.69** Actual single-crystal diffraction pattern of a small molecule collected with a Rigaku XtaLAB mini™. (Used by permission of Rigaku Corporation. www.rigaku.com.)

### 8.4.2 Crystal Growing

In order to determine the structure of a single crystal, such a crystal must be grown from the material to be studied. The crystal quality determines the quality of diffraction results obtained. One limitation of XRD is that data is obtained on only one single crystal of the bulk material, unlike other techniques where multiple replicates are usually analyzed. The growth of single crystals of materials often is not easy. Simple inorganic salts and small organic molecules can be crystallized as single crystals by very slow evaporation of a supersaturated solution of the salt or compound. Once one tiny single crystal forms, it will grow in preference to the formation of more small crystals. Sublimation under vacuum can be used. Proteins and other biomolecules are more difficult to grow as single crystals because they are complex. One method that often works is to suspend a drop of protein solution over a reservoir of buffer solution. Water diffusion from the drop often results in single-crystal growth. Different techniques are required to form metal crystals. The interested student can find many references and resources on the Internet, by searching the term "X-ray crystallography." The single crystal then has to be mounted; various mount types are available depending on the instrument and goniometer being used.

### 8.4.3 Crystal Structure Determination

From the diffraction pattern, the crystal structure can be determined mathematically and the compound identified. While the discussion of the details is beyond the scope of this text, small, benchtop automated single-crystal XRD systems have come into use. These instruments possess a variety of powerful data processing programs and libraries that permit the determination of high-resolution crystal structures of small molecules rapidly and automatically. Systems include the Rigaku XtaLAB mini™ and the Bruker X2S.

The XtaLAB mini™ software shows the approach used by these automated systems. Figure 8.70 lists the steps involved in obtaining a structure from the diffraction pattern. Once the single crystal of the analyte has been mounted, a "project" is opened and the data collected. Then, the data is evaluated and the structure solved using one or more of the stored mathematical approaches. Some of the various methods and programs can be seen on the computer screen. A model is created and refined, and a report with the crystal structure, lattice parameters, and molecular identification is produced. Figure 8.71 shows the refinement results for a particular crystal obtained using the program SHELX. The results after five cycles of refinement (which requires over 2000 observations and 231 variables) give a "goodness of fit" of 1.066, an indication that the result is highly probable. Perfect fit would be 1.000. The number of cycles, observations, and variables makes it clear that without modern computer processing, determination of a structure from an XRD pattern would take days or weeks of work, as it used to.

Measurement times for crystals of small molecules using such a system vary and depend on the complexity of the molecule. Potassium tetrachloroplatinate II, $K_2PtCl_4$, required less than 2 h of measurement time using the XtaLAB mini™, while a structure like raffinose, $C_{18}H_{32}O_{16}\cdot 5H_2O$, required 5 h and 30 min. The overall results from an analysis of the diffraction pattern would include the chemical structure, the name of the compound, the formula weight, the space group to which the crystal belongs, and the crystal lattice constants.

### 8.4.4 Powder X-Ray Diffractometry

Powdered crystalline samples can also be studied by XRD. The sample is loaded onto the specimen holder, which is placed in the X-ray beam in a setup similar to that used for single-crystal XRD. The sample must be powdered by hand or by mechanical grinding and is pressed into a sample

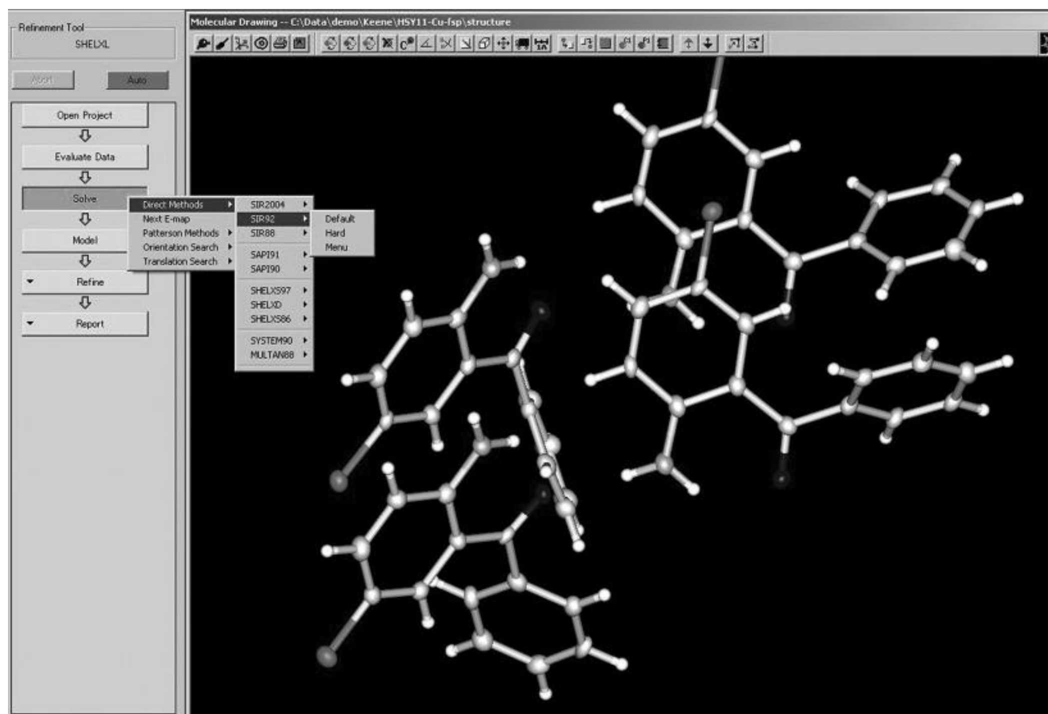


**Figure 8.70** Computer screen of the XtaLAB mini™ showing the automated program steps for solving a crystal structure, including a list of some of the mathematical methods available and the molecular structure resulting from the data processing. (Used by permission of Rigaku Corporation. www.rigaku.com.)

holder to form a flat surface or packed into a thin glass or polymer capillary tube. After mounting, the specimen is rotated relative to the X-ray source at a rate of (degrees θ)/min. Diffracted radiation comes from the sample according to the Bragg equation. The detector is simultaneously rotated at (degrees 2θ)/min, using traditional θ–2θ geometry. Alternatively, instruments such as the Thermo Fisher Scientific ARL X'TRA powder diffraction system are available using a θ–θ geometry (Bragg–Bretano geometry).

A powdered crystalline material contains many thousands of tiny crystals. These crystals are oriented in all possible directions relative to the beam of X-rays. Hence, instead of the sample generating only single diffraction spots, it generates cones of diffracted X-rays, with the point of all the cones at the sample (Figure 8.72). Each family of planes will have a different circular diameter, so the result is a series of concentric cones radiating from the sample. Imagine that inside the Rowland circle opposite the sample, we have a strip of X-ray film as shown in Figure 8.72 on the right. The circular cones of X-rays will hit the film, resulting in a series of curved lines on the film (Figure 8.72 left). A typical diffraction pattern from a powdered sample collected on film is shown in Figure 8.73. These are called Laue photographs, after Max von Laue, the German scientist who developed the technique. Film has been replaced by automated scanning with a standard X-ray detector as discussed for XRF or by the use of imaging detectors such as CCDs or image plates to give a 2D image. A cylindrical image plate detector used by Rigaku Corporation has an active area of 454 mm × 256 mm, a pixel size of 100 μm × 100 μm, extremely rapid readout, and a sensitivity of 1 X-ray photon per pixel for Cu $K_\alpha$ radiation. One X-ray photon per pixel is a quantum efficiency of 100%. The major advantage of these imaging detectors is that the images can be stored and

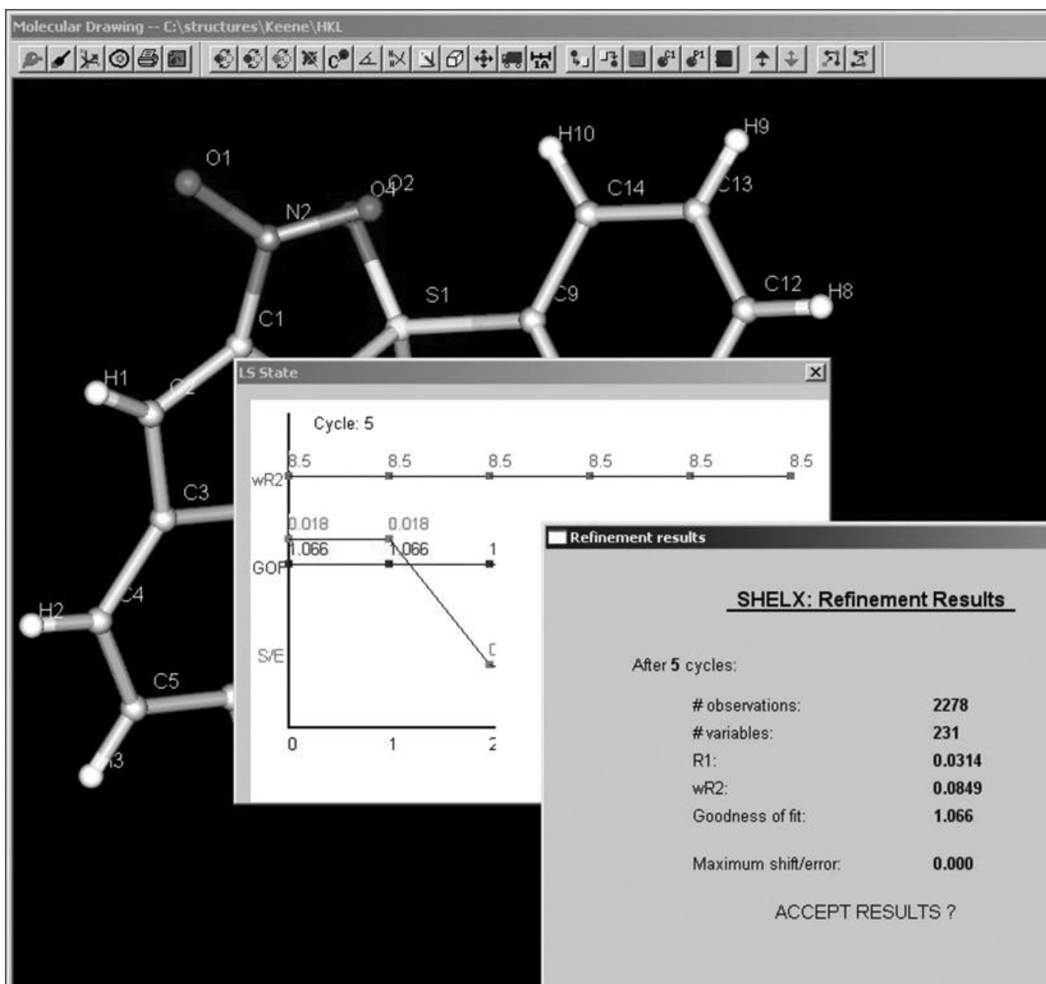


**Figure 8.71** Computer screen of the automated results of the refinement of a crystal structure by the XtaLAB mini™. (Used by permission of Rigaku Corporation. www.rigaku.com.)

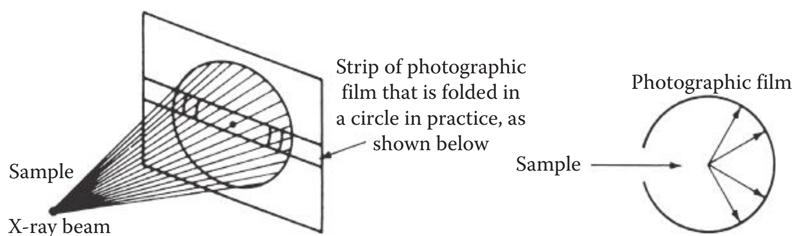


**Figure 8.72** Schematic of diffraction from a powdered crystalline sample. The powdered sample generates the concentric cones of diffracted X-rays because of the random orientation of crystallites in the sample. The X-ray tube exciting the sample is not shown in this diagram. The cones of diffracted light intersect X-ray film curved to fit the diameter of the Rowland circle. The result is a series of curved lines on the X-ray film.

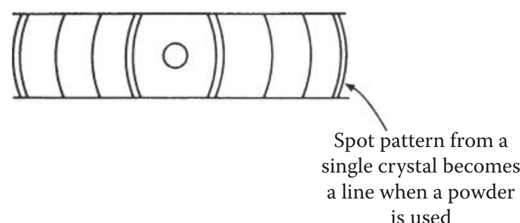


**Figure 8.73** A typical diffraction photograph, called a Laue photograph, from a powdered crystalline sample.

manipulated electronically without the need for a photographic film-developing lab. The Thermo Fisher Scientific ARL X'TRA uses a Peltier-cooled Si(Li) solid-state detector, which can be cooled to about −100°C, resulting in extremely low internal noise. This solid-state detector allows the user to electronically select photons based on their energy signature, which eliminates the need for beta filters or diffracted beam monochromators to remove Bremsstrahlung and sample fluorescence.

In order to obtain accurate XRD spectra, the sample must be ground finely and pressed, so that there is sufficient random orientation of the crystals in the sample. Nonrandom orientation (preferred orientation) will result in a distorted spectral pattern, like a broken line or series of spots instead of a complete curved line. Some materials exhibit preferred orientation, either naturally or by design, and can be identified through these distortions. Powder diffractometers come in a variety of sizes, including small benchtop units and field-portable units (Section 8.4.5.1).

### 8.4.5 Hybrid XRD/XRF Systems

Hybrid systems are designed to combine the speed and flexibility of XRD and XRF systems in one spectrometer. Such systems permit more complete characterization of a given crystalline sample. These systems are varied: some are XRF systems with a few powder XRD-based channels to identify compounds, such as a system designed with a CaO channel for the cement industry. The combination can go as far as including a complete powder diffractometer and XRF spectrometer for flexible compound identification and quantification. These types of systems are generally used in industries, including metal and alloy production, cement production, mining, and refractory materials production, for both R&D and process control.

Thermo Fisher Scientific's ARL 9900 series hybrid systems offer a variety of configurations of the XRF and powder XRD components for R&D, fast process analysis, qualitative and quantitative elemental analysis, and phase analysis. The system can be configured in many ways: with up to 32 monochromators for fast elemental analysis, up to three goniometers for analysis of specific elements (quantitative and standardless analysis), scanning the XRF spectrum (qualitative and semiquantitative analysis), a compact XRD system for process control, or a full powder XRD system. With the XRF unit, up to 83 elements (B to U) can be determined from ppm levels to 100%. The full XRD goniometer, called the NeXRD, provides qualitative and quantitative phase analysis. Full-pattern quantitative phase analysis results can be obtained in 5 min using automatic interpretation of the XRD pattern. The 9900 series has options for a variety of automated sample changers (12 or 98 position) and can be integrated with the ARL robotic sample preparation systems, allowing unattended continuous operation of the instrument. This system is a floor-mounted laboratory unit. The advantages of a hybrid unit for the laboratory are that it provides a single user interface for both XRF and XRD techniques, minimizes occupied floor space, merges elemental and phase analysis into a single report, and permits rapid, precise analysis of solid samples. One limitation of such systems is that they can only handle solid samples. Pictures and details are available at www.thermo.com./xray.

### *8.4.5.1 Compact and Portable Hybrid Systems*

A revolution in powder XRD/XRF systems has resulted from the development of portable, compact, rugged systems designed originally for rock and mineral analysis in the field. The Terra Mobile XRD/XRF system (from Innov-X and Olympus [www.olympus-ims.com; www.inxitu.com]) is a high-performance combination 2D powder diffraction/XRF system that is battery powered, completely self-contained, very rugged, and field portable (Figure 8.74a and b).

The Terra provides full phase ID of major, minor, and trace components in rocks and minerals and an XRF system capable of scanning from Ca to U. It has a sample handling system that can sieve powders to <150 μm and requires only 20 mg of sample. To obtain accurate powder XRD spectra, it is generally necessary to finely grind a sample and press a pellet, to ensure sufficient random orientation of the crystals in the sample. To avoid the problems of pressing a pellet, which is difficult to do in the field or on Mars, the Terra has a patented integrated sample vibration chamber. By vibrating the 15–20 mg sample, all orientations of the crystal structure are presented to the

(a)

(b)

**Figure 8.74** (a, b) Two images of geologists using the Terra Mobile XRD/XRF system in real mining applications in field conditions. (Courtesy of Olympus NDT. www.olympus-ims.com; www.inxitu.com.)

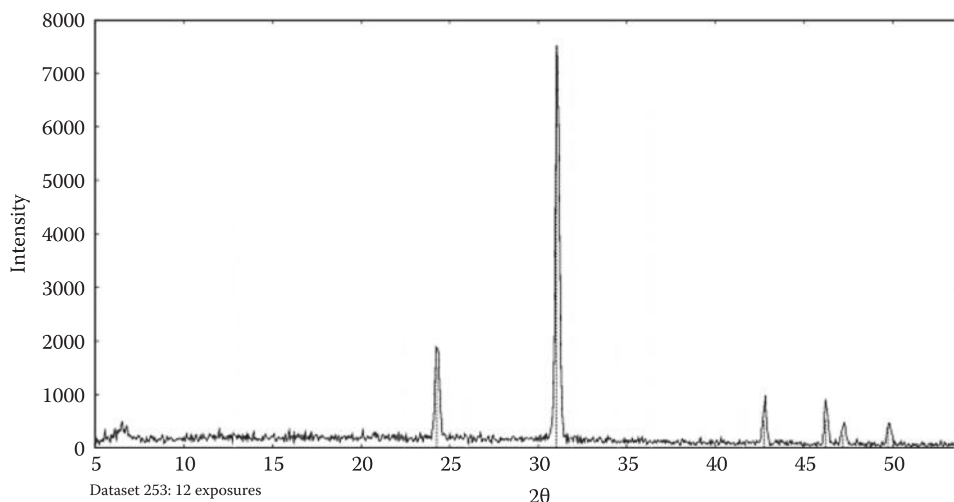


**Figure 8.75** Powder XRD spectrum of pure quartz, taken with the BTX Benchtop system using a Co target and 12 exposures (100 s). (Courtesy of Olympus NDT. www.olympus-ims.com; www.inxitu.com.)

instrument optics. This virtually eliminates the problem of preferred orientation induced by poor sample preparation. The system provides images of the XRD pattern and permits identification of preferred orientation and particle influences on the spectrum. The XRF uses energy discrimination to eliminate fluorescence, scatter, and other background and contains an XRF library for pattern confirmation. Peak identification in XRD and XRF is as accurate as that obtained with laboratory-based systems. The Terra system is now onboard the Mars Science Laboratory rover. Full-color images of the Curiosity rover and Terra XRD/XRF data from Mars are available at www.nasa.gov/mission_pages/msl.

Based on the Terra design is the BTX Benchtop XRD/XRF system (www.olympus-ims.com; www.inxitu.com). This system is a one-button operation compact XRD/XRF unit suitable for educational use as well as dedicated quality control powdered sample applications. It is easy to use, fast, small, and compact and requires minimal sample preparation and provides the high-quality results seen in many large laboratory units. A sample spectrum from the BTX system is shown in Figure 8.75.

### 8.4.6 Applications of XRD

The analytical applications of XRD are numerous. The method is nondestructive and gives detailed information on the structure of crystalline samples. Comparing powder diffraction patterns from crystals of unknown composition with patterns from crystals of known compounds permits the identification of unknown crystalline compounds. The number of peaks or lines, intensities of peaks or lines, and the angular positions of peaks or lines (in terms of 2θ) are used to identify the material (Figure 8.75).

Diffraction patterns are unique for each compound and serve as a fingerprint for a crystalline material. For example, as shown in Figure 8.76a and b, pure crystals of compound A and pure crystals of compound B give different diffraction patterns. A *mixture* containing both A and B will show diffraction peaks from both pure compounds (Figure 8.76c). If we had a mixture of 15% KCl and 85% NaCl, the diffraction pattern would show strong NaCl peaks with a weak pattern of KCl intermixed. A mixture containing 15% NaCl and 85% KCl would show the diffraction pattern of KCl

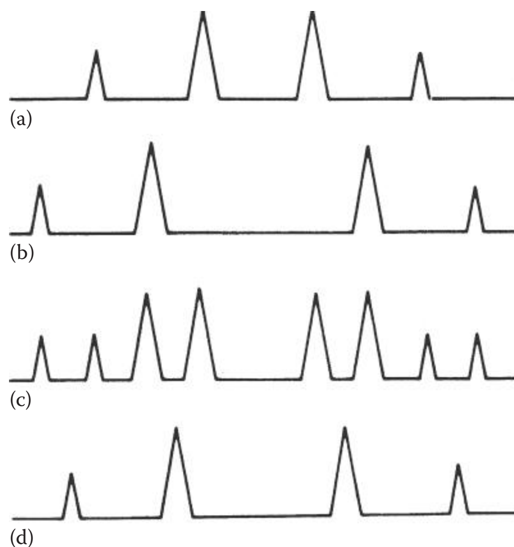


**Figure 8.76** Schematic X-ray powder diffraction patterns for simple inorganic salts. (a) Pure salt A. (b) Pure salt B. (c) A physical mixture of salt A and salt B. Note that the peaks for both pure salts can be seen in the mixture; every peak matches a peak in either (a) or (b). (d) A diffraction pattern for a mixed crystal containing the same elements present in both A and B, but chemically combined in the same crystal lattice. The diffraction pattern for the mixed crystal (a unique structure) is unique; it does not match either pure A or pure B.

with a weak pattern of NaCl. Such a mixture is a *multiphase material*, and interpretation of multiphase patterns is more difficult than for single-phase (pure) materials. If, on the other hand, the crystal were a *mixed crystal* of sodium potassium chloride, in which the sodium and potassium ions are in the *same crystal lattice*, there would be changes in the crystal's lattice size from that of pure NaCl or pure KCl. However, the mixed crystal is a single-phase material, resulting in a unique diffraction pattern as shown in Figure 8.76d. X-ray powder diffraction therefore can be used to distinguish between a *mixture of crystals*, which would show both diffraction patterns, and a *mixed crystal*, which would give a separate unique diffraction pattern. The exact crystallographic lattice constants can be measured using XRD. Powder diffraction pattern matching to identify unknowns is now done with a computer, software, and a powder diffraction pattern spectral library or database that can be searched by the computer. An example is shown in Figure 8.77. The International Centre for Diffraction Data (ICDD), located in Newtown Square, PA, United States, maintains a database of more than 50,000 single-phase powder XRD patterns (www.icdd.com).

In polymer characterization, it is possible to determine the degree of crystallinity of semicrystalline polymers. The noncrystalline (amorphous) portion simply scatters the X-ray beam to give a continuous background, whereas the crystalline portion gives diffraction lines. A typical schematic diffraction spectrum of a semicrystalline polymer is shown in Figure 8.78. The ratio of the area of diffraction peaks to scattered radiation is proportional to the ratio of crystalline to noncrystalline material in the polymer. The ultimate quantitative analysis must be confirmed using standard polymers with known percent crystallinity and basing the calculation on the known ratio of crystalline diffraction to amorphous scattering.

Using an XRD pattern and looking at the intensity of peaks, it is possible to determine if the crystals of a polymer or a metal are oriented in any particular direction. "Preferred orientation" can occur after the material has been rolled out into a sheet, for example. This is sometimes a very undesirable property, since the material may be very weak in one direction and strong in another, with

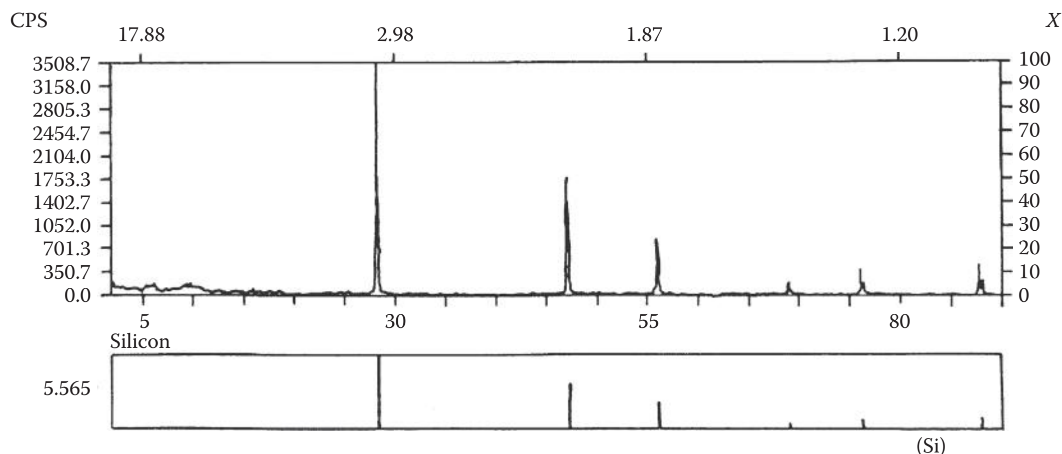


**Figure 8.77** The X-ray powder diffraction pattern of an unknown material is shown in the upper spectrum. A search of a computerized database identified the unknown as silicon, based on the match to the stored spectrum for silicon (lower spectrum).

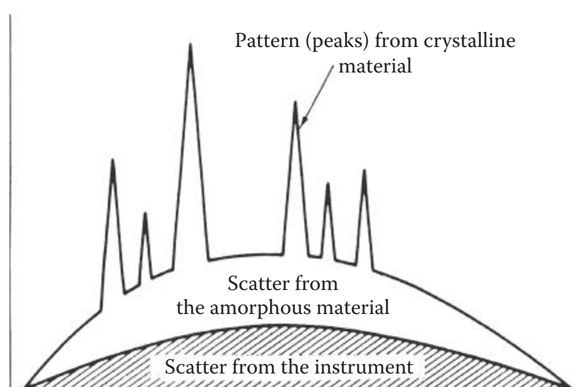


**Figure 8.78** Schematic diffraction pattern from a semicrystalline polymer, showing how both crystalline and amorphous phases may be detected. The amorphous portion results in broad scattering while the crystalline portion shows a typical diffraction peak pattern. A totally amorphous polymer would show no diffraction peaks. (There are no 100% crystalline polymers.) The units on the *x*-axis are degrees $\theta$.

the result that it tears easily in one direction. Sometimes, however, this is a desirable property, as, for example, in packaging material that we may wish to tear easily in one direction to open the package.

Powder XRD is used for phase analysis and compound identification in a variety of industries, especially mineral, mining, and metal production and for materials such as rocks, minerals, oxide materials, and products. Typical examples include the levels of Fe phases such as FeO, $Fe_2O_3$, $Fe_3O_4$, and FeC; determination of free lime in clinker and slags in the cement industry; phases related to the electrolysis of Al; and CaO, $CaCO_3$, and $Ca(OH)_2$ content.

XRD at different temperatures can be used to study phase transitions between different crystallographic forms of a material (e.g., tetragonal vs. monoclinic forms of yttria-stabilized zirconia). This approach can be used to measure thermal expansion coefficients and to study crystalline-to-amorphous transitions in materials.

A property of metals that can be determined by XRD is the state of anneal. Well-annealed metals are in an ordered crystal form and give sharp diffraction lines. If the metal is subjected to drilling, hammering, or bending, it becomes "worked" or "fatigued"; the crystal structure and the diffraction pattern change. Working a metal initially increases its strength, but continued deformation (fatigue) weakens the metal and can result in the metal breaking. (Try bending a paper clip slowly—you should note that it becomes harder to bend after one or two workings, but then if you continue to bend it at the same point, it will eventually become fatigued and break.) Disorder in metals and alloys can also result from rapid cooling from the molten state. Disorder results in lower density and a more brittle material. Electrical conductivity of metals is also affected by the order in the metal crystal. XRD can be used to distinguish between ordered and disordered materials and provide valuable information on the suitability of a material for a given use.

A very important use of XRD is in the determination of the structure of single crystals, that is, identifying the exact position in 3D space of every atom (molecules, ions) in the crystal. Single-crystal XRD was a major tool in elucidating the structure of ribonucleic acid (RNA) and deoxyribonucleic acid (DNA), insulin, vitamins, and proteins. Single-crystal diffractometry is used for structural determination of biomolecules, natural products, pharmaceuticals, inorganic coordination complexes, and organometallic compounds.

#### *8.4.6.1 Analytical Limitations of XRD*

Amorphous materials cannot be identified by XRD, so many polymeric and glassy materials cannot be studied. XRD is not a trace analysis technique. A component should be present at 3%–5% by weight at a minimum in order for diffraction peaks to be detected. The unique pattern from a mixed crystal, where one atom has replaced another in the lattice, was discussed earlier. A mixed crystal is analogous to a solid solution of a contaminant in a pure material. The contaminated material will appear to be a single phase, since it is a solid solution, but the lattice of the pure material will be expanded or contracted as the result of contaminant atoms of the "wrong" size in the lattice. There will be a unique diffraction pattern, but such a pattern may be hard to match. Mixtures may be difficult to identify because of overlapping peaks.

## 8.5 X-RAY EMISSION

In XRF, characteristic X-rays from an X-ray source are used to excite characteristic X-rays from a sample. X-ray emission differs in that particles such as electrons and alpha particles are the sources used to generate characteristic X-rays from a sample. Several types of X-ray emission systems will be described.

### 8.5.1 Electron Probe Microanalysis

A beam of electrons striking a target results in the emission of characteristic X-rays. This is the basis of the X-ray tube, as was discussed earlier in this chapter. A beam of electrons striking a sample will also generate characteristic X-rays from the sample. The use of a small diameter electron beam, on the order of 0.1–1.0 μm, to excite a sample is the basis of **electron probe microanalysis**. An electron probe microanalyzer is an X-ray emission spectrometer. The small diameter electron beam excites an area of the surface of the sample that is about 1 μm in diameter. Elemental composition and variation of composition on a microscopic scale can be obtained.

Two different instruments are available for microanalysis. The electron microprobe analyzer (EMA) uses high electron beam currents to provide elemental analysis of samples, with moderate spatial resolution and low magnification of the sample. The intensity of emitted X-rays from the

sample is high. The scanning electron microscope (SEM) is designed to provide high-resolution, high-magnification images of a sample. The SEM operates at low electron beam currents; the characteristic X-rays are of lower intensity than in the EMA but still provide elemental composition. In addition to X-ray spectra, other information may be obtained as a result of interactions of the electron beam with the sample. Some samples will exhibit UV or visible fluorescence (called *cathodoluminescence*); secondary electrons may be ejected, such as Auger electrons, and backscattered electrons are used to provide information about the sample topography and composition.

Both systems operate on similar principles. A tungsten filament emits electrons, which are focused by an electron optical system. The electron beam can scan the sample surface and can provide composition at a point, along a line or over a rectangular area, by *rastering* (moving) the beam across the surface in a series of parallel lines. The sample is mounted on a stage that can be accurately moved in the $x$- and $y$-direction and in the $z$-direction, normal to the plane of the sample. The system has an optical microscope, to permit alignment of the sample and selection of the area or feature of the sample to be analyzed.

The X-ray analysis system for the EMA is a WD spectrometer with gas-proportional counter detectors. In the SEM, an ED X-ray spectrometer with a Si(Li) detector is used. The entire electron and X-ray optical systems are operated under a vacuum of about $10^{-5}$ torr. Modern systems are completely automated with computer control of the instrument parameters, specimen stage movement, data collection, and data processing.

Samples must be solid and may be in almost any form. Thin films, bulk solids, particles, powders, machined pieces, and small objects (including biological specimens) can be analyzed. All elements from beryllium ($Z = 4$) to uranium can be determined at concentrations of about 100 ppm or greater. For qualitative analysis, the surface finish of the sample is not important. For quantitative analysis, the surface of the specimen must be flat. A common method for achieving a flat surface for an SEM sample is to embed the sample in epoxy and then carefully polish the hardened epoxy to expose a flat surface of the sample. Calibration standards should have flat surfaces as well, and the composition of the standards should be similar to that of the samples. Alternatively, an FP approach using pure element standards can be used. For nonconductive samples, a thin coating of osmium is deposited on the surface of the sample.

Applications of electron probe microanalysis are numerous in analytical chemistry, metallurgy, geology, medicine, biology, and materials science. In materials science, not only can the composition of the material be determined, but the location of elements in the solid structure can be visualized. Segregation of a particular element in grain boundaries between crystals can be seen, for example. Such segregation may have a dramatic effect on the properties of a material. Pure tungsten wire is too brittle to make a useful light bulb. The wire fractures easily as the light bulb is turned on (wire heats up) and off (wire cools down) because the crystals separate along the grain boundaries. By adding certain elements such as potassium to tungsten, an impure (doped) tungsten wire that is much more ductile results; this ductile wire can be heated and cooled many times without fracturing. Analysis of the doped tungsten using SEM shows that the added elements are located in the boundaries between the crystals. The elements in the grain boundaries cause the tungsten crystals to slide along the grain boundaries, permitting the tungsten wire to expand and contract on heating without fracturing. Thin films and multilayer materials can be analyzed and film thickness measured. Small particles filtered from air and water can be analyzed, and both particle count and particle size determined. The number, size, and type of particles in air are measures of air quality; this is very important in the manufacturing of semiconductor devices.

The distribution of elements in biological samples, mineral samples, soils, and other heterogeneous materials can be determined. Many other applications can be found in the literature. This is one of the few techniques that can provide spatial variation of composition at the micrometer scale. Other related techniques are discussed in Chapter 14.

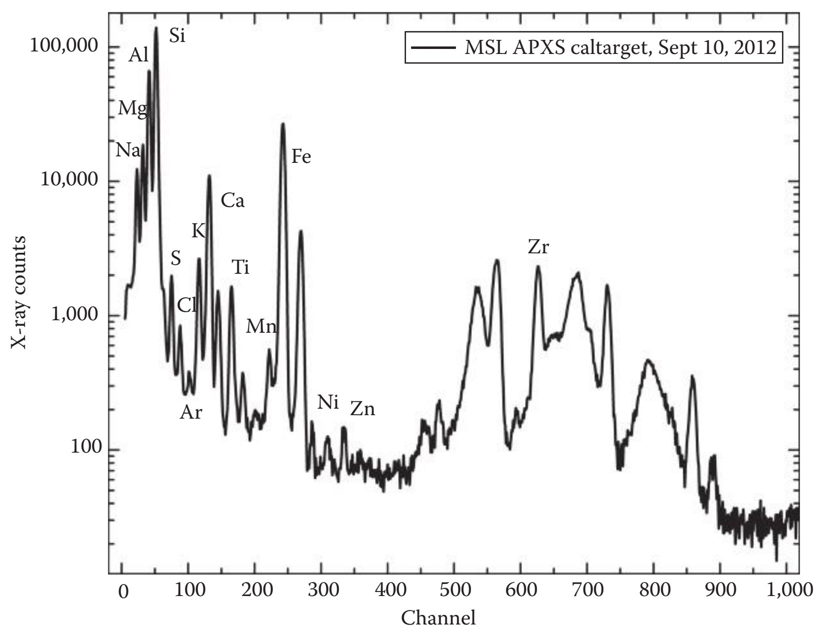


**Figure 8.79** Spectrum of the calibration target from the APXS on the Martian rover "Curiosity." (Image credit: NASA/JPL-Caltech/LANL.)

### 8.5.2 Particle-Induced X-Ray Emission

The use of a radioactive isotope as a source for XRF was discussed, and a list of common radioactive sources was given in Table 8.4. The use of one that generates "particles"—electrons or alpha particles—gives rise to the term PIXE. The 2012 NASA Martian Space Laboratory rover, Curiosity, has on board a PIXE instrument called an APXS. The APXS uses a Curium-244 source to excite characteristic X-rays from Martian rocks. The spectrometer includes a calibration target with multiple elements. The target is a well-characterized rock slab brought from Earth to enable accurate determination of the composition of Martian rocks. The calibration target spectrum is shown in Figure 8.79.

Figure 8.80 shows a Martian rock known as "Jake Matijevic" that has been studied using the APXS and the ChemCam laser-induced breakdown spectroscopy (LIBS) instrument (described in Chapter 7). The two black circles on the rock face show the areas studied by the APXS. The black dots are the laser pits from the LIBS instrument. The results of the APXS analysis are shown in Figure 8.81.

The spectra from the rock and target were collected for 1 h. Results showed that, compared to previous Martian rocks, the Jake rock is low in Fe and Mg, but high in Na, Al, Si, and K, which are often found in feldspar minerals. The results point to an igneous or volcanic origin for the rock.

## 8.6 COMMERCIAL X-RAY INSTRUMENT MANUFACTURERS

Commercial XRF systems include WDXRF and EDXRF laboratory-based instruments from floor models to benchtop systems, handheld X-ray analyzers based on EDXRF, field-portable XRF systems, and micro-XRF systems. Commercial XRD systems include single-crystal diffractometers,

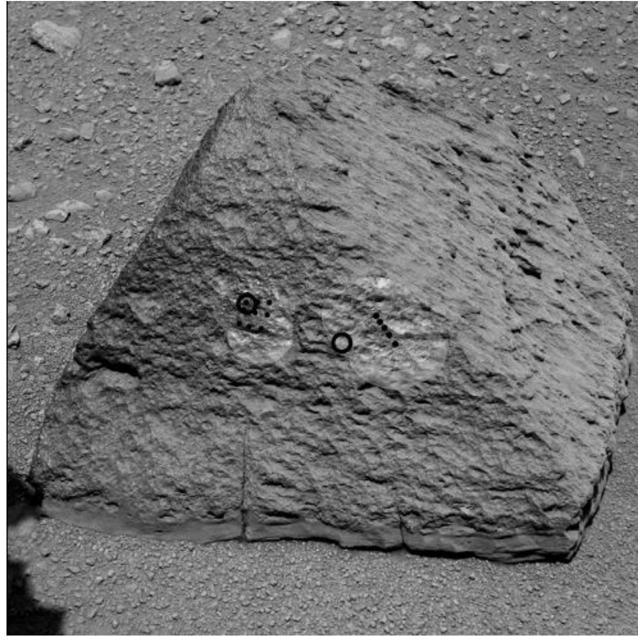

**Figure 8.80** The “Jake Matijevic” rock on Mars, showing the circles where the APXS instrument obtained data, as well as the laser pits (black dots) from the LIBS instrument. (Image credit: NASA/JPL-Caltech/LANL. Full-color images are available at www.nasa.gov/mission_pages/msl.)

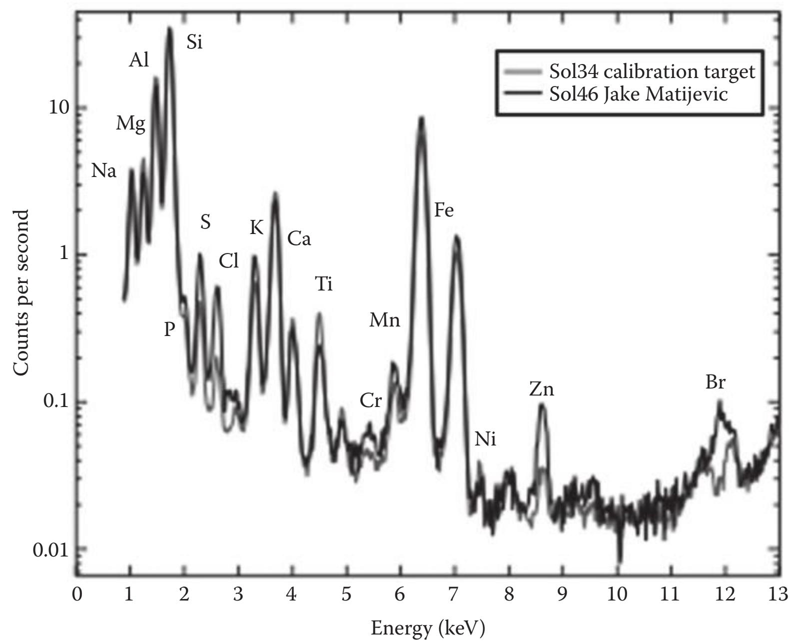


**Figure 8.81** Spectrum from “Jake” and the calibration target acquired by the APXS system. (Image credit: NASA/JPL-Caltech/LANL.)

powder XRD systems, and field-portable XRD systems. Hybrid XRD/XRF systems are available in laboratory and field-portable versions. Companies include but are not limited to Bruker, Horiba, PANalytical, Rigaku MSC and Applied Rigaku Technologies, Olympus (formerly Innov-X), SPECTRO, Thermo Fisher Scientific, EDAX, and Unisantis GmbH. The websites for most of these companies contain a wealth of information, including application notes, tutorials, videos, and on-demand webinars.

## SUGGESTED EXPERIMENTS/TUTORIALS

*Safety note*: The student is reminded that X-radiation poses significant health hazards. Safety is a very important issue with X-ray methods. X-radiation is ionizing radiation, a significant health hazard because it can damage or kill living cells and produce genetic mutations. Some instrumentation uses radioactive isotopes as sources; these sources are always producing ionizing radiation and cannot be “turned off.” Modern commercial instrumentation is equipped with the proper shielding and safety interlocks that will shut off the ionizing radiation automatically or protect the analyst from exposure when operated properly. Operators of X-ray instrumentation usually must undergo specialized safety training and wear radiation dosimeters to ensure that they are not being exposed to damaging X-rays. Only commercial equipment equipped with safety interlocks should be used and only after appropriate training and under the guidance of your instructor or radiation safety official at your facility. Under no circumstances should safety interlocks be tampered with. Experiments should never be performed with unconfined or unshielded X-ray sources. (An example of an unshielded X-ray source is the setup shown in Figure 8.14c.)

### X-Ray Absorption

**8.1** Take several metal disks made of different pure elements, each about 1 $in.^2$ in area and 1/8 in. in thickness. It is important that the thickness of each disk be constant. The disks should be made from (a) Mg, (b) Al, (c) Fe, (d) Ni, (e) Cu, (f) Sn, and (g) Pb. Expose them to an X-ray beam simultaneously on a single sheet of X-ray photographic film. Develop this film. Note that the absorption of X-rays by each disk is proportional to the atomic weight of the particular element.

**8.2** Take a piece of glass known to contain an entrapped bubble of air. Place it in front of X-ray film and expose it to X-rays. Note that the bubble can be detected on the film as a dark patch. Similar holes in metal castings (or other metal objects) can be detected by XRA, even though the holes are not visible to the naked eye.

### X-Ray Fluorescence

**8.3** Using the metal disks used in Experiment 8.1, record the fluorescence spectra of the different metals. Identify the K and L lines for each element. Plot the relationship between the wavelengths of these lines and the atomic numbers of the metals using a spreadsheet program such as Excel. Explain your results.

**8.4** Record the fluorescence spectrum of metal disks of unknown composition. By measuring the wavelength of the $K_\alpha$ line, identify the major components. Use disks of brass, bronze, stainless steel, and aluminum and coins of various denominations, for example.

**8.5** Using silver powder and copper powder, prepare mixtures with various ratios of these metals. Record the XRF spectrum of each mixture. Relate the silver/copper ratio to the ratio of the Ag $K_\alpha$ and Cu $K_\alpha$ lines. Measure the Ag/Cu ratio of various US silver coins minted (a) before 1964 and (b) after 1964.

**8.6** Record the fluorescence spectrum of sulfur. Locate the S $K_\alpha$ line. Record the fluorescence spectra of various grades of motor oil. Compare the sulfur contents of the oils by the intensities of the S $K_\alpha$ lines. The oil may be held in a polymer "zipper lock" bag during analysis if no liquid sample cups are available. Run a blank spectrum of the polymer bag as well to be certain it contains no detectable sulfur.

**8.7** Analyze small chips of various rocks, or samples of sand or soil from different geographic locations. Identify the elements present in each sample. Can you distinguish between sands or soils from different locations by their XRF spectra? Look for any trace or minor elements that may differentiate the samples. (Remember that peak intensities will vary due to surface roughness, so particle size differences between samples may account for peak height differences in the spectra.)

**8.8** Take the spectrum of various pieces of jewelry, supported on cellophane tape or a suitable heavy polymer film so that they do not fall into the spectrometer. Identify the elements present. Is your gold ring solid gold or gold-plated?

### X-Ray Diffraction

**8.9** Use a tungsten or copper X-ray source and a powder diffractometer. Load crushed NaCl powder into the sample holder. Measure the diffraction pattern of the NaCl. Repeat with powdered KCl. Note the difference in spectra. Make mixtures by varying the amounts of NaCl and KCl. Can you distinguish the mixtures and the relative amounts of each component from the powder patterns?

**8.10** For the student interested in crystal growth, potassium aluminum sulfate, also called alum, is a salt available in most pharmacies. It will form single crystals relatively easily from a supersaturated solution. Alum crystals are octahedral in shape and colorless. The related compound, chromium aluminum sulfate dodecahydrate, called chrome alum, forms dark-purple octahedral crystals. Mixing various proportions of supersaturated alum and chrome alum solutions allows the growth of mixed crystals that resemble amethysts in color. (The more alum in the mix, the lighter the purple color of the crystal.) Take the powder patterns of crushed pure alum and crushed pure chrome alum, and a mixture of the two compounds. After you have grown some mixed crystals, crush some and take their powder pattern. Is it different from the two pure materials and from the mixture? Explain your observations.

## PROBLEMS

**8.1** Draw a schematic diagram of an X-ray tube, label the major parts, and describe its operation.

**8.2** What is the origin of the $K_\alpha$ X-ray lines? The $K_\beta$ lines? The L lines?

**8.3** State Moseley's law. What was the importance of this law to chemistry in general?

**8.4** What are the three major analytical fields of X-ray spectroscopy? State three analytical applications of each field.

**8.5** The intensity of XRF is weak compared to some other spectroscopic techniques. What instrumental changes are made to maximize the fluorescence signal?

**8.6** What elements can be detected by XRF? What elements cannot be detected by XRF in air? Explain.

**8.7** Can X-rays from a tungsten target be used to excite copper atoms? Can X-rays from a copper target be used to excite tungsten atoms? Explain.

**8.8** Look at Figures 8.3a and 8.18. The spectrum in Figure 8.3 was obtained at a tube voltage of 30 kV; that in Figure 8.18 with *no* filter was obtained at 20 kV. Explain the difference in the spectra.

**8.9** What is the relationship between the wavelengths of the absorption edges and the related emission lines? Explain.
**8.10** Why can XRF not distinguish between $Cu^{2+}$ and $Cu^{1+}$ in a sample?
**8.11** Explain the difference between the two spectra in Figure 8.18. Why is a filter useful?
**8.12** Derive the Bragg equation using reflection from two parallel planes as the model.
**8.13** (a) Plot the signal-to-voltage relationship in an ionization counter and proportional counter.
(b) Which is the most sensitive? Why?
**8.14** Diagram a scintillation detector and describe its principle of operation.
**8.15** Describe how a Si(Li)-drifted detector operates.
**8.16** (a) What is meant by the mass absorption coefficient?
(b) What is the relationship between the mass absorption coefficient, atomic number, and atomic weight at the same wavelength?
**8.17** Describe the equipment used to collect XRD patterns from a single crystal.
**8.18** Why are X-ray powder diffraction patterns useful in analytical chemistry? What advantage does a powdered sample have over a single crystal in terms of identifying an unknown sample?
**8.19** Describe the basic components of a goniometer.
**8.20** Look up the Ge line energies in Appendix 8.A and predict where you would find a Ge escape peak in an EDXRF spectrum of pure Cu using a Ge(Li) detector. Where would the escape peak occur if a Si(Li) detector were used for the same sample?
**8.21** Predict what sum peaks you might see as artifacts in the EDXRF spectrum of pure Cu.
**8.22** Looking at the cell in Figure 8.63b with the origin in the back lower left corner (marked O), explain why the (440) plane is closer to the origin than the (110) plane. Remember that the Miller indices are the reciprocals of the intercepts. Draw the planes. (You may find drawing a 2D picture is easier than a 3D one).
**8.23** What axis is the (110) plane in Si parallel to? Draw the (110) plane in a cubic unit cell such as the one shown in Figure 8.63b.

To interpret Problems 8.24 through 8.31, students should use the following table of tube voltage/filter combinations optimized for element ranges as well as Table 8.A.2. These spectra were collected on a Thermo Scientific EDXRF using different voltages, filters, and atmospheres. The conditions are given in each spectrum. Check the voltage and filter combinations used for the elements that can be detected using that combination.

| Filter | Tube Voltage (kV) | Elements Optimized | Other Elements Detected |
|---|---|---|---|
| None | 8–15 | Na–S (K lines) | K–Fe (K lines) |
| | | Zn–Mo (L lines) | Tc–Ce (L lines) |
| Cellulose | 8–15 | Cl–Sc (K lines) | Al–Zn (K lines) |
| | | Tc–Cs (L ines | Zr–Gd (L ines) |
| Al, 0.127 mm | 10–20 | Ti–Mn (K lines) | Cl–Br (K lines) |
| | | Ba–Sm ( L lines) | Ag–Hf (L lines) |
| Thin (0.05 mm Rh) | 20–30 | Fe–Ge (K lines) | K–Mo (K lines) |
| | | Eu–Au (L lines) | Ba–U (L lines) |
| Five (0.127 mm Rh) | 30–45 | As–Mo (K lines) | Ti–Mo (K lines) |
| | | Hg–U ( L lines) | |
| Six (0.63 mm Cu) | 45–50 | Tc–La (K lines) | Zn–La (L lines) |

**8.24** Identify the binary inorganic salt that gives the following spectrum.

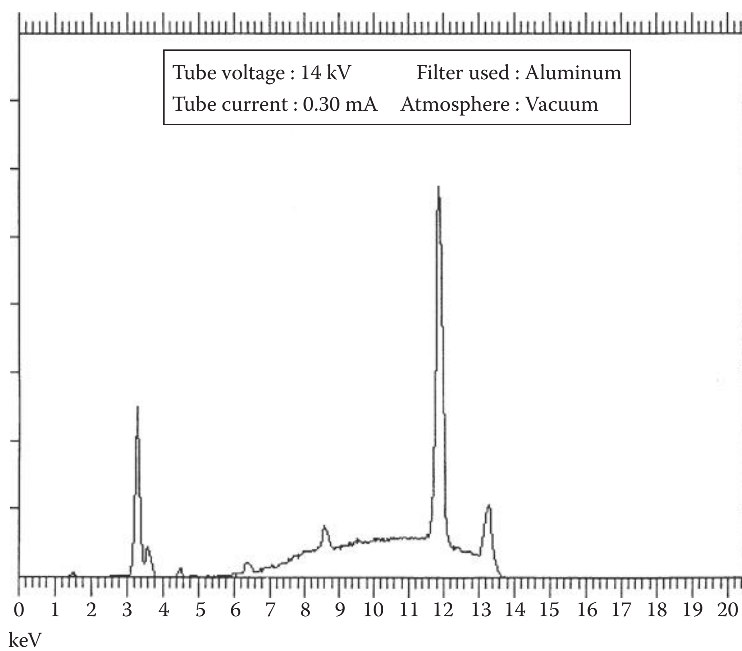


**8.25** Identify the elements present in this spectrum.

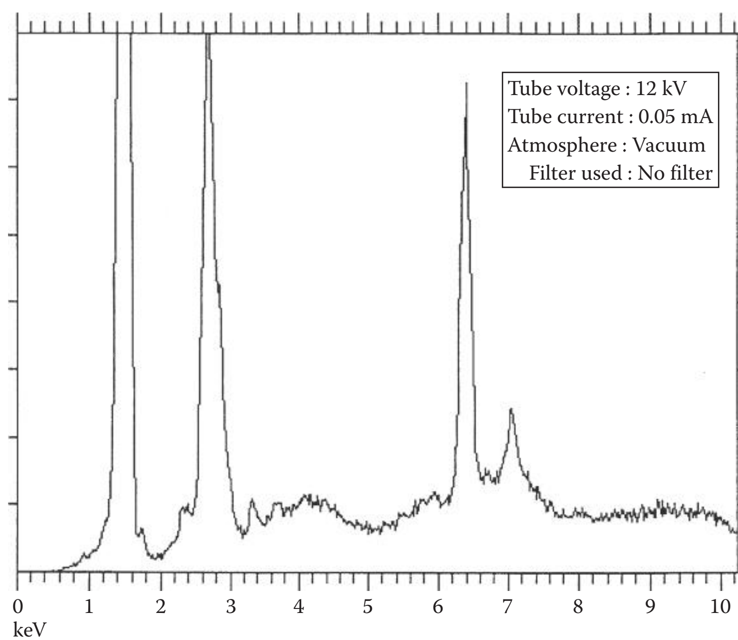

**8.26** Identify the elements present in this spectrum.

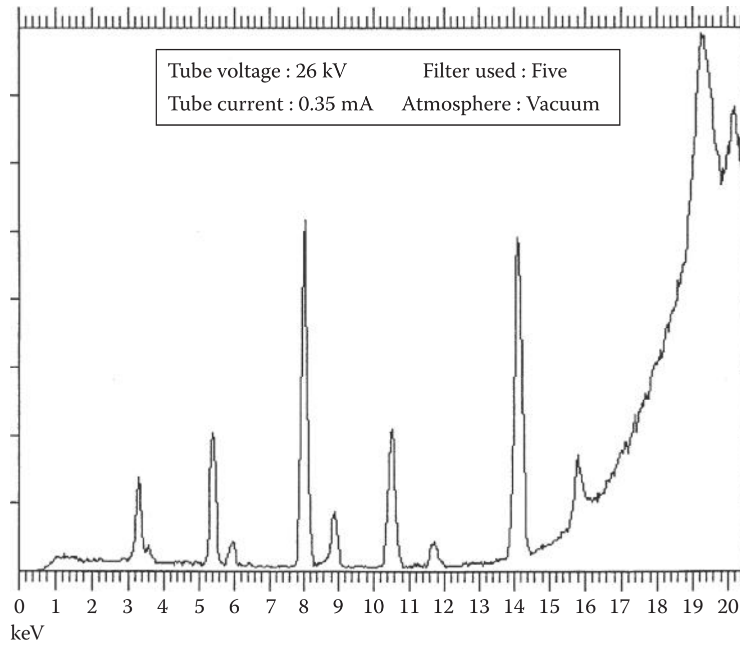


**8.27** Identify the elements present and label the lines.

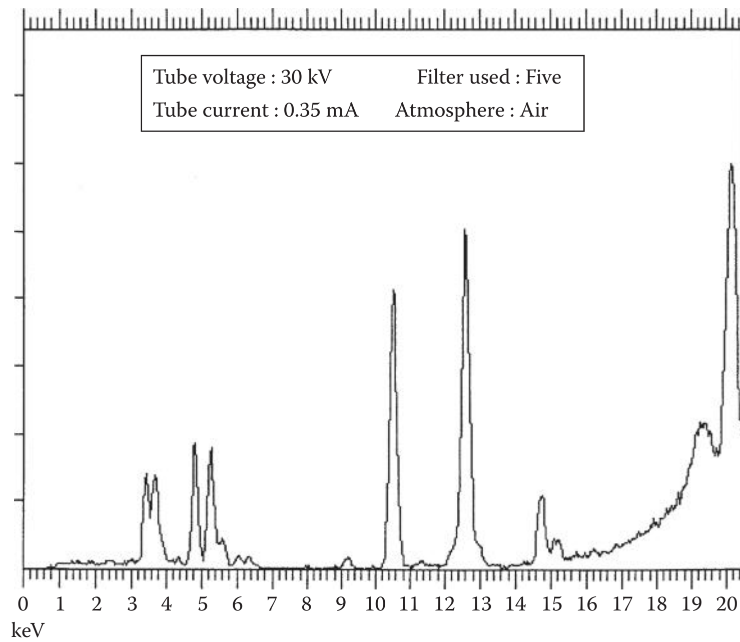

**8.28** Identify the elements present—there are at least seven. (Hint: Many are high Z elements.)

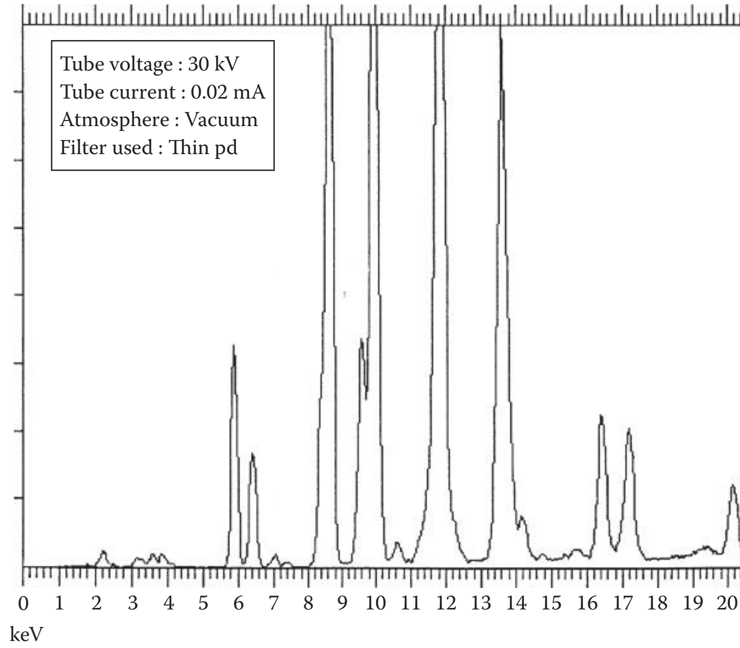


**8.29** More high Z elements to identify. Label the lines.

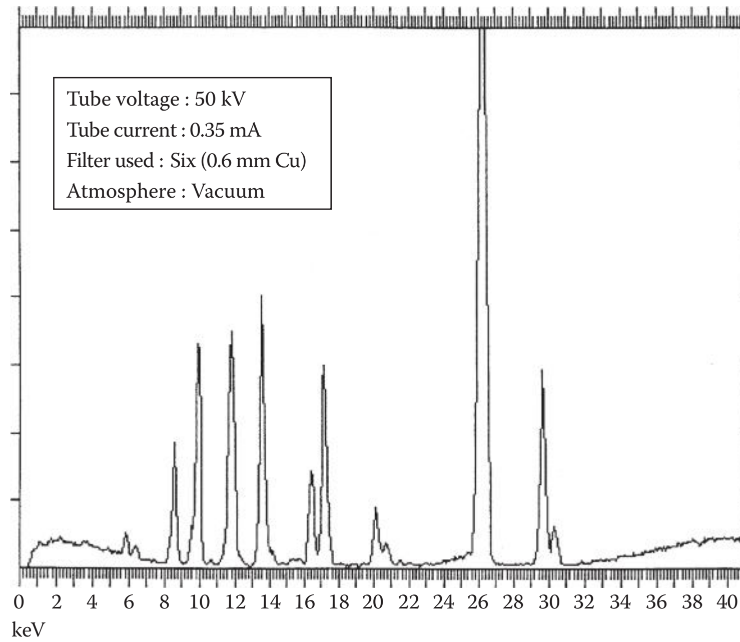

**8.30** This is the spectrum of the X-ray tube. The line spectrum was obtained with NO filter in the X-ray tube path. The dotted spectrum was obtained using a 0.63 mm Cu filter. (1) Identify the X-ray tube anode. (2) What do we call the radiation emitted by the filtered X-ray tube? (3) What elements will be excited using the filtered tube radiation? (4) Why do you want the tube voltage so high? (50 kV is high voltage.) (5) Why not use the unfiltered X-ray tube spectrum to excite your sample? Can you list two elements that could not be determined using the unfiltered X-ray tube, other than the anode element itself?

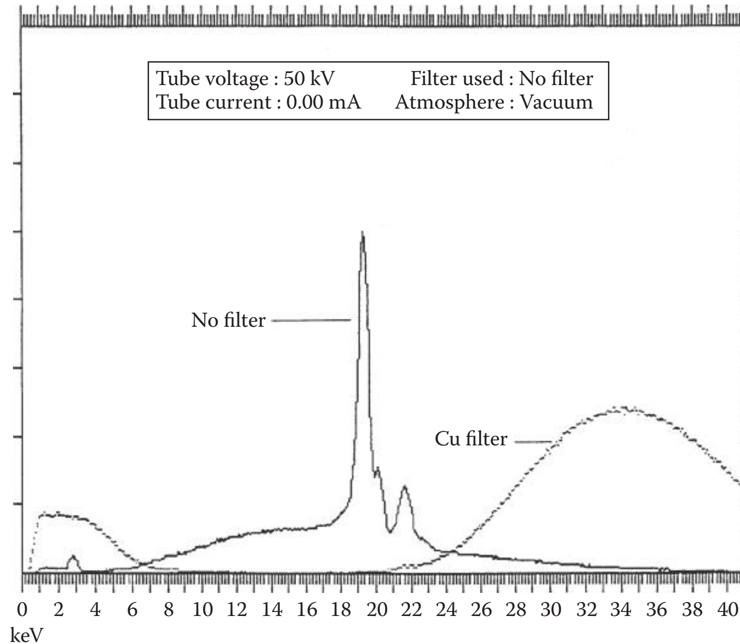


**8.31** A sample with many elements. Identify as many as you can. This sample is loaded with stuff! GOOD LUCK!!!

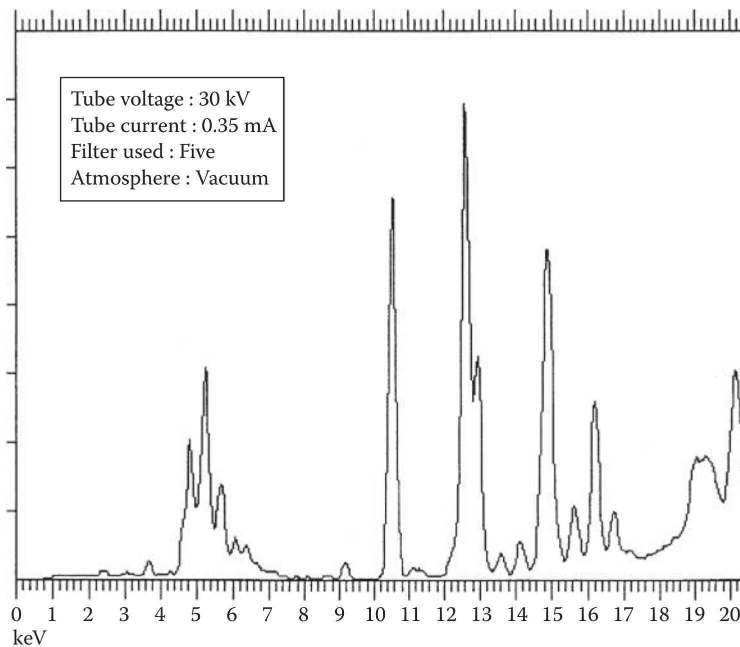

## 8.A APPENDIX: CHARACTERISTIC X-RAY WAVELENGTHS (Å) AND ENERGIES (keV)*

**Table 8.A.1 K Series Lines (Å)**

| **Line** | | $\alpha_{1,2}$ | $\alpha_1$ | $\alpha_2$ | $\beta_1$ | | $\beta_3$ |
|---|---|---|---|---|---|---|---|
| **Approximate Intensity** | | **150** | **100** | **50** | | **15** | |
| **Element** | **Z** | | | | | | |
| Li | 3 | 230 | | | | | |
| B | 4 | 113 | | | | | |
| B | 5 | 67 | | | | | |
| C | 6 | 44 | | | | | |
| N | 7 | 31.603 | | | | | |
| O | 8 | 23.707 | | | | | |
| F | 9 | 18.307 | | | | | |
| Ne | 10 | 14.615 | | | 14.460 | | |
| Na | 11 | 11.909 | | | 11.574 | | 11.726 |
| Mg | 12 | 9.889 | | | 9.559 | | 9.667 |
| Al | 13 | 8.339 | 8.338 | 8.341 | 7.960 | | 8.059 |
| Si | 14 | 7.126 | 7.125 | 7.127 | | 6.778 | |
| P | 15 | 6.155 | 6.154 | 6.157 | 5.804 | | |
| S | 16 | 5.373 | 5.372 | 5.375 | 5.032 | | |
| Cl | 17 | 4.729 | 4.728 | 4.731 | 4.403 | | |
| Ar | 18 | 4.192 | 4.191 | 4.194 | 3.886 | | |
| K | 19 | 3.744 | 3.742 | 3.745 | 3.454 | | |
| Ca | 20 | 3.360 | 3.359 | 3.362 | 3.089 | | |
| Sc | 21 | 3.032 | 3.031 | 3.034 | 2.780 | | |
| Ti | 22 | 2.750 | 2.749 | 2.753 | | 2.514 | |
| V | 23 | 2.505 | 2.503 | 2.507 | | 2.285 | |
| Cr | 24 | 2.291 | 2.290 | 2.294 | | 2.085 | |
| Mn | 25 | 2.103 | 2.102 | 2.105 | | 1.910 | |
| Fe | 26 | 1.937 | 1.936 | 1.940 | | 1.757 | |
| Co | 27 | 1.791 | 1.789 | 1.793 | | 1.621 | |
| Ni | 28 | 1.659 | 1.658 | 1.661 | | 1.500 | |
| Cu | 29 | 1.542 | 1.540 | 1.544 | 1.392 | | 1.393 |
| Zn | 30 | 1.437 | 1.435 | 1.439 | 1.296 | | |
| Ga | 31 | 1.341 | 1.340 | 1.344 | 1.207 | | 1.208 |
| Ge | 32 | 1.256 | 1.255 | 1.258 | 1.129 | | 1.129 |
| As | 33 | 1.177 | 1.175 | 1.179 | 1.057 | | 1.058 |
| Se | 34 | 1.106 | 1.105 | 1.109 | 0.992 | | 0.993 |
| Br | 35 | 1.041 | 1.040 | 1.044 | 0.933 | | 0.933 |
| Kr | 36 | 0.981 | 0.980 | 0.984 | 0.879 | | 0.879 |
| Rb | 37 | 0.927 | 0.926 | 0.930 | 0.829 | | 0.830 |
| Sr | 38 | 0.877 | 0.875 | 0.880 | 0.783 | | 0.784 |
| Y | 39 | 0.831 | 0.829 | 0.833 | 0.740 | | 0.741 |
| Zr | 40 | 0.788 | 0.786 | 0.791 | 0.701 | | 0.702 |
| Nb | 41 | 0.748 | 0.747 | 0.751 | 0.665 | | 0.666 |
| Mo | 42 | 0.710 | 0.709 | 0.713 | 0.632 | | 0.633 |
| Tc | 43 | 0676 | 0.675 | 0.679 | | 0.601 | |

(*continued*)

* Appendices 8.A and 8.B are modified from Markowicz, used with permission. The data in these tables were obtained from the following sources: Clark (1963), Burr (1974), and Jenkins et al. (1991).

**Table 8.A.1 (continued) K Series Lines (Å)**

| **Line** | | $\alpha_{1,2}$ | $\alpha_1$ | $\alpha_2$ | $\beta_1$ | | $\beta_3$ |
|---|---|---|---|---|---|---|---|
| **Approximate Intensity** | | **150** | **100** | **50** | | **15** | |
| **Element** | **Z** | | | | | | |
| Ru | 44 | 0.644 | 0.643 | 0.647 | 0.572 | | 0.573 |
| Rh | 45 | 0.614 | 0.613 | 0.617 | 0.546 | | 0.546 |
| Pd | 46 | 0.587 | 0.585 | 0.590 | 0.521 | | 0.521 |
| Ag | 47 | 0.561 | 0.559 | 0.564 | 0.497 | | 0.498 |
| Cs | 48 | 0.536 | 0.535 | 0.539 | 0.475 | | 0.476 |
| In | 49 | 0.514 | 0.512 | 0.517 | 0.455 | | 0.455 |
| Sn | 50 | 0.492 | 0.491 | 0.495 | 0.435 | | 0.436 |
| Sb | 51 | 0.472 | 0.470 | 0.475 | 0.417 | | 0.418 |
| Te | 52 | 0.453 | 0.451 | 0.456 | 0.400 | | 0.401 |
| I | 53 | 0.435 | 0.433 | 0.438 | 0.384 | | 0.385 |
| Xe | 54 | 0.418 | 0.416 | 0.421 | 0.369 | | 0.360 |
| Cs | 55 | 0.402 | 0.401 | 0.405 | 0.355 | | 0.355 |
| Ba | 56 | 0.387 | 0.385 | 0.390 | 0.341 | | 0.342 |
| La | 57 | 0.373 | 0.371 | 0.376 | 0.328 | | 0.329 |
| Ce | 58 | 0.359 | 0.357 | 0.362 | 0.316 | | 0.317 |
| Pr | 59 | 0.346 | 0.344 | 0.349 | 0.305 | | 0.305 |
| Nd | 60 | 0.334 | 0.332 | 0.337 | 0.294 | | 0.294 |
| Pm | 61 | 0.322 | 0.321 | 0.325 | | 0.283 | |
| Sm | 62 | 0.311 | 0.309 | 0.314 | 0.274 | | 0.274 |
| Eu | 63 | 0.301 | 0.299 | 0.304 | 0.264 | | 0.265 |
| Gd | 64 | 0.291 | 0.289 | 0.294 | 0.255 | | 0.256 |
| Tb | 65 | 0.281 | 0.279 | 0.284 | 0.246 | | 0.246 |
| Dy | 66 | 0.272 | 0.270 | 0.275 | 0.237 | | 0.238 |
| Ho | 67 | 0.263 | 0.261 | 0.266 | 0.230 | | 0.231 |
| Er | 68 | 0.255 | 0.253 | 0.258 | 0.222 | | 0.223 |
| Tm | 69 | 0.246 | 0.244 | 0.250 | 0.215 | | 0.216 |
| Yb | 70 | 0.238 | 0.236 | 0.241 | 0.208 | | 0.208 |
| Lu | 71 | 0.231 | 0.229 | 0.234 | 0.202 | | 0.203 |
| Hf | 72 | 0.224 | 0.222 | 0.227 | 0.195 | | 0.196 |
| Ta | 73 | 0.217 | 0.215 | 0.220 | 0.190 | | 0.191 |
| W | 74 | 0.211 | 0.209 | 0.213 | 0.184 | | 0.185 |
| Re | 75 | 0.204 | 0.202 | 0.207 | 0.179 | | 0.179 |
| Os | 76 | 0.198 | 0.196 | 0.201 | 0.173 | | 0.174 |
| Ir | 77 | 0.193 | 0.191 | 0.196 | 0.168 | | 0.169 |
| Pt | 78 | 0.187 | 0.158 | 0.190 | 0.163 | | 0.164 |
| Au | 79 | 0.182 | 0.180 | 0.185 | 0.159 | | 0.160 |
| Hg | 80 | 0.177 | 0.175 | 0.180 | 0.154 | | 0.155 |
| Tl | 81 | 0.172 | 0.170 | 0.175 | 0.150 | | 0.151 |
| Pb | 82 | 0.167 | 0.165 | 0.170 | 0.146 | | 0.147 |
| Bi | 83 | 0.162 | 0.161 | 0.165 | 0.142 | | 0.143 |
| Po | 84 | 0.185 | 0.156 | 0.161 | 0.138 | | |
| At | 85 | | 0.152 | 0.157 | 0.134 | | 0.135 |
| Rn | 86 | | 0.148 | 0.153 | 0.131 | | 0.132 |
| Fr | 87 | | 0.144 | 0.149 | 0.127 | | 0.128 |
| Ra | 88 | | 0.144 | 0.149 | 0.127 | | 0.128 |
| Ac | 89 | | 0.140 | 0.145 | 0.124 | | 0.125 |
| Th | 90 | 0.135 | 0.133 | 0.138 | 0.117 | | 0.118 |
| Pa | 91 | | 0.131 | 0.136 | 0.115 | | 0.116 |
| U | 92 | 0.128 | 0.126 | 0.131 | 0.111 | | 0.112 |

**Table 8.A.2 Energies of Principal K and L X-Ray Emission Lines (keV)**

| Z | Element | $K_{\beta_2}$ | $K_{\beta_1}$ | $K_{\alpha_1}$ | $K_{\alpha_2}$ | $L_{\gamma_1}$ | $L_{\beta_2}$ | $L_{\beta_1}$ | $L_{\alpha_1}$ | $L_{\alpha_2}$ |
|---|---|---|---|---|---|---|---|---|---|---|
| 3 | Li | | | 0.052 | | | | | | |
| 4 | Be | | | 0.110 | | | | | | |
| 5 | B | | | 0.185 | | | | | | |
| 6 | C | | | 0.282 | | | | | | |
| 7 | N | | | 0.392 | | | | | | |
| 8 | C | | | 0.523 | | | | | | |
| 9 | F | | | 0.677 | | | | | | |
| 10 | Ne | | | 0.851 | | | | | | |
| 11 | Na | | 1.067 | 1.041 | | | | | | |
| 12 | Mg | | 1.297 | 1.254 | | | | | | |
| 13 | Al | | 1.553 | 1.487 | 1.486 | | | | | |
| 14 | Si | | 1.832 | 1.40 | 1.739 | | | | | |
| 15 | P | | 2.136 | 2.015 | 2.014 | | | | | |
| 16 | S | | 2.464 | 2.309 | 2.306 | | | | | |
| 17 | Cl | | 2.815 | 2.622 | 2.621 | | | | | |
| 18 | Ar | | 3.192 | 2.957 | 2.955 | | | | | |
| 19 | K | | 3.589 | 3.313 | 3.310 | | | | | |
| 20 | Ca | | 4.012 | 3.691 | 3.688 | | | 0.344 | 0.341 | |
| 21 | Sc | | 4.460 | 4.090 | 4.085 | | | 0.399 | 0.395 | |
| 22 | Ti | | 4.931 | 4.510 | 4.504 | | | 0.458 | 0.492 | |
| 23 | V | | 5.427 | 4.952 | 4.944 | | | 0.519 | 0.510 | |
| 24 | Cr | | 5.946 | 5.414 | 5.405 | | | 0.581 | 0.571 | |
| 25 | Mn | | 6.490 | 5.898 | 5.887 | | | 0.647 | 0.636 | |
| 26 | Fe | | 7.057 | 6.403 | 6.390 | | | 0.717 | 0.704 | |
| 27 | Co | | 7.647 | 6.930 | 6.915 | | | 0.790 | 0.775 | |
| 28 | Ni | 8.328 | 8.264 | 7.477 | 7.460 | | | 0.866 | 0.849 | |
| 29 | Cu | 8.976 | 8.904 | 8.047 | 8.027 | | | 0.943 | 0.928 | |
| 30 | Zn | 9.657 | 9.571 | 8.638 | 8.615 | | | 1.032 | 1.009 | |
| 31 | Ga | 10.365 | 10.263 | 9.251 | 9.234 | | | 1.122 | 1.096 | |
| 32 | Ge | 11.100 | 10.981 | 9.885 | 9.854 | | | 1.216 | 1.166 | |
| 33 | As | 11.863 | 11.725 | 10.543 | 10.507 | | | 1.517 | 1.282 | |
| 34 | Se | 12.651 | 12.495 | 11.221 | 11.181 | | | 1.419 | 1.379 | |
| 35 | Br | 13.465 | 13.290 | 11.923 | 11.877 | | | 1.526 | 1.480 | |
| 36 | Kr | 14.313 | 14.112 | 12.648 | 12.597 | | | 1.638 | 1.587 | |
| 37 | Rb | 15.184 | 14.960 | 13.394 | 13.335 | | | 1.752 | 1.694 | 1.692 |
| 38 | Sr | 16.083 | 15.834 | 14.164 | 14.097 | | | 1.872 | 1.806 | 1.805 |
| 39 | Y | 17.011 | 16.736 | 14.957 | 14.882 | | | 1.996 | 1.922 | 1.920 |
| 40 | Zr | 17.969 | 17.666 | 15.774 | 15.690 | 2.302 | 2.219 | 2.124 | 2.042 | 2.040 |
| 41 | Nb | 18.951 | 18.261 | 16.614 | 16.520 | 2.462 | 2.367 | 2.257 | 2.166 | 2.163 |
| 42 | Mo | 19.964 | 19.607 | 17.478 | 17.373 | 2.623 | 2.518 | 2.395 | 2.293 | 2.290 |
| 43 | Tc | 21.012 | 20.585 | 18.410 | 18.328 | 2.792 | 2.674 | 2.538 | 2.424 | 2.420 |
| 44 | Ru | 22.072 | 21.655 | 19.278 | 19.149 | 2.964 | 2.836 | 2.683 | 2.558 | 2.554 |
| 45 | Rh | 23.169 | 22.721 | 20.214 | 20.072 | 3.144 | 3.001 | 2.834 | 2.696 | 2.692 |
| 46 | Pd | 24.297 | 23.816 | 21.175 | 21.018 | 3.328 | 3.172 | 2.990 | 2.838 | 2.833 |
| 47 | Ag | 25.454 | 24.942 | 22.162 | 21.988 | 3.519 | 3.348 | 3.151 | 2.994 | 2.978 |
| 48 | Cd | 26.641 | 26.093 | 23.172 | 22.982 | 3.716 | 3.528 | 3.316 | 3.133 | 3.127 |
| 49 | In | 27.859 | 27.274 | 24.207 | 24.000 | 3.920 | 3.713 | 3.487 | 3.287 | 3.279 |
| 50 | Sn | 29.106 | 28.483 | 25.270 | 25.042 | 4.131 | 3.904 | 3.662 | 3.444 | 3.436 |
| 51 | Sb | 30.387 | 29.723 | 26.357 | 26.109 | 4.347 | 4.100 | 3.543 | 3.605 | 3.595 |

(*continued*)

**Table 8.A.2 (continued) Energies of Principal K and L X-Ray Emission Lines (keV)**

| Z | Element | $K_{\beta_2}$ | $K_{\beta_1}$ | $K_{\alpha_1}$ | $K_{\alpha_2}$ | $L_{\gamma_1}$ | $L_{\beta_2}$ | $L_{\beta_1}$ | $L_{\alpha_1}$ | $L_{\alpha_2}$ |
|---|---|---|---|---|---|---|---|---|---|---|
| 52 | Te | 31.698 | 30.993 | 27.471 | 27.200 | 4.570 | 4.301 | 4.029 | 3769 | 3.758 |
| 53 | I | 33.016 | 32.292 | 28.610 | 28.315 | 4.800 | 4.507 | 4.220 | 3.937 | 3.926 |
| 54 | Xe | 34.446 | 33.644 | 29.802 | 29.485 | 5.036 | 4.720 | 4.422 | 4.111 | 4.098 |
| 55 | Cs | 35.819 | 34.984 | 30.970 | 30.623 | 5.280 | 4.936 | 4.620 | 4.286 | 4.272 |
| 56 | Ba | 37.255 | 35.376 | 32.191 | 31.815 | 5.531 | 5.156 | 4.828 | 4.467 | 4.451 |
| 57 | La | 38.728 | 37.799 | 33.440 | 33.033 | 5.789 | 5.384 | 5.043 | 4.651 | 4.635 |
| 58 | Ce | 40.231 | 39.255 | 34.717 | 34.276 | 6.052 | 5.613 | 5.262 | 4.840 | 4.823 |
| 59 | Pr | 41.772 | 40.746 | 36.023 | 35.548 | 6.322 | 5.850 | 5.489 | 5.034 | 5.014 |
| 60 | Nd | 43.298 | 42.269 | 37.359 | 36.845 | 6.602 | 6.090 | 5.722 | 5.230 | 5.208 |
| 61 | Pm | 44.955 | 43.945 | 38.649 | 38.160 | 6.891 | 6.336 | 5.956 | 5.431 | 5.408 |
| 62 | Sm | 46.553 | 45.400 | 40.124 | 39.523 | 7.180 | 6.587 | 6.206 | 5.636 | 5.609 |
| 63 | Eu | 48.241 | 47.027 | 41.529 | 40.877 | 7.478 | 6.842 | 6.456 | 5.846 | 5.816 |
| 64 | Gd | 49.961 | 48.718 | 42.983 | 42.280 | 7.788 | 7.102 | 6.714 | 6.039 | 6.027 |
| 65 | Tb | 51.737 | 50.391 | 44.470 | 43.737 | 8.104 | 7.368 | 6.979 | 6.275 | 6.241 |
| 66 | Dy | 53.491 | 52.178 | 45.985 | 45.193 | 8.418 | 7.638 | 7.249 | 6.495 | 6.457 |
| 67 | Ho | 55.292 | 53.934 | 47.528 | 46.686 | 8.748 | 7.912 | 7.528 | 6.720 | 6.680 |
| 68 | Er | 57.088 | 55.690 | 49.099 | 48.205 | 9.089 | 8.188 | 7.810 | 6.948 | 6.904 |
| 69 | Tm | 58.969 | 57.576 | 50.730 | 49.762 | 9.424 | 8.472 | 8.103 | 7.181 | 7.135 |
| 70 | Yb | 60.959 | 59.352 | 52.360 | 51.326 | 9.779 | 8.758 | 8.401 | 7.414 | 7.367 |
| 71 | Lu | 62.946 | 61.282 | 54.063 | 52.959 | 10.142 | 9.048 | 8.709 | 7.654 | 7.604 |
| 72 | Hf | 64.936 | 63.209 | 55.757 | 54.579 | 10.514 | 9.346 | 9.021 | 7.898 | 7.843 |
| 73 | Ta | 66.999 | 65.210 | 57.524 | 56.270 | 10.892 | 9.649 | 9.341 | 8.145 | 8.087 |
| 74 | W | 69.090 | 67.233 | 59.310 | 57.973 | 11.283 | 9.959 | 9.670 | 8.396 | 8.333 |
| 75 | Re | 71.220 | 69.298 | 61.131 | 59.707 | 11.684 | 10.273 | 10.008 | 8.651 | 8.584 |
| 76 | Os | 73.393 | 71.404 | 62.991 | 61.477 | 12.094 | 10.596 | 10.354 | 8.910 | 8.840 |
| 77 | Ir | 75.605 | 73.549 | 64.886 | 63.278 | 12.509 | 10.918 | 10.706 | 9.173 | 9.098 |
| 78 | Pt | 77.866 | 75.736 | 66.820 | 65.111 | 12.939 | 11.249 | 11.069 | 9.441 | 9.360 |
| 79 | Au | 80.165 | 77.968 | 68.794 | 66.980 | 13.379 | 11.582 | 11.439 | 9.711 | 9.625 |
| 80 | Hg | 82.526 | 80.258 | 70.821 | 68.894 | 13.828 | 11.923 | 11.823 | 9.987 | 9.896 |
| 81 | Tl | 84.904 | 82.558 | 72.860 | 70.320 | 14.288 | 12.268 | 12.210 | 10.266 | 10.170 |
| 82 | Pb | 87.343 | 94.922 | 74.957 | 72.794 | 14.762 | 12.620 | 12.611 | 10.549 | 10.448 |
| 83 | Bi | 89.833 | 87.335 | 77.097 | 74.805 | 15.244 | 12.977 | 13.021 | 10.836 | 10.729 |
| 84 | Po | 92.386 | 89.809 | 79.296 | 76.868 | 15.740 | 13.338 | 13.441 | 11.128 | 11.014 |
| 85 | At | 94.976 | 92.319 | 81.525 | 78.956 | 16.248 | 13.705 | 13.873 | 11.424 | 11.304 |
| 86 | Rn | 97.616 | 94.877 | 83.800 | 81.080 | 16.768 | 14.077 | 14.316 | 11.724 | 11.597 |
| 87 | Fr | 100.305 | 97.483 | 86.119 | 83.243 | 17.301 | 14.459 | 14.770 | 12.029 | 11.894 |
| 88 | Ra | 103.048 | 100.136 | 88.485 | 85.446 | 17.845 | 14.839 | 15.233 | 12.338 | 12.194 |
| 89 | Ac | 105.838 | 102.846 | 90.894 | 87.681 | 18.405 | 15.227 | 15.712 | 12.650 | 12.499 |
| 90 | Th | 108.671 | 105.592 | 93.334 | 89.942 | 18.977 | 15.620 | 16.200 | 12.966 | 12.808 |
| 91 | Pa | 111.575 | 108.408 | 95.851 | 92.271 | 19.559 | 16.022 | 16.700 | 13.291 | 13.120 |
| 92 | U | 114.549 | 111.289 | 98.428 | 94.648 | 20.163 | 16.425 | 17.218 | 13.613 | 12.438 |
| 93 | Np | 117.533 | 114.181 | 101.005 | 97.023 | 20.774 | 16.837 | 17.740 | 13.945 | 12.758 |
| 94 | Pu | 120.592 | 117.146 | 103.653 | 99.457 | 21.401 | 17.254 | 18.278 | 14.279 | 14.082 |
| 95 | Am | 123.706 | 120.163 | 106.351 | 101.932 | 22.042 | 17.667 | 18.829 | 14.618 | 14.411 |
| 96 | Cm | 126.875 | 123.235 | 109.098 | 104.448 | 22.699 | 18.106 | 19.393 | 14.961 | 14.743 |
| 97 | Bk | 130.101 | 126.362 | 111.896 | 107.023 | 23.370 | 18.540 | 19.971 | 15.309 | 15.079 |
| 98 | Cf | 133.383 | 129.544 | 114.745 | 109.603 | 24.056 | 18.980 | 20.562 | 15.661 | 15.420 |
| 99 | Es | 136.724 | 132.781 | 118.646 | 112.244 | 24.758 | 19.426 | 21.166 | 16.018 | 15.764 |
| 100 | Fm | 140.122 | 136.075 | 120.598 | 114.926 | 27.475 | 19.879 | 21.785 | 16.379 | 16.113 |

*Note:* The conversion equation between energy in keV and wavelength in Å is $E$ (keV) = 12.4/λ (Å).

**Table 8.A.3 Correspondence between Old Siegbahn and New IUPAC Notation X-Ray Diagram Lines**

| Siegbahn | IUPAC | Siegbahn | IUPAC | Siegbahn | IUPAC |
|---|---|---|---|---|---|
| $K_{\alpha_1}$ | $K–L_3$ | $L_{\alpha_1}$ | $L_3–M_5$ | $L_{\gamma 1}$ | $L_2–N_4$ |
| $K_{\alpha_2}$ | $K–L_2$ | $L_{\alpha 2}$ | $L_{3_}M_4$ | $L_{\gamma 2}$ | $L_1–N_2$ |
| $K_{\beta_1}$ | $K–M_3$ | $L_{\beta_1}$ | $L_2–M_4$ | $L_{\gamma 3}$ | $L_1–N_3$ |
| $K_{\beta_2^1}$ | $K–N_3$ | $L_{\beta 2}$ | $L_3–N_5$ | $L_{\gamma 4}$ | $L_1–O_4$ |
| $K_{\beta_2^{11}}$ | $K–N_2$ | $L_{\beta 3}$ | $L_1–M_3$ | $L_{\gamma 4}$ | $L_1–O_2$ |
| $K_{\beta_3}$ | $K–M_2$ | $L_{\beta 4}$ | $L_1–M_2$ | $L_{\gamma 5}$ | $L_2–N_1$ |
| $K_{\beta_4^1}$ | $K–N_5$ | $L_{\beta 5}$ | $L_3–O_{4,5}$ | $L_{\gamma 6}$ | $L_2–O_4$ |
| $K_{\beta_4^{11}}$ | $K–N_4$ | $L_{\beta 6}$ | $L_3–N_1$ | $L_{\gamma 8}$ | $L_2–O_1$ |
| $K_{\beta_{4x}}$ | $K–N_4$ | $L_{\beta 7}$ | $L_3–O_1$ | $L_{\gamma 8}$ | $L_2–N_{6(7)}$ |
| $K_{\beta_5^1}$ | $K–M_5$ | $L_{\beta'_7}$ | $L_3–N_{6,7}$ | $L_{\eta}$ | $L_2–M_1$ |
| $K_{\beta_5^{11}}$ | $K–M_4$ | $L_{\beta 9}$ | $L_1–M_5$ | $L_l$ | $L_3–M_1$ |
| | | $L_{\beta 10}$ | $L_1–M_4$ | $L_s$ | $L_3–M_3$ |
| | | $L_{\beta 15}$ | $L_3–N_4$ | $L_t$ | $L_3–M_2$ |
| | | $L_{\beta 17}$ | $L_2–M_3$ | $L_u$ | $L_3–N_{6,7}$ |
| | | | | $L_v$ | $L_2–N_{6(7)}$ |
| | | | | $M_{\alpha_1}$ | $M_5–N_7$ |
| | | | | $M_{\alpha_2}$ | $M_5–N_6$ |
| | | | | $M\beta$ | $M_4–N_6$ |
| | | | | $M_{\gamma}$ | $M_3–N_5$ |
| | | | | $M_{\zeta}$ | $M_{4,5}–N_{2,3}$ |

## 8.B APPENDIX: ABSORPTION EDGE WAVELENGTHS AND ENERGIES

**Table 8.B.1 Critical Absorption Wavelengths and Critical Absorption Energies**

| Atomic Number | Element | K Edge | | $L_1$ Edge | | $L_2$ Edge | | $L_3$ Edge | | $M_4$ Edge | | $M_5$ Edge | |
|---|---|---|---|---|---|---|---|---|---|---|---|---|---|
| | | Å | keV | Å | keV | Å | keV | Å | keV | Å | keV | Å | keV |
| 1 | H | 918 | 0.014 | | | | | | | | | | |
| 2 | He | 504 | 0.025 | | | | | | | | | | |
| 3 | Li | 226.953 | 0.055 | | | | | | | | | | |
| 4 | Be | 106.9 | 0.116 | | | | | | | | | | |
| 5 | B | 64.6 | 0.192 | | | | | | | | | | |
| 6 | C | 43.767 | 0.283 | | | | | | | | | | |
| 7 | N | 31.052 | 0.399 | | | | | | | | | | |
| 8 | O | 23.367 | 0.531 | | | | | | | | | | |
| 9 | F | 18.05 | 0.687 | | | | | | | | | | |
| 10 | Ne | 14.19 | 0.874 | 258 | 0.048 | 564 | 0.022 | 564 | 0.022 | | | | |
| 11 | Na | 11.48 | 1.08 | 225 | 0.055 | 365 | 0.034 | 365 | 0.034 | | | | |
| 12 | Mg | 9.512 | 1.303 | 197 | 0.063 | 248 | 0.050 | 253 | 0.049 | | | | |
| 13 | Al | 7.951 | 1.559 | 143 | 0.087 | 170 | 0.073 | 172 | 0.072 | | | | |
| 14 | Si | 6.745 | 1.837 | 105 | 0.118 | 125 | 0.099 | 127 | 0.098 | | | | |
| 15 | P | 5.787 | 2.142 | 81.0 | 0.153 | 96.1 | 0.129 | 96.9 | 0.128 | | | | |
| 16 | S | 5.018 | 2.470 | 64.2 | 0.193 | 75.6 | 0.164 | 79.1 | 0.163 | | | | |
| 17 | Cl | 4.397 | 2.819 | 52.1 | 0.238 | 61.1 | 0.203 | 61.4 | 0.202 | | | | |
| 18 | Ar | 3.871 | 3.202 | 43.2 | 0.287 | 50.2 | 0.247 | 50.6 | 0.245 | | | | |
| 19 | K | 3.437 | 3.606 | 36.4 | 0.341 | 41.8 | 0.297 | 42.2 | 0.294 | | | | |
| 20 | Ca | 3.070 | 4.037 | 30.7 | 0.399 | 35.2 | 0.352 | 35.5 | 0.349 | | | | |
| 21 | Sc | 2.757 | 4.495 | 26.8 | 0.462 | 30.2 | 0.411 | 30.8 | 0.402 | | | | |
| 22 | Ti | 2.497 | 4.963 | 23.4 | 0.530 | 27.0 | 0.460 | 27.3 | 0.454 | | | | |
| 23 | V | 2.269 | 5.462 | 20.5 | 0.604 | 23.9 | 0.519 | 24.2 | 0.512 | | | | |
| 24 | Cr | 2.070 | 5.987 | 18.3 | 0.679 | 21.3 | 0.583 | 21.6 | 0.574 | | | | |
| 25 | Mn | 1.896 | 6.535 | 16.3 | 0.762 | 19.1 | 0.650 | 19.4 | 0.639 | | | | |
| 26 | Fe | 1.743 | 7.109 | 14.6 | 0.849 | 17.2 | 0.721 | 17.5 | 0.708 | | | | |
| 27 | Co | 1.608 | 7.707 | 13.3 | 0.929 | 15.6 | 0.794 | 15.9 | 0.779 | | | | |
| 28 | Ni | 1.488 | 8.329 | 12.22 | 1.015 | 14.2 | 0.871 | 14.5 | 0.853 | | | | |

| | | | | | | | | | | | | | |
|---|---|---|---|---|---|---|---|---|---|---|---|---|---|
| 29 | Cu | 1.380 | 8.978 | 11.27 | 1.100 | 13.0 | 0.953 | 13.3 | 0.933 | | | | |
| 30 | Zn | 1.283 | 9.657 | 10.33 | 1.200 | 11.87 | 1.045 | 12.13 | 1.022 | | | | |
| 31 | Ga | 1.196 | 10.365 | 9.54 | 1.30 | 10.93 | 1.134 | 11.10 | 1.117 | | | | |
| 32 | Ge | 1.117 | 11.100 | 8.73 | 1.42 | 9.94 | 1.248 | 10.19 | 1.217 | | | | |
| 33 | As | 1.045 | 11.860 | 8.107 | 1.529 | 9.124 | 1.358 | 9.39 | 1.32 | | | | |
| 34 | Se | 0.980 | 12.649 | 7.506 | 1.651 | 8.416 | 1.473 | 8.67 | 1.43 | | | | |
| 35 | Br | 0.920 | 13.471 | 6.97 | 1.78 | 7.80 | 1.59 | 8.00 | 1.55 | | | | |
| 36 | Kr | 0.866 | 14.319 | 6.46 | 1.92 | 7.21 | 1.72 | 7.43 | 1.67 | | | | |
| 37 | Rb | 0.816 | 15.197 | 5.998 | 2.066 | 6.643 | 1.865 | 6.89 | 1.80 | | | | |
| 38 | Sr | 0.770 | 16.101 | 5.583 | 2.220 | 6.172 | 2.008 | 6.387 | 1.940 | | | | |
| 39 | Y | 0.728 | 17.032 | 5.232 | 2.369 | 5.755 | 2.153 | 5.962 | 2.079 | | | | |
| 40 | Zr | 0.689 | 17.993 | 4.867 | 2.546 | 5.378 | 2.304 | 5.583 | 2.220 | | | | |
| 41 | Nb | 0.653 | 18.981 | 4.581 | 2.705 | 5.026 | 2.467 | 5.223 | 2.373 | | | | |
| 42 | Mo | 0.620 | 19.996 | 4.298 | 2.883 | 4.718 | 2.627 | 4.913 | 2.523 | | | | |
| 43 | Tc | 0.589 | 21.045 | 4.060 | 3.054 | 4.436 | 2.795 | 4.632 | 2.677 | | | | |
| 44 | Ru | 0.561 | 22.112 | 3.83 | 3.24 | 4.180 | 2.965 | 4.369 | 2.837 | | | | |
| 45 | Rh | 0.534 | 23.217 | 3.626 | 3.418 | 3.942 | 3.144 | 4.130 | 3.001 | | | | |
| 46 | Pd | 0.509 | 24.341 | 3.428 | 3.616 | 3.724 | 3.328 | 3.908 | 3.171 | | | | |
| 47 | Ag | 0.486 | 25.509 | 3.254 | 3.809 | 3.514 | 3.527 | 3.698 | 3.351 | | | | |
| 48 | Cd | 0.464 | 26.704 | 3.085 | 4.018 | 3.326 | 3.726 | 3.504 | 3.537 | | | | |
| 49 | In | 0.444 | 27.920 | 2.926 | 4.236 | 3.147 | 3.938 | 3.324 | 3.728 | | | | |
| 50 | Sn | 0.425 | 29.182 | 2.777 | 4.463 | 2.982 | 4.156 | 3.156 | 3.927 | | | | |
| 51 | Sb | 0.407 | 30.477 | 2.639 | 4.695 | 2.830 | 4.380 | 3.000 | 4.131 | | | | |
| 52 | Te | 0.390 | 31.800 | 2.511 | 4.937 | 2.687 | 4.611 | 2.855 | 4.340 | | | | |
| 53 | I | 0.374 | 33.155 | 2.389 | 5.188 | 2.553 | 4.855 | 2.719 | 4.557 | | | | |
| 54 | Xe | 0.359 | 34.570 | 2.274 | 5.451 | 2.429 | 5.102 | 2.592 | 4.780 | | | | |
| 55 | Cs | 0.345 | 35.949 | 2.167 | 5.719 | 2.314 | 5.356 | 2.474 | 5.010 | | | | |
| 56 | Ba | 0.331 | 37.399 | 2.068 | 5.994 | 2.204 | 5.622 | 2.363 | 5.245 | 15.56 | 0.7967 | 15.89 | 0.7801 |
| 57 | La | 0.318 | 38.920 | 1.973 | 6.282 | 2.103 | 5.893 | 2.258 | 5.488 | | | | |
| 58 | Ce | 0.307 | 40.438 | 1.889 | 6.559 | 2.011 | 6.163 | 2.164 | 5.727 | | | | |
| 59 | Pr | 0.295 | 41.986 | 1.811 | 6.844 | 1.924 | 6.441 | 2.077 | 5.967 | 13.122 | 0.9448 | 13.394 | 0.9257 |

(*continued*)

**Table 8.B.1 (continued) Critical Absorption Wavelengths and Critical Absorption Energies**

| Atomic Number | Element | K Edge | | $L_1$ Edge | | $L_2$ Edge | | $L_3$ Edge | | $M_4$ Edge | | $M_5$ Edge | |
|---|---|---|---|---|---|---|---|---|---|---|---|---|---|
| | | Å | keV | Å | keV | Å | keV | Å | keV | Å | keV | Å | keV |
| 60 | Nd | 0.285 | 43.559 | 1.735 | 7.142 | 1.843 | 6.725 | 1.995 | 6.213 | 12.459 | 0.9951 | 23.737 | 0.9734 |
| 61 | Pm | 0.274 | 45.207 | 1.665 | 7.448 | 1.767 | 7.018 | 1.918 | 6.466 | | | | |
| 62 | Sm | 0.265 | 46.833 | 1.599 | 7.752 | 1.703 | 7.279 | 1.845 | 6.719 | 11.288 | 1.0983 | 11.552 | 1.0732 |
| 63 | Eu | 0.256 | 48.501 | 1.536 | 8.066 | 1.626 | 7.621 | 1.775 | 6.981 | 10.711 | 1.1575 | 11.013 | 1.1258 |
| 64 | Gd | 0.247 | 50.215 | 1.477 | 8.391 | 1.561 | 7.938 | 1.710 | 7.250 | | | | |
| 65 | Tb | 0.238 | 51.984 | 1.421 | 8.722 | 1.501 | 8.256 | 1.649 | 7.517 | | | | |
| 66 | Dy | 0.231 | 53.773 | 1.365 | 9.081 | 1.438 | 8.619 | 1.579 | 7.848 | | | | |
| 67 | Ho | 0.223 | 55.599 | 1.317 | 9.408 | 1.390 | 8.918 | 1.535 | 8.072 | | | | |
| 68 | Er | 0.216 | 57.465 | 1.268 | 9.773 | 1.338 | 9.260 | 1.482 | 8.361 | 8.601 | 1.4415 | 8.847 | 1.4013 |
| 69 | Tm | 0.209 | 59.319 | 1.222 | 10.141 | 1.288 | 9.626 | 1.433 | 8.650 | | | 8.487 | 1.4609 |
| 70 | Yb | 0.202 | 61.282 | 1.182 | 10.487 | 1.243 | 9.972 | 1.386 | 8.941 | | | | |
| 71 | Lu | 0.196 | 63.281 | 1.140 | 10.870 | 1.199 | 10.341 | 1.341 | 8.239 | | | | |
| 72 | Hf | 0.190 | 65.292 | 1.100 | 11.271 | 1.155 | 10.732 | 1.297 | 9.554 | | | | |
| 73 | Ta | 0.184 | 67.379 | 1.061 | 11.681 | 1.114 | 11.128 | 1.255 | 9.874 | 6.87 | 1.804 | 7.11 | 1.743 |
| 74 | W | 0.178 | 69.479 | 1.025 | 12.097 | 1.075 | 11.533 | 1.216 | 10.196 | 6.59 | 1.880 | 6.83 | 1.814 |
| 75 | Re | 0.173 | 71.590 | 0.990 | 12.524 | 1.037 | 11.953 | 1.177 | 10.529 | 6.33 | 1.958 | 6.560 | 1.890 |
| 76 | Os | 0.168 | 73.856 | 0.956 | 12.968 | 1.001 | 12.380 | 1.140 | 10.867 | 6.073 | 2.042 | 6.30 | 1.967 |
| 77 | Ir | 0.163 | 76.096 | 0.923 | 13.427 | 0.967 | 12.817 | 1.106 | 11.209 | 5.83 | 2.126 | 6.05 | 2.048 |
| 78 | Pt | 0.158 | 78.352 | 0.893 | 13.875 | 0.934 | 13.266 | 1.072 | 11.556 | 5.59 | 2.217 | 5.81 | 2.133 |
| 79 | Au | 0.153 | 80.768 | 0.863 | 14.354 | 0.903 | 13.731 | 1.040 | 11.917 | 5.374 | 2.307 | 5.584 | 2.220 |
| 80 | Hg | 0.149 | 83.046 | 0.835 | 14.837 | 0.872 | 14.210 | 1.008 | 12.3 | 5.157 | 2.404 | 5.36 | 2.313 |
| 81 | Tl | 0.415 | 85.646 | 0.808 | 15.338 | 0.843 | 14.695 | 0.979 | 12.655 | 4.952 | 2.504 | 5.153 | 2.406 |
| 82 | Pb | 0.141 | 88.037 | 0.782 | 15.858 | 0.815 | 15.205 | 0.950 | 13.041 | 4.757 | 2.606 | 4.955 | 2.502 |
| 83 | Bi | 0.137 | 90.420 | 0.757 | 16.376 | 0.789 | 15.713 | 0.923 | 13.422 | 4.572 | 2.711 | 4.764 | 2.603 |
| 84 | Po | 0.133 | 93.112 | 0.732 | 16.935 | 0.763 | 16.244 | 0.897 | 13.817 | | | | |

| | | | | | | | | | | | | | |
|---|---|---|---|---|---|---|---|---|---|---|---|---|---|
| 85 | At | 0.130 | 95.740 | 0.709 | 17.490 | 0.739 | 16.784 | 0.872 | 14.215 | | | | |
| 86 | Rn | 0.126 | 98.418 | 0.687 | 18.058 | 0.715 | 17.337 | 0.848 | 14.618 | | | | |
| 87 | Fr | 0.123 | 101.147 | 0.665 | 18.638 | 0.693 | 17.904 | 0.825 | 15.028 | | | | |
| 88 | Ra | | | 0.645 | 19.229 | 0.671 | 18.478 | 0.803 | 15.439 | | | | |
| 89 | Ac | 0.116 | 106.759 | 0.625 | 19.842 | 0.650 | 19.078 | 0.782 | 15.865 | | | | |
| 90 | Th | 0.113 | 109.741 | 0.606 | 20.458 | 0.630 | 19.677 | 0.761 | 16.293 | 3.557 | 3.485 | 3.729 | 3.325 |
| 91 | Pa | 0.110 | 112.581 | 0.588 | 21.102 | 0.611 | 20.311 | 0.741 | 16.731 | 3.436 | 3.608 | 3.618 | 3.436 |
| 92 | U | 0.108 | 115.610 | 0.56 | 21.764 | 0.592 | 20.938 | 0.722 | 17.160 | 3.333 | 3.720 | 3.497 | 3.545 |
| 93 | Np | 0.105 | 118.619 | 0.553 | 22.417 | 0.574 | 21.596 | 0.704 | 17.614 | | | | |
| 94 | Pu | 0.102 | 121.720 | 0.537 | 23.097 | 0.557 | 22.262 | 0.686 | 18.066 | | | | |
| 95 | Am | 0.099 | 124.816 | 0.521 | 23.793 | 0.540 | 22.944 | 0.669 | 18.525 | | | | |
| 96 | Cm | 0.097 | 128.088 | 0.506 | 24.503 | 0.525 | 23.640 | 0.653 | 18.990 | | | | |
| 97 | Bk | 0.094 | 131.357 | 0.491 | 25.230 | 0.509 | 24.352 | 0.637 | 19.461 | | | | |
| 98 | Cf | 0.092 | 134.683 | 0.477 | 25.971 | 0.494 | 25.080 | 0.622 | 19.938 | | | | |
| 99 | Es | 0.090 | 138.067 | 0.464 | 26.729 | 0.480 | 25.824 | 0.607 | 20.422 | | | | |
| 100 | Fm | 0.088 | 141.510 | 0.451 | 27.503 | 0.466 | 26.584 | 0.593 | 20.912 | | | | |

## BIBLIOGRAPHY

American Society for Testing and Materials. *Annual Book of ASTM Standards*. ASTM: West Conshohocken, PA, 2002.

Application reviews. *Anal. Chem*. June 1994.

Bertin, E.P. *Principles and Practice of X-Ray Spectrometric Analysis*, 2nd edn. Plenum Press: New York, 1975.

Bertin, E.P. *Introduction to X-Ray Spectrometric Analysis*. Plenum Press: New York, 1978.

Burr, A. In Robinson, J.W. (ed.), *Handbook of Spectroscopy*, Vol. 1. CRC Press: Boca Raton, FL, 1994.

Clark, G.L. (ed.) *Encyclopedia of X-Rays and Gamma Rays*. Reinhold Publishing: New York, 1963.

Criss, J.W.; Birks, L.S. *Anal. Chem*., *40*, 1080–1086, 1968.

Ellis, A.T. In Van Griekin, R.E.; Markowicz, A.A. (eds.), *Handbook of X-Ray Spectrometry*, 2nd edn. Marcel Dekker, Inc.: New York, 2002.

Formica, J. X-ray diffraction. In Settle, F. (ed.), *Handbook of Instrumental Techniques for Analytical Chemistry*. Prentice-Hall, Inc.: Upper Saddle River, NJ, 1997.

Gross, A. The characterization of historic pigments by µXRF spectrometry. Bruker Nano Lab Report XRF 422, www.bruker.com. 2010.

Hahn, O.; Oltrogge, D.; Bevers, H. *Archaeometry*, 2003.

Havrilla, G.J. X-ray fluorescence spectrometry. In Settle, F. (ed.), *Handbook of Instrumental Techniques for Analytical Chemistry*. Prentice-Hall, Inc.: Upper Saddle River, NJ, 1997.

Helson, L.A.; Kuczumov, A. In Van Griekin, R.E.; Markowicz, A.A. (eds.), *Handbook of X-Ray Spectrometry*, 2nd edn. Marcel Dekker, Inc.: New York, 2002.

Herglotz, H.K.; Birks, L.S. *X-Ray Spectrometry*. Marcel Dekker, Inc.: New York, 1978.

Jenkins, R. X-ray fluorescence. *Anal. Chem*., *36*, 1009A, 1984.

Jenkins, R. *X-Ray Fluorescence Spectrometry*, 2nd edn. John Wiley & Sons, Inc.: New York, 1999.

Jenkins, R.; Gould, R.W.; Gedcke, D. *Quantitative X-Ray Spectrometry*. Marcel Dekker, Inc.: New York, 1981.

Jenkins, R.; Manne, R.; Robin, J.; Senemaud, C. *Pure Appl. Chem*., *63*(5), 785, 1991.

Jenkins, R.; Snyder, R.L. *Introduction to X-Ray Powder Diffractometry*. John Wiley & Sons, Inc.: New York, 1996.

Lubhofsky, H.A.; Schweikert, E.A.; Myers, E.A. *Treatise on Analytical Chemistry*, 2nd edn. Wiley Interscience: New York, 1986.

Markowicz, A.A. In Van Griekin, R.E., Markowicz, A.A. (eds.), *Handbook of X-Ray Spectrometry*, 2nd edn. Marcel Dekker, Inc.: New York, 2002.

Parsons, M.L. X-ray methods. In Ewing, G.W. (ed.), *Analytical Instrumentation Handbook*, 2nd edn. Marcel Dekker, Inc.: New York, 1997.

Robinson, J.W. *Handbook of Spectroscopy*, Vol. 1. CRC Press: Boca Raton, FL, 1974.

Robinson, J.W. *Practical Handbook of Spectroscopy*. CRC Press: Boca Raton, FL, 1991.

Stout, G.H.; Jensen, L.H. *X-Ray Structure Determination*. Macmillan Publishing Co., Inc.: New York, 1968.

Teo, B.K.; Joy, D.C. (eds.) *EXAFS Spectroscopy: Techniques and Applications*. Plenum Press: New York, 1981.

Van Griekin, R.E.; Markowicz, A.A. (eds.) *Handbook of X-Ray Spectrometry*, 2nd edn. Marcel Dekker, Inc.: New York, 2002.